# Applications of Particle Physics to the Early Universe

by

Leonardo Senatore

Submitted to the Department of Physics
in partial fulfillment of the requirements for the degree of

Doctor of Philosophy in Physics

at the

MASSACHUSETTS INSTITUTE OF TECHNOLOGY

June 2006



Author .....
Department of Physics
May 5, 2006

Certified by .....
Alan Guth
Victor F. Weisskopf Professor of Physics
Thesis Supervisor

Certified by .....
Nima Arkani-Hamed
Professor of Physics
Thesis Supervisor

Accepted by .....
Thomas J. Greytak
Associate Department Head for Education

# Applications of Particle Physics to the Early Universe

by

Leonardo Senatore

Submitted to the Department of Physics
on May 5, 2006, in partial fulfillment of the
requirements for the degree of
Doctor of Philosophy in Physics

## Abstract

In this thesis, I show some of the results of my research work in the field at the crossing between Cosmology and Particle Physics. The Cosmology of several models of the Physics Beyond the Standard Model is studied. These range from an inflationary model based on the condensation of a ghost-like scalar field, to several models motivated by the possibility that our theory is described by a landscape of vacua, as probably implied by String Theory, which have influence on the theory of Baryogenesis, of Dark Matter, and of Big Bang Nucleosynthesis. The analysis of the data of the experiment WMAP on the CMB for the search of a non-Gaussian signal is also presented and it results in an upper limit on the amount on non-Gaussianities which is at present the most precise and extended available.

Thesis Supervisor: Alan Guth
Title: Victor F. Weisskopf Professor of Physics

Thesis Supervisor: Nima Arkani-Hamed
Title: Professor of Physics

# Acknowledgments

I would like to acknowledge my supervisors, Prof. Alan Guth, from whom I learnt the scientific rigor, and Prof. Nima Arkani-Hamed, whose enthusiasm is always an inspiration; the other professors with whom I had the pleasure to interact with: Prof. Matias Zaldarriaga, Prof. Max Tegmark, and in particular Prof. Paolo Creminelli, with whom I ended up spending a large fraction of my time both at work and out of work; all the many Post-Docs and students who helped me, in particular Alberto Nicolis; and eventually all the friends I have met in the journey which brought me here. Often I was in the need of help, and I have always found someone that, smiling, was happy to give it to me. It is difficult to imagine, being a foreign far from home, if without all these people I would have been able to arrive to this point.

At the end, a special thank must go to my parents and to my girlfriend, who have always been close to me.

# Contents

# Chapter 1

# Introduction

During my studies towards a PhD in Theoretical Physics, I have focused mainly on the connections between Cosmology and Particle Physics.

In the very last few years, there has been a huge improvement in the field of Observational Cosmology, in particular thanks to the experiments on the cosmic microwave background (CMB) and on large scale structures. The much larger precision of the observational data in comparison with just a few years ago has made it possible to make the connection with the field of Theoretical Physics much stronger. This has occurred at a time in which the field of Particle Physics is experiencing a deficiency of experimental data, so that the indications coming from the observational field of Cosmology have become very important, or even vital. This is particularly true, for example, for the possible Physics associated with the ultra-violet (UV) completion of Einstein's General Relativity (GR), as, for example, String Theory.

Because of this, Cosmology has become both a field where new ideas from Particle Physics can be tested, potentially even verified or ruled out with great confidence, and finally applied in search for a more complete understanding of the early history of the universe, and also a field which, with its observations, can motivate new ideas on the Physics of the fundamental interactions.

Some scientific events which occurred during my years as a graduate student have particularly influenced my work.

From the cosmological side, the results produced by the Wilkinsons Microwave

Anisotropy Probe (WMAP) experiment on the CMB have greatly improved our knowledge of the current cosmological parameters [1]. These new measurements have gone into the direction of verifying the generic predictions of the presence of a primordial inflationary phase in our universe, even though not yet at the necessary high confidence level to insert inflation in the standard paradigm for the history of the early universe. The first careful study of the non-Gaussian features of the CMB has been of particular importance for my work, as I will highlight later. Further, these new data have shown with high confidence the detection of the presence of a form of energy, called Dark Energy, very similar to the one associated with a cosmological constant, which at present dominates the whole energy of the universe.

This last very unexpected discovery from Cosmology is an example of how cosmological observations can affect the field of Theoretical Physics. In fact, this observation has been of great influence on the development of a new set of ideas in Theoretical Physics which have strongly influenced my work. In fact, the problem of the smallness of the cosmological constant is one of the biggest unsolved problems of present Theoretical Physics, and, until these discoveries, it had been hoped that a UV complete theory of Quantum Gravity, once understood, would have given a solution. However, from the theoretical side, String Theory, which is, up to now, the only viable candidate for being a UV completion of GR, has shown that there exist consistent solutions with a non-null value of the cosmological constant, and that there could be a huge Landscape of consistent solutions, with different low energy parameters. Therefore, the theoretical possibility that the cosmological constant could be non zero, and that it could have many different values according to the different possible histories of the universe, together with the observational fact that the cosmological constant in our universe appears to be non zero, has led to a revival of a proposal by Weinberg [2] that the environmental, or anthropic, argument that structures should be present in our universe in order for there to be life, could force the value of the cosmological constant to be small. Recently, this argument has then been extended to the possibility that also other parameters of the low energy theory might be determined by environmental arguments [3, 4]. For obvious reasons, this general class of ideas is

usually referred to as Landscape motivated, and here I will do the same.

In this thesis, I will illustrate some of the works I did into these directions. I consider useful to explain them in the chronological order in which they were developed.

In chapter 2, I will develop a model of inflation where the acceleration of the universe is driven by the ghost condensate [5] . The ghost condensate is a recently proposed mechanism through which the vacuum of a scalar field can be characterized by a constant, not null, speed for the field [6]. The inflationary model based on this has the interesting features of generically predicting a detectable level of non-Gaussianities in the CMB, and of being the first example which shows that it is possible to have an inflationary model where the Hubble rate grows with time. The studies performed in this work have resulted in the publication in the journal **Physical Review D** of the paper in [7].

In chapter 3, in the context of Split Supersymmetry [3], which is a recently proposed supersymmetric model motivated by the Landscape where the scalar superpartners are very heavy, and the higgs mass is finely tuned for environmental reasons, I will study the possibility that the dark matter of the universe is made up of particles which interact only gravitationally, such as the gravitino. This possibility, if realized in nature, would have deep consequences on the possible spectrum of Split Supersymmetry and its possible detection at the next Large Hadron Collider (LHC). I will conclude that observational bounds from Big Bang Nucleosynthesis strongly constrain the possibility that the gravitino is the dark matter in the context of Split Supersimmetry, while other hidden sector candidates are still allowed. The studies performed in this work have resulted in the publication in the journal **Physical Review D** of the paper in [8].

In chapter 4, I will study a model developed in the context of the Landscape, in which the hierarchy between the Weak scale and the Plank scale is explained in terms of requiring that baryons are generated in our universe through the mechanism of Electroweak Baryogenesis. While the signature of this model at LHC could be

very little, the constraint from baryogenesis implies that the system is expected to show up within next generation experiments on the electron electric dipole moment (EDM). The studies performed in this work have resulted in the publication in the journal **Physical Review D** of the paper in [9].

In chapter 5, I will show a work in which I performed the analysis of the actual data on the CMB from the WMAP experiment, in search of a signal of non-Gaussianity in the temperature fluctuations. I will improve the analysis done by the WMAP team, and I will extend it to other physically motivated models. At the moment, the limit I will quote on the amplitude of the non-Gaussian signal is the most stringent and complete available. The studies performed in this work have resulted in the publication of the paper in [10], accepted for publication by the **Journal of Cosmology and Astroparticle Physics** in May 2006.

In chapter 6, again inspired by the possibility that there is a Landscape of vacua in the fundamental theory, and that the Higgs particle mass might be finely tuned for environmental reasons, I will study the minimal model beyond the Standard Model that would account for the dark matter in the universe as well as gauge coupling unification. I will find that this minimal model can allow for exceptionally heavy dark matter particles, well beyond the reach of LHC, but that the model should however reveal itself within next generation experiments on the EDM. I will embed the model in a Grand Unified Extradimenesional Theory with an extra dimension in an interval, and I will study in detail its properties. The studies performed in this work has resulted in the publication in the journal **Physical Review D** of the paper in [11].

This will conclude a summary of some of the research work I have been doing during these years.

Both the field of Cosmology and of Particle Physics are expecting great results from the very next years.

Improvement of the data from WMAP experiment, as well as the launch of Plank and CMBPol experiments are expected to give us enough data to understand with

confidence the primordial inflationary era of our universe. A detection in the CMB of a tilt in the power spectrum of the scalar perturbations, or of a polarization induced by a background of gravitational waves, or of a non-Gaussian signal would shed light into the early phases of the universe, and therefore also on the Physics at very high energy well beyond what at present is conceivable to reach at particle accelerators. Combined with a definite improvement in the data on the Supernovae, expected in the very near future, these new experiment might shed light also on the great mystery of the present value of the Dark Energy, testing with great accuracy the possibility that it is constituted by a cosmological constant.

The turning on of LHC will probably let us understand if the solution to the hierarchy problem is to be solved in some natural way, as for example with TeV scale Supersymmetry, or if there is evidence of a tuning which points towards the presence of a Landscape.

It is a pleasure to realize that by the next very few years, many of these deep questions might have an answer.

# Bibliography


[1] D. N. Spergel *et al.* [WMAP Collaboration], "First Year Wilkinson Microwave Anisotropy Probe (WMAP) Observations: Determination of Cosmological Parameters," Astrophys. J. Suppl. **148**, 175 (2003) [arXiv:astro-ph/0302209].

[2] S. Weinberg, "Anthropic Bound On The Cosmological Constant," Phys. Rev. Lett. **59** (1987) 2607.

[3] N. Arkani-Hamed and S. Dimopoulos, "Supersymmetric unification without low energy supersymmetry and signatures for fine-tuning at the LHC," JHEP **0506**, 073 (2005) [arXiv:hep-th/0405159].

[4] N. Arkani-Hamed, S. Dimopoulos and S. Kachru, "Predictive landscapes and new physics at a TeV," arXiv:hep-th/0501082.

[5] N. Arkani-Hamed, P. Creminelli, S. Mukohyama and M. Zaldarriaga, "Ghost inflation," JCAP **0404**, 001 (2004) [arXiv:hep-th/0312100].

[6] N. Arkani-Hamed, H. C. Cheng, M. A. Luty and S. Mukohyama, "Ghost condensation and a consistent infrared modification of gravity," JHEP **0405**, 074 (2004) [arXiv:hep-th/0312099].

[7] L. Senatore, "Tilted ghost inflation," Phys. Rev. D **71**, 043512 (2005) [arXiv:astro-ph/0406187].

[8] L. Senatore, "How heavy can the fermions in split SUSY be? A study on gravitino and extradimensional LSP," Phys. Rev. D **71**, 103510 (2005) [arXiv:hep-ph/0412103].

[9] L. Senatore, "Hierarchy from baryogenesis," Phys. Rev. D **73**, 043513 (2006) [arXiv:hep-ph/0507257].

[10] P. Creminelli, A. Nicolis, L. Senatore, M. Tegmark and M. Zaldarriaga, "Limits on non-Gaussianities from WMAP data," arXiv:astro-ph/0509029.

[11] R. Mahbubani and L. Senatore, "The minimal model for dark matter and unification," Phys. Rev. D **73**, 043510 (2006) [arXiv:hep-ph/0510064].

# Chapter 2

# Tilted Ghost Inflation

In a ghost inflationary scenario, we study the observational consequences of a tilt in the potential of the ghost condensate. We show how the presence of a tilt tends to make contact between the natural predictions of ghost inflation and the ones of slow roll inflation. In the case of positive tilt, we are able to build an inflationary model in which the Hubble constant $H$ is growing with time. We compute the amplitude and the tilt of the 2-point function, as well as the 3-point function, for both the cases of positive and negative tilt. We find that a good fraction of the parameter space of the model is within experimental reach.

## 2.1 Introduction

Inflation is a very attractive paradigm for the early stage of the universe, being able to solve the flatness, horizon, monopoles problems, and providing a mechanism to generate the metric perturbations that we see today in the CMB [1].

Recently, ghost inflation has been proposed as a new way for producing an epoch of inflation, through a mechanism different from that of slow roll inflation [2, 3]. It can be thought of as arising from a derivatively coupled ghost scalar field $\phi$ which

condenses in a background where it has a non zero velocity:

$$\langle \dot{\phi} \rangle = M^2 \rightarrow \langle \phi \rangle = M^2 t \tag{2.1}$$

where we take $M^2$ to be positive.

Unlike other scalar fields, the velocity $\langle \dot{\phi} \rangle$ does not redshift to zero as the universe expands, but it stays constant, and indeed the energy momentum tensor is identical of that of a cosmological constant. However, the ghost condensate is a physical fluid, and so, it has physical fluctuations which can be defined as:

$$\phi = M^2 t + \pi \tag{2.2}$$

The ghost condensate then gives an alternative way of realizing De Sitter phases in the universe. The symmetries of the theory allow us to construct a systematic and reliable effective Lagrangian for $\pi$ and gravity at energies lower than the ghost cut-off $M$. Neglecting the interactions with gravity, around flat space, the effective Lagrangian for $\pi$ has the form:

$$S = \int d^4x \frac{1}{2}\dot{\pi}^2 - \frac{\alpha}{2M^2}(\nabla^2\pi)^2 - \frac{\beta}{2M^2}\dot{\pi}(\nabla\pi)^2 + ... \tag{2.3}$$

where $\alpha$ and $\beta$ are order one coefficients. In [2], it was shown that, in order for the ghost condensate to be able to implement inflation, the shift symmetry of the ghost field $\phi$ had to be broken. This could be realized adding a potential to the ghost. The observational consequences of the theory were no tilt in the power spectrum, a relevant amount of non gaussianities, and the absence of gravitational waves. The non gaussianities appeared to be the aspect closest to a possible detection by experiments such as WMAP. Also the shape of the 3-point function of the curvature perturbation $\zeta$ was different from the one predicted in standard inflation. In the same paper [2], the authors studied the possibility of adding a small tilt to the ghost potential, and they did some order of magnitude estimate of the consequences in the case the potential decreases while $\phi$ increases.

In this chapter, we perform a more precise analysis of the observational consequences of a ghost inflation with a tilt in the potential. We study the 2-point and 3-point functions. In particular, we also imagine that the potential is tilted in such a way that actually the potential increases as the value of $\phi$ increases with time. This configuration still allows inflation, since the main contribution to the motion of the ghost comes from the condensation of the ghost, which is only slightly affected by the presence of a small tilt in the potential. This provides an inflationary model in which $H$ is growing with time. We study the 2-point and 3-point function also in this case.

The chapter is organized as follows. In section 2.2, we introduce the concept of the tilt in the ghost potential; in section 2.3 we study the case of negative tilt, we compute the 2-point and 3-point functions, and we determine the region of the parameter space which is not ruled out by observations; in section 2.4 we do the same as we did in section 2.3 for the case of positive tilt; in section 2.5 we summarize our conclusions.

## 2.2 Density Perturbations

In an inflationary scenario, we are interested in the quantum fluctuations of the $\pi$ field, which, out of the horizon, become classical fluctuations. In [3], it was shown that, in the case of ghost inflation, in longitudinal gauge, the gravitational potential $\Phi$ decays to zero out of the horizon. So, the Bardeen variable is simply:

$$\zeta = -\frac{H}{\dot{\phi}}\pi \tag{2.4}$$

and is constant on superhorizon scales. It was also shown that the presence of a ghost condensate modifies gravity on a time scale $\Gamma^{-1}$, with $\Gamma \sim M^3/M_{Pl}^2$, and on a length scale $m^{-1}$, with $m \sim M^2/M_{Pl}$. The fact that these two scales are different is not a surprise since the ghost condensate breaks Lorentz symmetry.

Requiring that gravity is not modified today on scales smaller than the present

Hubble horizon, we have to impose $\Gamma < H_0$, which implies that gravity is not modified during inflation:

$$\Gamma \ll m \ll H \tag{2.5}$$

This is equivalent to the decoupling limit $M_{Pl} \to \infty$, keeping $H$ fixed, which implies that we can study the Lagrangian for $\pi$ neglecting the metric perturbations.

Now, let us consider the case in which we have a tilt in the potential. Then, the zero mode equation for $\pi$ becomes:

$$\ddot{\pi} + 3H\dot{\pi} + V' = 0 \tag{2.6}$$

which leads to the solution:

$$\dot{\pi} = -\frac{V'}{3H} \tag{2.7}$$

We see that this is equivalent to changing the velocity of the ghost field.

In order for the effective field theory to be valid, we need that the velocity of $\pi$ to be much smaller than $M^2$, so, in agreement with [2], we define the parameter:

$$\begin{aligned} \delta^2 &= -\frac{V'}{3HM^2} \text{ for } V' < 0 \\ \delta^2 &= +\frac{V'}{3HM^2} \text{ for } V' > 0 \end{aligned} \tag{2.8}$$

to be $\delta^2 \ll 1$. We perform the analysis for small tilt, and so at first order in $\delta^2$.

At this point, it is useful to write the 0-0 component of the stress energy tensor, for the model of [3]:

$$T_{00} = -M^4 P(X) + 2M^4 P'(X)\dot{\phi}^2 + V(\phi) \tag{2.9}$$

where $X = \partial_\mu \phi \partial^\mu \phi$. The authors show that the field, with no tilted potential, is attracted to the minimum of the function $P(X)$, such that, $P(X_{min}) = M^2$. So, adding a tilt to the potential can be seen as shifting the ghost field away from the minimum of $P(X)$.

Now, we proceed to studying the two point function and the three point function

for both the cases of a positive tilt and a negative tilt.

## 2.3 Negative Tilt

Let us analyze the case $V' < 0$.

### 2.3.1 2-Point Function

To calculate the spectrum of the $\pi$ fluctuations, we quantize the field as usual:

$$\pi_k(t) = w_k(t)\hat{a}_k + w_k^*(t)\hat{a}_{-k}^\dagger \tag{2.10}$$

The dispersion relation for $w_k$ is:

$$\omega_k^2 = \alpha\frac{k^4}{M^2} + \beta\delta^2 k^2 \tag{2.11}$$

Note, as in [3], that the sign of $\beta$ is the same as the sign of $< \dot{\phi} >= M^2$. In all this chapter we shall restrict to $\beta \geq 0$, and so the sign of $\beta$ is fixed.

We see that the tilt introduces a piece proportional to $k^2$ in the dispersion relation. This is a sign that the role of the tilt is to transform ghost inflation to the standard slow roll inflation. In fact, $\omega^2 \sim k^2$ is the usual dispersion relation for a light field.

Defining $w_k(t) = u_k(t)/a$, and going to conformal time $d\eta = dt/a$, we get the following equation of motion:

$$u_k'' + (\beta\delta^2 k^2 + \alpha\frac{k^4 H^2\eta^2}{M^2} - \frac{2}{\eta^2})u_k = 0 \tag{2.12}$$

If we were able to solve this differential equation, than we could deduce the power spectrum. But, unfortunately, we are not able to find an exact analytical solution. Anyway, from (2.12), we can identify two regimes: one in which the term $\sim k^4$ dominates at freezing out, $\omega \sim H$, and one in which it is the term in $\sim k^2$ that dominates at that time. Physically, we know that most of the contribution to the

shape of the wavefunction comes from the time around horizon crossing. So, in order for the tilt to leave a signature on the wavefunction, we need it to dominate before freezing out.There will be an intermediate regime in which both the terms in $k^2$ and $k^4$ will be important around horizon crossing, but we decide not to analyze that case as not too much relevant to our discussion. So, we restrict to:

$$\delta^2 \gg \delta_{cr}^2 \equiv \frac{\alpha^{1/2}}{\beta}\frac{H}{M} \tag{2.13}$$

where *cr* stays for *crossing*. In that case, the term in $k^2$ dominates before freezing out, and we can approximate the differential equation (2.12) to:

$$u_k'' + (\bar{k}^2 - \frac{2}{\eta^2})u_k = 0 \tag{2.14}$$

where $\bar{k} = \beta^{1/2}\delta k$. Notice that this is the same differential equation we would get for the slow roll inflation upon replacing $k$ with $\bar{k}$.

Solving with the usual vacuum initial condition, we get:

$$w_k = -H\eta\frac{e^{-i\bar{k}\eta}}{2^{1/2}\bar{k}^{1/2}\eta}(1 - \frac{i}{\bar{k}\eta}) \tag{2.15}$$

which leads to the power spectrum:

$$P_\pi = \frac{k^3}{2\pi^2}|w_k(\eta \to 0)|^2 = \frac{H^2}{4\pi^2\beta^{3/2}\delta^3} \tag{2.16}$$

and, using $\zeta = -\frac{H}{\dot{\phi}}\pi$,

$$P_\zeta = \frac{H^4}{4\pi^2\beta^{3/2}\delta^3 M^4} \tag{2.17}$$

This is the same result as in slow roll inflation, replacing $k$ with $\bar{k}$. Notice that, on the contrary with respect to standard slow roll inflation, the denominator is not suppressed by slow roll parameters, but by the $\delta^2$ term.

The tilt is given by:

$$n_s - 1 \equiv \frac{dln(P_\zeta)}{dln(k)} = (4\frac{dln(H)}{dlnk} - \frac{3}{2}\frac{dln\beta}{dlnk} - \frac{3}{2}\frac{dln\delta^2}{dlnk} - 2\frac{dln\dot{\phi}}{dlnk})|_{k=\frac{aH}{\beta^{1/2}\delta}} = \quad (2.18)$$
$$= \frac{2M^2V'}{HV} + \frac{V''}{H^2}\Big(\frac{1}{2\delta^2} + \frac{2}{9} + \frac{4M^4}{V}(1 - 2P''M^8)\Big)$$

where $k = \frac{aH}{\beta^{1/2}\delta}$ is the momenta at freezing out, and where $P$ and its derivatives are evaluated at $X_{min}$.

Notice the appearance of the term $\sim \frac{1}{\delta^2}$, which can easily be the dominant piece. Please remind that, anyway, this is valid only for $\delta^2 \gg \delta^2_{cr}$. Notice also that, for the effective field theory to be valid, we need:

$$\frac{V'}{3H} \ll M^2 \quad (2.19)$$

so, $\frac{M^2V'}{HV} \ll \frac{M^4}{V}$. This last piece is in general $\ll 1$ if the ghost condensate is present today. In order to get an estimate of the deviation from scale invariance, we can see that the larger contribution comes from the piece in $\sim \frac{V''}{\delta^2H^2}$. From the validity of the effective field theory, we get:

$$\delta^2M^2H \cong |V'| \gtrsim |V''|\Delta\phi = |V''|(M^2/H)N_e \Rightarrow |V''| < \delta^2\frac{H^2}{N_e} \quad (2.20)$$

where $N_e$ is the number of e-foldings to the end of inflation. So, we deduce that the deviation of the tilt can be as large as:

$$|n_s - 1| \leq \frac{1}{N_e} \quad (2.21)$$

This is a different prediction from the exact $n_s = 1$ in usual ghost inflation.

### 2.3.2 3-Point Function

Let us come to the computation of the three point function. The leading interaction term (or the least irrelevant one), is given by [2]:

$$L_{int} = -\beta \frac{e^{Ht}}{2M^2}(\dot{\pi}(\nabla\pi)^2) \tag{2.22}$$

Using the formula in [4]:

$$< \pi_{k_1}(t)\pi_{k2}(t)\pi_{k3}(t) >= -i\int_{t_0}^{t} dt' < [\pi_{k_1}(t)\pi_{k2}(t)\pi_{k3}(t), \int d^3x H_{int}(t')] > \tag{2.23}$$

we get [2]:

$$\begin{aligned} &< \pi_{k_1}\pi_{k_2}\pi_{k_3} >= \frac{i\beta}{M^2}(2\pi)^3\delta^3(\sum k_i) \\ &w_1(0)w_2(0)w_3(0)((\vec{k_2}.\vec{k_3})I(1,2,3) + cyclic + c.c) \end{aligned} \tag{2.24}$$

where *cyclic* stays for cyclic permutations of the $k$'s, and where

$$I(1,2,3) = \int_{-\infty}^{0} \frac{1}{H\eta} w_1^*(\eta)' w_2^*(\eta) w_3^*(\eta) \tag{2.25}$$

and the integration is performed with the prescription that the oscillating functions inside the horizon become exponentially decreasing as $\eta \to -\infty$.

We can do the approximation of performing the integral with the wave function (2.15). In fact, the typical behavior of the wavefunction will be to oscillate inside the horizon, and to be constant outside of it. Since we are performing the integration on a path which exponentially suppresses the wavefunction when it oscillates, and since in the integrand there is a time derivative which suppresses the contribution when a wavefunction is constant, we see that the main contribution to the three point function comes from when the wavefunctions are around freezing out. Since, in that case, we are guaranteed that the term in $k^2$ dominates, then we can reliably approximate the

wavefunctions in the integrand with those in (2.15). Using that $\zeta = -\frac{H}{\dot{\phi}}\pi$,we get:

$$< \zeta_{k_1}\zeta_{k_2}\zeta_{k_3} >= (2\pi)^3\delta^3(\sum k_i)\frac{H^8}{4\beta^3\delta^8 M^8} \tag{2.26}$$
$$\frac{1}{k_t^3\prod_{i=1}^3 k_i^3}\Big(k_1^2(\vec{k_2}.\vec{k_3})\Big((k_2+k_3)k_t + k_t^2 + 2k_3k_2\Big) + cyclic\Big)$$

where $k_i = |\vec{k_i}|$. Let us define

$$F(k_1,k_2,k_3) = \frac{1}{k_t^3\prod k_i^3}\Big(k_1^2(\vec{k_2}.\vec{k_3})\Big((k_2+k_3)k_t + k_t^2 + 2k_3k_2\Big) + cyclic\Big) \tag{2.27}$$

which, apart for the $\delta$ function, holds the $k$ dependence of the 3-point function.

The obtained result agrees with the order of magnitude estimates given in [2]:

$$\frac{<\zeta^3>}{(<\zeta^2>)^{3/2}} \sim \frac{1}{\delta^8}(\frac{H}{M})^8\frac{1}{(\frac{1}{\delta^3}(\frac{H}{M})^2)^{3/2}} \sim \frac{1}{\delta^{7/2}}(\frac{H}{M})^2 \tag{2.28}$$

The total amount of non gaussianities is decreasing with the tilt. This is in agreement with the fact that the tilt makes the ghost inflation model closer to slow roll inflation, where, usually, the total amount of non gaussianities is too low to be detectable.

The 3-point function we obtained can be better understood if we do the following observation. This function is made up of the sum of three terms, each one obtained on cyclic permutations of the $k$'s. Each of these terms can be split into a part which is typical of the interaction and of scale invariance, and the rest which is due to the wave function. For the first cyclic term, we have:

$$Interaction = \frac{(\vec{k_2}.\vec{k_3})}{k_1k_2^3k_3^3} \tag{2.29}$$

while, the rest, which I will call wave function, is:

$$Wavefunction = \frac{((k_2+k_3)k_t + k_t^2 + 2k_2k_3)}{k_t^3} \tag{2.30}$$

The interaction part appears unmodified also in the untilted ghost inflation case. While the wave function part is characteristic of the wavefunction, and changes in

the two cases.

Our 3-point function can be approximately considered as a function of only two independent variables. The delta function, in fact, eliminates one of the three momenta, imposing the vectorial sum of the three momenta to form a closed triangle. Because of the symmetry of the De Sitter universe, the 3-point function is scale invariant, and so we can choose $|\vec{k}_1| = 1$. Using rotation invariance, we can choose $\vec{k}_1 = \hat{e}_1$, and impose $\vec{k}_2$ to lie in the $\hat{e}_1, \hat{e}_2$ plane. So, we have finally reduced the 3-point function from being a function of 3 vectors, to be a function of 2 variables. From this, we can choose to plot the 3-point function in terms of $x_i \equiv \frac{k_i}{k_1}$, $i = 1, 2$. The result is shown in fig.2-1. Note that we chose to plot the three point function with a measure equal to $x_2^2 x_3^2$. The reason for this is that this results in being the natural measure in the case we wish to represent the ratio between the signal associated to the 3-point function with respect to the signal associated to the 2-point function [5]. Because of the triangular inequality, which implies $x_3 \leq 1 - x_2$, and in order to avoid to double represent the same momenta configuration, we set to zero the three point function outside the triangular region: $1 - x_2 \leq x_3 \leq x_2$. In order to stress the difference with the case of standard ghost inflation, we plot in fig.2-2 the correspondent 3-point function for the case of ghost inflation without tilt. Note that, even though the two shapes are quite similar, the 3-point function of ghost inflation without tilt changes signs as a function of the $k$'s, while the 3-point function in the tilted case has constant sign.

An important observation is that, in the limit as $x_3 \to 0$ and $x_2 \to 1$, which corresponds to the limit of very long and thin triangles, we have that the 3 point function goes to zero as $\sim \frac{1}{x_3}$. This is expected, and in contrast with the usual slow roll inflation result $\sim \frac{1}{x_3^3}$. The reason for this is the same as the one which creates the same kind of behavior in the ghost inflation without tilt [2]. The limit of $x_3 \to 0$ corresponds to the physical situation in which the mode $k_3$ exits from the horizon, freezes out much before the other two, and acts as a sort of background. In this limit, let us imagine a spatial derivative acting on $\pi_3$, which is the background in the interaction Lagrangian. The 2-point function $< \pi_1 \pi_2 >$ depends on the position

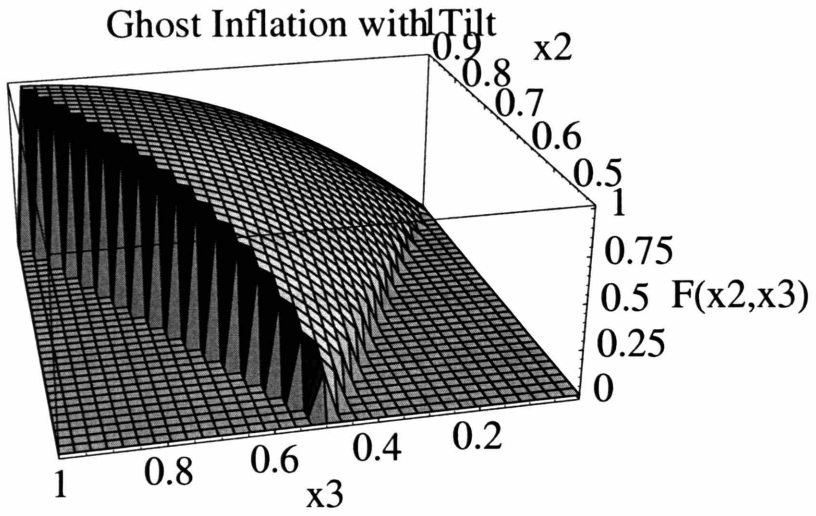


Figure 2-1: Plot of the function $F(1, x_2, x_3)x_2^2 x_3^2$ for the tilted ghost inflation 3-point function. The function has been normalized to have value 1 for the equilateral configuration $x_2 = x_3 = 1$, and it has been set to zero outside of the region $1 - x_2 \leq x_3 \leq x_2$

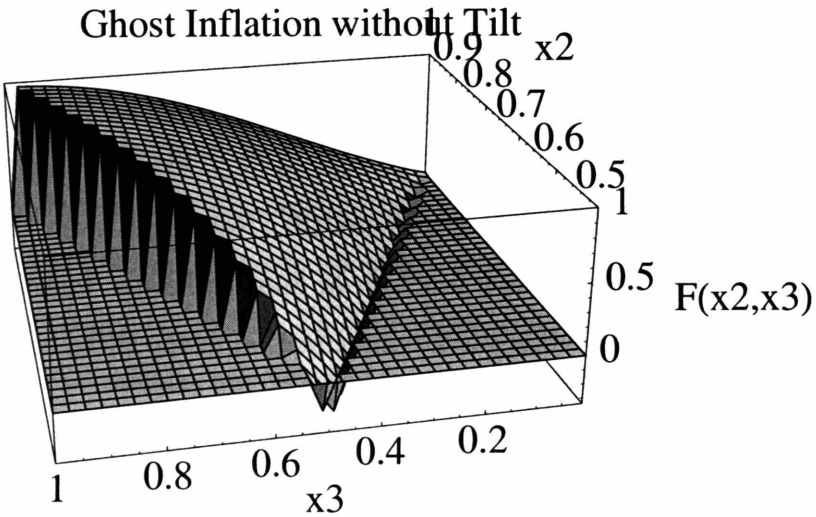


Figure 2-2: Plot of the similarly defined function $F(1, x_2, x_3)x_2^2 x_3^2$ for the standard ghost inflation 3-point function. The function has been normalized to have value 1 for the equilateral configuration $x_2 = x_3 = 1$, and it has been set to zero outside of the region $1 - x_2 \leq x_3 \leq x_2$ [5]

on the background wave, and, at linear order, will be proportional to $\partial_i \pi_3$. The variation of the 2-point function along the $\pi_3$ wave is averaged to zero in calculating

the 3-point function $< \pi_{k_1}\pi_{k_2}\pi_{k_3} >$, because the spatial average $< \pi_3\partial_i\pi_3 >$ vanishes. So, we are forced to go to the second order, and we therefore expect to receive a factor of $k_3^2$, which accounts for the difference with the standard slow roll inflation case. In the model of ghost inflation, the interaction is given by derivative terms, which favors the correlation of modes freezing roughly at the same time, while the correlation is suppressed for modes of very different wavelength. The same situation occurs in standard slow roll inflation when we study non-gaussianities generated by higher derivative terms [6].

The result is in fact very similar to the one found in [6]. In that case, in fact, the interaction term could be represented as:

$$L_{int} \sim \dot{\varphi}^2(-\dot{\varphi}^2 + e^{-2Ht}(\partial_i\varphi)^2) \tag{2.31}$$

where one of the time derivative fields is contracted with the classical solution. This interaction gives rise to a 3-point function, which can be recast as:

$$< \zeta_{k_1}\zeta_{k_2}\zeta_{k_3} > \sim \Big(\frac{(k_1^2(\vec{k_2}.\vec{k_3}))}{\prod_i(k_i^3)k_t^3}((k_2+k_3)k_t + k_t^2 + 2k_2k_3) + cyclic\Big) + \tag{2.32}$$
$$\frac{12}{\prod_i(k_i^3)k_t^3}(k_1^3 + k_2^3 + k_3^3)$$

We can easily see that the first part has the same $k$ dependence as our tilted ghost inflation. That part is in fact due to the interaction with spatial derivative acting, and it is equal to our interaction. The integrand in the formula for the 3-point function is also evaluated with the same wave functions, so, it gives necessarily the same result as in our case. The other term is due instead to the term with three time derivatives acting. This term is not present in our model because of the spontaneous breaking of Lorentz symmetry, which makes that term more irrelevant that the one with spatial derivatives, as it is explained in [2]. This similarity could have been expected, because, adding a tilt to the ghost potential, we are converging towards standard slow roll inflation. Besides, since we have a shift symmetry for the ghost field, the interaction term which will generate the non gaussianities will be a higher

derivative term, as in [6].

We can give a more quantitative estimate of the similarity in the shape between our three point function and the three point functions which appear in other models. Following [5], we can define the cosine between two three point functions $F_1(k_1, k_2, k_3)$, $F_2(k_1, k_2, k_3)$, as:

$$cos(F_1, F_2) = \frac{F_1 \cdot F_2}{(F_1 \cdot F_1)^{1/2}(F_2 \cdot F_2)^{1/2}} \tag{2.33}$$

where the scalar product is defined as:

$$F_1(k_1, k_2, k_3) \cdot F_2(k_1, k_2, k_3) = \int_{1/2}^{1} dx_2 \int_{1-x_2}^{x_2} dx_3 x_2^4 x_3^4 F_1(1, x_2, x_3) F_2(1, x_2, x_3) \tag{2.34}$$

where, as before, $x_i = \frac{k_i}{k_1}$. The result is that the cosine between ghost inflation with tilt and ghost inflation without tilt is approximately 0.96, while the cosine with the distribution from slow roll inflation with higher derivatives is practically one. This means that a distinction between ghost inflation with tilt and slow roll inflation with higher derivative terms , just from the analysis of the shape of the 3-point function, sounds very difficult. This is not the case for distinguishing from these two models and ghost inflation without tilt.

Finally, we would like to make contact with the work in [7], on the Dirac-Born-Infeld (DBI) inflation. The leading interaction term in DBI inflation is, in fact, of the same kind as the one in (2.31), with the only difference being the fact that the relative normalization between the term with time derivatives acting and the one with space derivatives acting is weighted by a factor $\gamma^2 = (1 - v_p^2)^{-1}$, where $v_p$ is the gravity-side proper velocity of the brane whose position is the Inflaton. This relative different normalization between the two terms is in reality only apparent, since it is cancelled by the fact that the dispersion relation is $w \sim \frac{k}{\gamma}$. This implies the the relative magnitude of the term with space derivatives acting, and the one of time derivatives acting are the same, making the shape of the 3-point function in DBI inflation exactly equal to the one in slow roll inflation with higher derivative couplings, as found in [6].

### 2.3.3 Observational Constraints

We are finally able to find the observational constraints that the negative tilt in the ghost inflation potential implies.

In order to match with COBE:

$$P_\zeta = \frac{1}{4\pi^2\beta^{3/2}\delta^3}(\frac{H}{M})^4 \cong (4.8\ 10^{-5})^2 \Rightarrow \frac{H}{M} \cong 0.018\beta^{3/8}\delta^{3/4} \tag{2.35}$$

From this, we can get a condition for the visibility of the tilt. Remembering that $\delta^2_{cr} = \frac{\alpha^{1/2}}{\beta}(\frac{H}{M})$, we get that, in order for $\delta$ to be visible:

$$\delta^2 \gg \delta^2_{cr} = 0.018\frac{\alpha^{1/2}\delta^{3/4}}{\beta^{5/8}} \Rightarrow \delta^2 \gg \delta^2_{visibility} = 0.0016\frac{\alpha^{4/5}}{\beta} \tag{2.36}$$

In the analysis of the data (see for example [8]), it is usually assumed that the non-gaussianities come from a field redefinition:

$$\zeta = \zeta_g - \frac{3}{5}f_{NL}(\zeta_g^2 - <\zeta_g^2>) \tag{2.37}$$

where $\zeta_g$ is gaussian. This pattern of non-gaussianity, which is local in real space, is characteristic of models in which the non-linearities develop outside the horizon. This happens for all models in which the fluctuations of an additional light field, different from the inflaton, contribute to the curvature perturbations we observe. In this case the non linearities come from the evolution of this field into density perturbations. Both these sources of non-linearity give non-gaussianity of the form (2.37) because they occur outside the horizon. In the data analysis, (2.37) is taken as an ansatz, and limits are therefore imposed on the scalar variable $f_{NL}$. The angular dependence of the 3-point function in momentum space implied by (2.37) is given by:

$$<\zeta_{k_1}\zeta_{k_2}\zeta_{k_3}> = (2\pi)^3\delta^3(\sum_i \vec{k}_i)(2\pi)^4(-\frac{3}{5}f_{NL}P_R^2)\frac{4\sum_i k_i^3}{\prod_i 2k_i^3} \tag{2.38}$$

In our case, the angular distribution is much more complicated than in the previous expression, so, the comparison is not straightforward. In fact, the cosine between the

two distributions is -0.1. We can nevertheless compare the two distributions (2.27) and (2.37) for an equilateral configuration, and define in this way an "effective" $f_{NL}$ for $k_1 = k_2 = k_3$. Using COBE normalization, we get:

$$f_{NL} = -\frac{0.29}{\delta^2} \tag{2.39}$$

The present limit on non-gaussianity parameter from the WMAP collaboration [8] gives:

$$-58 < f_{NL} < 138 \text{ at } 95\% \text{ C.L.} \tag{2.40}$$

and it implies:

$$\delta^2 > 0.005 \tag{2.41}$$

which is larger than $\delta^2_{visibility}$ (which nevertheless depends on the coupling constants $\alpha$,$\beta$).

Since for $\delta^2 \gg \delta^2_{visibility}$ we do see the effect of the tilt, we conclude that there is a minimum constraint on the tilt: $\delta^2 > 0.005$.

In reality, since the shape of our 3-point function is very different from the one which is represented by $f_{NL}$, it is possible that an analysis done specifically for this shape of non-gaussianities may lead to an enlargement of the experimental boundaries. As it is shown in [5], an enlargement of a factor 5-6 can be expected. This would lead to a boundary on $\delta^2$ of the order $\delta^2 \gtrsim 0.001$, which is still in the region of interest for the tilt.

Most important, we can see that future improved measurements of Non Gaussianity in CMB will immediately constraint or verify an important fraction of the parameter space of this model.

Finally, we remind that the tilt can be quite different from the scale invariant result of standard ghost inflation:

$$|n_s - 1| \lesssim \frac{1}{N_e} \tag{2.42}$$

## 2.4 Positive Tilt

In this section, we study the possibility that the tilt in the potential of the ghost is positive, $V' > 0$. This is quite an unusual condition, if we think to the case of the slow roll inflation. In this case, in fact, the value of $H$ is actually increasing with time. This possibility is allowed by the fact that, on the contrary with respect to what occurs in the slow roll inflation, the motion of the field is not due to an usual potential term, but is due to a spontaneous symmetry breaking of time diffeomorphism, which gives a VEV to the velocity of the field. So, if the tilt in the potential is small enough, we expect to be no big deviance from the ordinary motion of the ghost field, as we already saw in section one.

In reality, there is an important difference with respect to the case of negative tilt: a positive tilt introduces a wrong sign kinetic energy term for $\pi$. The dispersion relation, in fact, becomes:

$$\omega^2 = \alpha \frac{k^4}{M^2} - \beta \delta^2 k^2 \tag{2.43}$$

The $k^2$ term is instable. The situation is not so bad as it may appear, and the reason is the fact that we will consider a De Sitter universe. In fact, deep in the ultraviolet the term in $k^4$ is going to dominate, giving a stable vacuum well inside the horizon. As momenta are redshifted, the instable term will tend to dominate. However, there is another scale entering the game, which is the freeze out scale $\omega(k) \sim H$. When this occurs, the evolution of the system is freezed out, and so the presence of the instable term is forgotten.

So, there are two possible situations, which resemble the ones we met for the negative tilt. The first is that the term in $k^2$ begins to dominate after freezing out. In this situation we would not see the effect of the tilt in the wave function. The second case is when there is a phase between the ultraviolet and the freezing out in which the term in $k^2$ dominates. In this case, there will be an instable phase, which will make the wave function grow exponentially, until the freezing out time, when this growing will be stopped. We shall explore the phase space allowed for this scenario,

which occurs for

$$\delta^2 \gg \delta_{cr}^2 = \frac{\alpha^{1/2}}{\beta}\frac{H}{M} \tag{2.44}$$

and we restrict to it.

Before actually beginning the computation, it is worth to make an observation. All the computation we are going to do could be in principle be obtained from the case of positive tilt, just doing the transformation $\delta^2 \rightarrow -\delta^2$ in all the results we obtained in the former section. Unfortunately, we can not do this. In fact, in the former case, we imposed that the term in $k^2$ dominates at freezing out, and then solved the wave equation with the initial ultraviolet vacua defined by the term in $k^2$, and not by the one in $k^4$, as, because of adiabaticity, the field remains in the vacua well inside the horizon. On the other hand, in our present case, the term in $k^2$ does not define a stable vacua inside the horizon, so, the proper initial vacua is given by the term in $k^4$ which dominates well inside the horizon. This leads us to solve the full differential equation:

$$u'' + (-\beta\delta^2 k^2 + \alpha\frac{k^4 H^2 \eta^2}{M^2} - \frac{2}{\eta^2})u = 0 \tag{2.45}$$

Since we are not able to find an analytical solution, we address the problem with the semiclassical WKB approximation. The equation we have is a Schrodinger like eigenvalue equation, and the effective potential is:

$$\tilde{V} = \beta\delta^2 k^2 - \alpha\frac{k^4 H^2 \eta^2}{M^2} + \frac{2}{\eta^2} \tag{2.46}$$

Defining:

$$\eta_0^2 = \frac{\beta\delta^2 M^2}{\alpha H^2 k^2} \tag{2.47}$$

we have the two semiclassical regions:

for $\eta \ll \eta_0$, the potential can be approximated to:

$$\tilde{V} \cong -\alpha\frac{k^4 H^2 \eta^2}{M^2} \tag{2.48}$$

while, for $\eta \gg \eta_0$:

$$\tilde{V} \cong \beta\delta^2 k^2 + \frac{2}{\eta^2} \tag{2.49}$$

The semiclassical approximation tells us that the solution, in these regions, is given by:

for $\eta \ll \eta_0$:

$$u \cong \frac{A_1}{(p(\eta))^{1/2}} e^{-i\int_{\eta}^{\eta_{cr}} p(\eta')d\eta'} \tag{2.50}$$

while, for $\eta \gg \eta_0$:

$$u \cong \frac{A_2}{(p(\eta))^{1/2}} e^{\int_{\eta_{cr}}^{\eta} p(\eta')d\eta'} \tag{2.51}$$

where $p(\eta) = (|V(\eta)|)^{1/2}$.

The semiclassical approximation fails for $\eta \sim \eta_0$. In that case, one can match the two solution using a standard linear approximation for the potential, and gets $A_2 = A_1 e^{-i\pi/4}$ [9]. It is easy to see that the semiclassical approximation is valid when $\delta^2 \gg \delta_{cr}^2$.

Let us determine our initial wave function. In the far past, we know that the solution is the one of standard ghost inflation [2]:

$$u = (\frac{\pi}{8})^{1/2}(-\eta)^{1/2} H_{3/4}^{(1)}(\frac{Hk^2\alpha}{2M}\eta^2) \tag{2.52}$$

We can put this solution, for the remote past, in the semiclassical form, to get:

$$u = \frac{1}{(\frac{2H\alpha k^2}{M}(-\eta))^{1/2}} e^{i(-\frac{5}{8}\pi + \frac{\beta\delta^2 M}{2H})} e^{i\frac{Hk^2\alpha}{2M}\eta^2} \tag{2.53}$$

So, using our relationship between $A_1$ and $A_2$, we get, for $\eta \gg \eta_0$, the following wave function for the ghost field:

$$w = u/a = -\frac{1}{2^{1/2}\bar{k}^{1/2}} e^{i(-\frac{7}{8}\pi + \frac{\beta\delta^2 M}{2H})} e^{\frac{\beta\delta^2 M}{\alpha H}} (H\eta e^{\bar{k}\eta} + \frac{H}{i\bar{k}} e^{-\bar{k}\eta}) \tag{2.54}$$

Notice that this is exactly the same wave function we would get if we just rotated $\delta \rightarrow i\delta$ in the solutions we found in the negative tilt case. But the normalization

would be very different, in particular missing the exponential factor, which can be large. It is precisely this exponential factor that reflects the phase of instability in the evolution of the wave function.

From this observation, the results for the 2-point ant 3-point functions are immediately deduced from the case of negative tilt, paying attention to the factors coming from the different normalization constants in the wave function.

So, we get:

$$P_\zeta = \frac{1}{4\pi^2}\frac{e^{\frac{2\beta\delta^2 M}{\alpha H}}}{\beta^{3/2}\delta^3}(\frac{H}{M})^4 \tag{2.55}$$

Notice the exponential dependence on $\alpha, \beta, H/M$, and $\delta^2$.

The tilt gets modified, but the dominating term $\sim \frac{1}{\delta^2}$ is not modified:

$$\begin{aligned} n_s - 1 &= V'(\frac{2M^2}{HV} + \frac{2\pi\beta}{\alpha}\frac{\delta^2 M}{H^2 M_{Pl}^2}) + \\ &+\frac{V''}{H^2}(\frac{1}{2\delta^2} + \frac{2}{9} + \frac{4M^4}{V}(1 - 2P''M^8) - \frac{2\beta}{3\alpha}\frac{H}{M} + \frac{\pi}{3}\frac{\delta^2 M^3}{H^3 M_{Pl}^2}(2 - 4P''M^8)) \end{aligned} \tag{2.56}$$

For the three point function, we get:

$$\begin{aligned} &< \zeta_{k_1}\zeta_{k_2}\zeta_{k_3} >= (2\pi)^3\delta^3(\sum k_i)\frac{H^8}{4\beta^3\delta^8 M^8} \\ &\frac{1}{k_t^3\prod k_i^3}\Big(k_1^2(\vec{k_2}.\vec{k_3})\Big((k_2+k_3)k_t + k_t^2 + 2k_3k_2\Big) + cyclic\Big)e^{6\frac{\beta\delta^2 M}{\alpha H}} \end{aligned} \tag{2.57}$$

which has the same $k$'s dependence as in the former case of negative tilt. Estimating the $f_{NL}$ as in the former case, we get:

$$f_{NL} \sim -\frac{0.29}{\delta^2}e^{6\frac{\beta\delta^2 M}{\alpha H}} \tag{2.58}$$

Notice again the exponential dependence.

Combining the constraints from the 2-point and 3-point functions, it is easy to see that a relevant fraction of the parameter space is already ruled out. Anyway, because of the exponential dependence on the parameters $\delta^2, \frac{H}{M}$, and the coupling constants $\alpha$, and $\beta$, which allows for big differences in the observable predictions, there are many

configurations that are still allowed.

## 2.5 Conclusions

We have presented a detailed analysis of the consequences of adding a small tilt to the potential of ghost inflation.

In the case of negative tilt, we see that the model represent an hybrid between ghost inflation and slow roll inflation. When the tilt is big enough to leave some signature, we see that there are some important observable differences with the original case of ghost inflation. In particular, the tilt of the 2-point function of $\zeta$ is no more exactly scale invariant $n_s = 1$, which was a strong prediction of ghost inflation. The 3-point function is different in shape, and is closer to the one due to higher derivative terms in slow roll inflation. Its total magnitude tends to decrease as the tilt increases. It must be underlined that the size of these effects for a relevant fraction of the parameter space is well within experimental reach.

In the case of a positive tilt to the potential, thanks to the freezing out mechanism, we are able to make sense of a theory with a wrong sign kinetic term for the fluctuations around the condensate, which would lead to an apparent instability. Consequently, we are able to construct an interesting example of an inflationary model in which $H$ is actually increasing with time. Even though a part of the parameter space is already excluded, the model is not completely ruled out, and experiments such as WMAP and Plank will be able to further constraint the model.

# Bibliography


[1] A. H. Guth, "The Inflationary Universe: A Possible Solution To The Horizon And Flatness Problems," Phys. Rev. D **23** (1981) 347. A. D. Linde, "A New Inflationary Universe Scenario: A Possible Solution Of The Horizon, Flatness, Homogeneity, Isotropy And Primordial Monopole Problems," Phys. Lett. B **108** (1982) 389. J. M. Bardeen, P. J. Steinhardt and M. S. Turner, "Spontaneous Creation Of Almost Scale - Free Density Perturbations In An Inflationary Universe," Phys. Rev. D **28** (1983) 679.

[2] N. Arkani-Hamed, P. Creminelli, S. Mukohyama and M. Zaldarriaga, "Ghost inflation," JCAP **0404** (2004) 001 [arXiv:hep-th/0312100].

[3] N. Arkani-Hamed, H. C. Cheng, M. A. Luty and S. Mukohyama, "Ghost condensation and a consistent infrared modification of gravity," arXiv:hep-th/0312099.

[4] J. Maldacena, "Non-Gaussian features of primordial fluctuations in single field inflationary models," JHEP **0305** (2003) 013 [arXiv:astro-ph/0210603]. See also V.Acquaviva, N.Bartolo, S.Matarrese and A.Riotto,"Second-order cosmological perturbations from inflation", Nucl.Phyis. B 667, 119 (2003) [astro-ph/0207295]

[5] D. Babich, P. Creminelli and M. Zaldarriaga, "The shape of non-Gaussianities," arXiv:astro-ph/0405356.

[6] P. Creminelli, On non-gaussianities in single-field inflation, JCAP **0310** (2003) 003 [arXiv:astro-ph/0306122].

[7] M. Alishahiha, E. Silverstein and D. Tong, "DBI in the sky," arXiv:hep-th/0404084.

[8] E. Komatsu *et al.*, "First Year Wilkinson Microwave Anisotropy Probe (WMAP) Observations: Tests of Gaussianity," Astrophys. J. Suppl. **148** (2003) 119 [arXiv:astro-ph/0302223].

[9] See for example: Ladau, Lifshitz, Quantum Machanics, Vol.III, Butterworth Heinemann ed. 2000.

# Chapter 3

# How heavy can the Fermions in Split Susy be? A study on Gravitino and Extradimensional LSP.

In recently introduced Split Susy theories, in which the scale of Susy breaking is very high, the requirement that the relic abundance of the Lightest SuperPartner (LSP) provides the Dark Matter of the Universe leads to the prediction of fermionic superpartners around the weak scale. This is no longer obviously the case if the LSP is a hidden sector field, such as a Gravitino or an other hidden sector fermion, so, it is interesting to study this scenario. We consider the case in which the Next-Lightest SuperPartner (NLSP) freezes out with its thermal relic abundance, and then it decays to the LSP. We use the constraints from BBN and CMB, together with the requirement of attaining Gauge Coupling Unification and that the LSP abundance provides the Dark Matter of the Universe, to infer the allowed superpartner spectrum. As very good news for a possible detaction of Split Susy at LHC, we find that if the Gravitino is the LSP, than the only allowed NLSP has to be very purely photino like. In this case, a photino from 700 GeV to 5 TeV is allowed, which is difficult to test

at LHC. We also study the case where the LSP is given by a light fermion in the hidden sector which is naturally present in Susy breaking in Extra Dimensions. We find that, in this case, a generic NLSP is allowed to be in the range 1-20 TeV, while a Bino NLSP can be as light as tens of GeV.

## 3.1 Introduction

Two are the main reasons which lead to the introduction of Low Energy Supersymmetry for the physics beyond the Standard Model: a solution of the hierarchy problem, and gauge coupling unification.

The problem of the cosmological constant is usually neglected in the general treatment of beyond the Standard Model physics, justifying this with the assumption that its solution must come from a quantum theory of gravity. However, recently [1], in the light of the landscape picture developed by a new understanding of string theory, it has been noted that, if the cosmological constant problem is solved just by a choice of a particular vacua with the right amount of cosmological constant, the statistical weight of such a fine tuning may dominate the fine tuning necessary to keep the Higgs light. Therefore, it is in this sense reasonable to expect that the vacuum which solves the cosmological constant problem solves also the hierarchy problem.

As a consequence of this, the necessity of having Susy at low energy disappears, and Susy can be broken at much higher scales ($10^6 - 10^9$ GeV).

However, there is another important prediction of Low Energy Susy which we do not want to give up, and this is gauge coupling unification. Nevertheless, gauge coupling unification with the same precision as with the usual Minimal Supersymmetric Standard Model (MSSM) can be achieved also in the case in which Susy is broken at high scales. An example of this is the theories called Split Susy [1, 2] where there is an hierarchy between the scalar supersymmetric partners of Standard Model (SM) particles (squarks, sleptons, and so on) and the fermionic superpartners of SM particles (Gaugino, Higgsino), according to which, the scalars can be very heavy at

an intermediate scale of the order of $10^9$ GeV, while the fermions can be around the weak scale. The existence for this hierarchy can be justified by requiring that the chiral symmetry protects the mass of the fermions partners.

While the chiral symmetry justifies the existence of light fermions, it can not fix the mass of the fermionic partners precisely at the weak scale. As a consequence, this theory tends to make improbable the possibility of finding Susy at LHC, because in principle there could be no particles at precisely 1 TeV. In this chapter, for Split Susy, we do a study at one-loop level of the range of masses allowed by gauge coupling unification, finding that these can vary in a range that approximately goes up to 20 TeV. A possible way out from this depressing scenario comes from realizing that cosmological observations indicate the existence of Dark Matter (DM) in the universe. The standard paradigm is that the Dark Matter should be constituted by stable weakly interacting particles which are thermal relics from the initial times of the universe. The Lightest Supersymmetric Partner (LSP) in the case of conserved R-parity is stable, and, if it is weakly interacting, such as the Neutralino, it provides a perfect candidate for the DM. In particular, an actual calculation shows that in order for the LSP to provide all the DM of the universe, its mass should be very close to the TeV scale. This is the very good news for LHC we were looking for. Just to stress this result, it is the requirement the the DM is given by weakly interacting LSP that forces the fermions in Split Susy to be close to the weak scale, and accessible at LHC.

In three recent papers [2, 3, 4], the predictions for DM in Split Susy were investigated, and revealed some regions in which the Neutralino can be as light as $\sim 200$ GeV (Bino-Higgsino), and some others instead where it is around a 1 TeV (Pure Higgsino) or even 2 TeV (Pure Wino). As we had anticipated, all these scales are very close to one TeV, even though only the Bino-Higgsino region is very good for detection at LHC.

Since the Dark Matter Observation is really the constraint that tells us if this kind of theories will be observable or not at LHC, it is worth to explore all the possibilities for DM in Split Susy. In particular, a possible and well motivated case which had been not considered in the literature, is the case in which the LSP is a very weakly

interacting fermion in a hidden sector.

In this chapter, we will explore this possibility in the case in which the LSP is either the Gravitino, or a light weakly interacting fermion in the hidden sector which naturally appears in Extra Dimensional Susy breaking models of Split Susy [1, 5].

We will find that, if the Gravitino is the LSP, than all possible candidates for the NLSP are excluded by the combination of imposing gauge coupling unification and the constraint on hadronic decays coming from BBN. Just the requirement of having the Gravitino to provide all the Dark Matter of the univese and to still have gauge coupling unification would have allowed weakly interacting fermionic superpartneres as heavy as 5 TeV, with very bad consequences on the detactibility of Split Susy at LHC. This means that these constraints play a very big role. The only exception to this result occurs if the NLSP is very photino like, avoiding in this way the stringent constraints on hadronic decays coming from BBN. However, as we will see, already a small barionic decay branching ratio of $10^{-3}$ is enough to rule out also this possibility.

For the Extradimensional LSP, we will instead find a wide range of possibilities, with NLSP allowed to span from 30 GeV to 20 TeV.

The chapter is organized as follows. In section 4.2, we study the constraints on the spectrum coming from the requirement of obtaining gauge coupling unification. In section 4.3, we briefly review the relic abundance of Dark Matter in the case the LSP is an hidden sector particle. In section 4.4, we discuss the cosmological constraints coming from BBN and CMB. In section 4.5, we show the results for Gravitino LSP. In section 4.6, we do the same for a dark sector LSP arising in extra dimensional implementation of Split Susy. In section 4.7, we draw our conclusions.

## 3.2 Gauge Coupling Unification

Gauge coupling unification is a necessary requirement in Split Susy theories. Here we investigate at one loop level how heavy can be the fermionic supersymmetric partner for which gauge coupling unification is allowed. We will consider the Bino, Wino, and Higgsino as degenerate at a scale $M_2$, while we will put the Gluinos at a different

scale $M_3$.

Before actually beginning the computation, it is interesting to make an observation about the lower bound on the mass of the fermionic superpartners. Since the Bino is gauge singlet, it has no effect on one-loop gauge coupling unification. In Split Susy, with the scalar superpartners very heavy, the Bino is very weakly interacting, its only relevant vertex being the one with the light Higgs and the Higgsino. This means that, while for the other supersymmetric partners LEP gives a lower bound of $\sim$ 50-100 GeV [11], for the Bino in Split Susy there is basically no lower limit.

Going back to the computation of gauge coupling unification, we perform the study at 1-loop level. The renormalization group equations for the gauge couplings are given by:

$$\Lambda \frac{dg_i}{d\Lambda} = \frac{1}{(4\pi)^2} b_i(\Lambda) g_i^3 \tag{3.1}$$

where $b_i(\Lambda)$ depends of the scale, keeping truck of the different particle content of the theory according to the different scales, and $i = 1, 2, 3$ represent respectively $\sqrt{5/3}g', g, g_s$. We introduce two different scales for the Neutralinos, $M_2$, and for the Gluinos $M_3$, and for us $M_3 > M_2$.

In the effective theory below $M_2$, we have the SM, which implies:

$$b^{SM} = (\frac{41}{10}, -\frac{19}{7}, -7) \tag{3.2}$$

Between $M_2$ and $M_3$:

$$b^{split1} = (\frac{9}{2}, -\frac{7}{6}, -7) \tag{3.3}$$

Between $M_3$ and $\tilde{m}$, which is the scale of the scalars:

$$b^{split2} = (\frac{9}{2}, -\frac{7}{6}, -5) \tag{3.4}$$

and finally, above $\tilde{m}$ we have the SSM:

$$b^{ssm} = (\frac{33}{5}, 1, -3) \tag{3.5}$$

The way we proceed is as follows: we compute the unification scale $M_{GUT}$ and $\alpha_{GUT}$ as deduced by the unification of the SU(2) and U(1) couplings. Starting from this, we deduce the value of $\alpha_s$ at the weak scale $M_Z$, and we impose it to be within the $2\sigma$ experimental result $\alpha_s(M_Z) = 0.119 \pm 0.003$. We use the experimental data: $\sin^2(\theta_W(M_Z)) = 0.23150 \pm 0.00016$ and $\alpha^{-1}(M_Z) = 128.936 \pm 0.0049$[12].

A further constraint comes from Proton decay $p \to \pi^0 e^+$, which has lifetime:

$$\tau(p \to \pi_0 e^+) = \frac{8 f_\pi^2 M_{GUT}^4}{\pi m_p \alpha_{GUT}^2 ((1+D+F)A\alpha_N)^2} = \tag{3.6}$$
$$= \left(\frac{M_{GUT}}{10^{16}\text{GeV}}\right)^4 \left(\frac{1/35}{\alpha_{GUT}}\right)^2 \left(\frac{0.015\text{GeV}^3}{\alpha_N}\right) 1.3 \times 10^{35}\text{yr}$$

where we have taken the chiral Lagrangian factor $(1 + D + F)$ and the operator renormalization $A$ to be $(1 + D + F)A \simeq 20$. For the Hadronic matrix element $\alpha_N$, we take the lattice result [13] $\alpha_N = 0.015\text{GeV}^3$. From the Super-Kamiokande limit [14], $\tau(p \to \pi^0 e^+) > 5.3 \times 10^{33}$yr, we get:

$$M_{GUT} > \left(\frac{\alpha_N}{0.015\text{GeV}^3}\right)^{1/2} \left(\frac{\alpha_{GUT}}{1/35}\right)^{1/2} 4 \times 10^{15}\text{GeV} \tag{3.7}$$

An important point regards the mass thresholds of the theory. In fact, the spectrum of the theory will depend strongly on the initial condition for the masses at the supersymmetric scale $\tilde{m}$. As we will see, in particular, the Gluino mass $M_3$ has a very important role for determining the allowed mass range for the Next-Lightest Supersymmetric Particle (NLSP), which is what we are trying to determine. In the light of this, we will consider $M_2$ as a free parameter, with the only constraint of being smaller than $\tilde{m}$. $M_3$ will be then a function of $M_2$ and $\tilde{m}$, and its actual value will depend on the kind of initial conditions we require. In order to cover the larger fraction of parameter space as possible, we will consider two distinct and well motivated initial conditions. First, we will require gaugino mass unification at $\tilde{m}$. This initial condition is the best motivated in the approach of Split Susy, where unification plays a fundamental role. Secondarily, we will require anomaly mediated gauigino mass initial conditions at the scale $\tilde{m}$. This second kind of initial conditions will give results

quite different from those of Gaugino mass unification, and, even if in this case the Gravitino can not be the NLSP, the field $\psi_X$, which will be a canditate LSP from extradimensions that we will introduce in the next sections, could be still the LSP.

### 3.2.1 Gaugino Mass Unification

Here we study the case in which we apply gaugino mass unification at the scale $\tilde{m}$.

In [2], a 2-loop study of the renormalization group equations for the Gaugino mass starting from this initial condition was done, and it was found that, according to $\tilde{m}$ and $M_2$, the ratio between $M_3$ and $M_2$ can vary in a range $\sim 3-8$. We shall use their result for $M_3$, as the value of $M_3$ will have influence on the results, tending to increase the upper limit on the fermions' mass.

At one loop level, we can obtain analytical results. After integration of eq.(3.1), we get the following expressions:

$$M_{GUT} = \left(e^{8\pi^2 \frac{1}{g_1^2(M_Z)} - \frac{1}{g_2^2(M_Z)}} M_Z^{\left(b_1^{sm} - b_2^{sm}\right)} M_2^{\left((b_1^{split1} - b_1^{sm}) - (b_2^{split1} - b_2^{sm})\right)} \right. \\ \left. M_3^{\left((b_1^{split2} - b_1^{split1}) - (b_2^{split2} - b_2^{split1})\right)} \tilde{m}^{\left((b_1^{ssm} - b_1^{split2}) - (b_2^{ssm} - b_2^{split2})\right)}\right)^{\left(\frac{1}{b_1^{ssm} - b_2^{ssm}}\right)} \tag{3.8}$$

$$\frac{1}{g_{GUT}^2} = \frac{1}{g_2^2(M_Z)} - \frac{1}{8\pi^2} \ln\left(M_Z^{-b_2^{sm}} M_2^{(-b_2^{split1} + b_2^{sm})} \right. \\ \left. M_3^{(b_2^{split2} + b_2^{split1})} \tilde{m}^{(-b_2^{ssm} + b_2^{split2})} M_{GUT}^{b_2^{ssm}}\right) \tag{3.9}$$

$$\frac{1}{g_s^2(M_Z)} = \frac{1}{g^2(M_{GUT})} + \frac{1}{8\pi^2} \ln\left(M_Z^{-b_3^{sm}} M_2^{(-b_3^{split1} + b_3^{sm})} \right. \\ \left. M_3^{(-b_3^{split2} + b_3^{split1})} \tilde{m}^{(-b_3^{ssm} + b_3^{split2})} M_{GUT}^{b_3^{ssm}}\right) \tag{3.10}$$

It turns out that two loops effect are important to determine the predicted value of $\alpha_s(M_Z)$. Since our main purpose is to have a rough idea of the maximum scale for the fermionic masses allowed by Gauge Coupling Unification, we proceed in the

following way. In [2], 2-loop gauge coupling unification was studied for $M_2 = 300$ GeV and 1 TeV. Since the main effect of the 2-loop contribution is to raise the predicted value of $\alpha_s(M_Z)$, we translate our predicted value of $\alpha_s(M_Z)$ to match the result in [2] for the correspondent values of $M_2$. Having set in this way the predicted scale for $\alpha_s(M_Z)$, we check what is the upper limit on fermion masses in order to reach gauge coupling unification. The amount of translation we have to do is: 0.008.

In fig.3-1, we plot the prediction for $\alpha_s(M_z)$ for $M_2 = 300$ GeV, 1 TeV, and 5 TeV. We see that for 5 TeV, unification becomes impossible. And so, 5 TeV is the upper limit on fermionic superpartner allowed from gauge coupling unification. Note that the role of the small difference between $M_3$ and $M_2$ is to raise this limit.

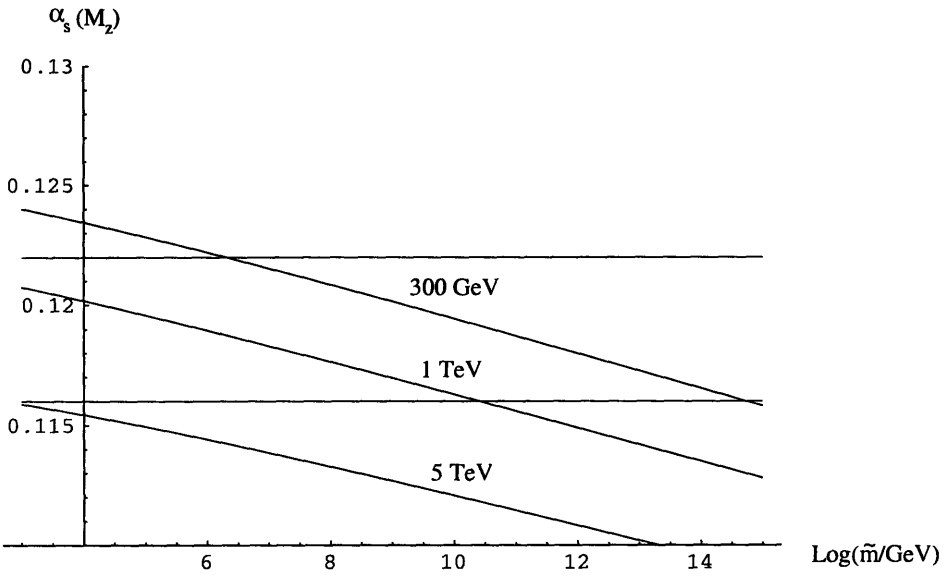


Figure 3-1: In the case of gaugino mass unification at scale $\tilde{m}$, we plot the unification prediction for $\alpha_s(M_Z)$. The results for $M_2 = 300$ GeV, 1 TeV and 5 TeV are shown. The horizontal lines represent the experimental bounds

In fig.3-2, and fig.3-3,we plot the predictions for $\alpha_{GUT}(M_{GUT})$ and for $M_{GUT}$, for the same range of masses. We see that unification is reached in the perturbative regime, with unification scale large enough to avoid proton decay limits. Note, however, that for $M_2 = 5$ TeV, the limit is close to a possible detection.

Finally, note that with this Gaugino mass initial conditions, the Wino can not be the NLSP if the Gravitino is the LSP, as shown in [2].

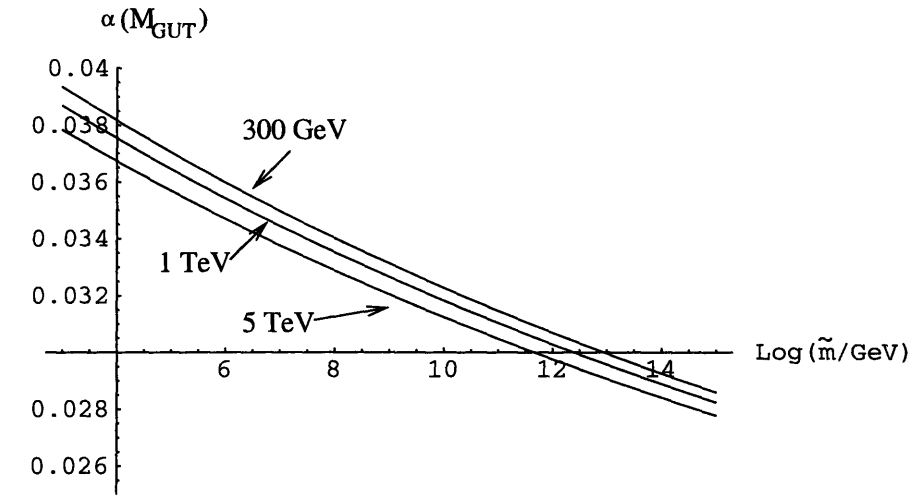


Figure 3-2: In the case of Gaugino mass unification at scale $\tilde{m}$, we plot the prediction for $\alpha_s(M_{GUT})$. The results for $M_2 = 300$ GeV, 1 TeV and 5 TeV are shown.

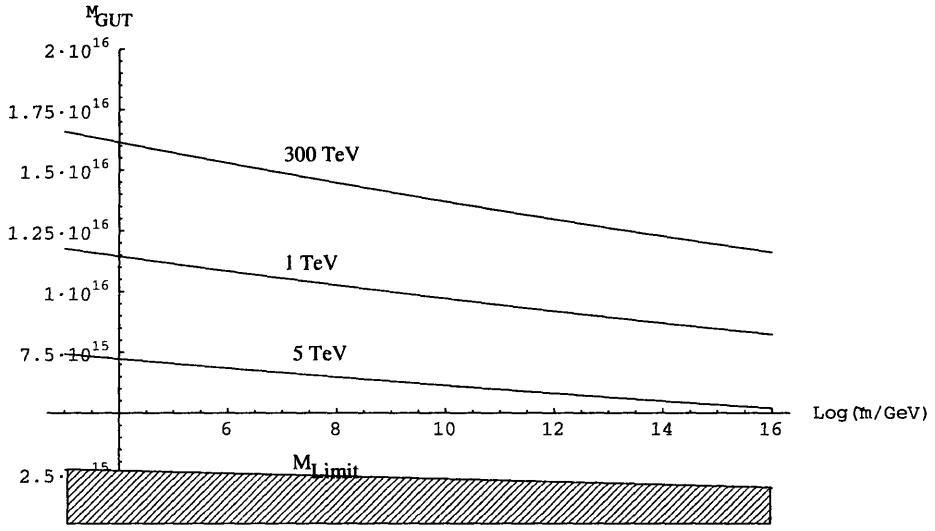


Figure 3-3: In the case of Gaugino mass unification at scale $\tilde{m}$, we plot the prediction for $M_{GUT}$. The results for $M_2 = 300$ GeV, 1 TeV and 5 TeV are shown, together with the lower bound on $M_{GUT}$ from Proton decay.

As we will see later, a particular interesting case for the LSP in the hidden sector is given by a Bino NLSP. For this case, we need to do a more accurate computation, splitting the mass of the Gauginos, from that of the Higgsinos, and taking the Wino mass roughly two times larger than the Bino mass, as inferred from [2] for gaugino mass unification initial conditions. In fig.3-4, we show what is the allowed region for

the mass of the Bino and the ratio of the Hissino mass and Bino mass, such that gauge coupling unification is attained with a mass for the scalars, $\tilde{m}$, in the range $10^5$ GeV-$10^{18}$ GeV. Raising the Higgsino mass with respect to the Bino mass has the effect of lowering the maximum mass for the fermionic superpartners. This is due to the fact that, raising the Higgsino mass, the unification value for the U(1) and SU(2) couplings is reduced, so that the prediction for $\alpha_s(M_Z)$ is lowered.

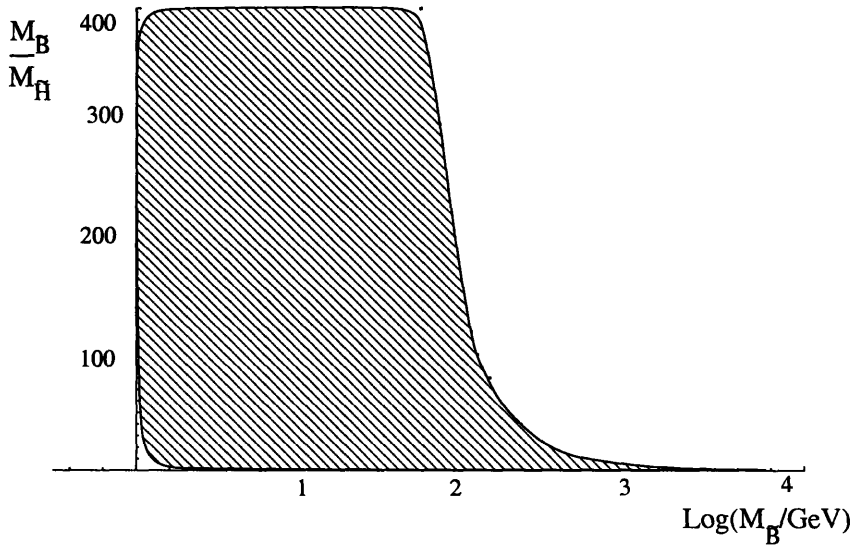


Figure 3-4: Shaded is the allowed region for the Bino mass and the ratio of the Higgsino mass and the Bino mass, in order to obtain Gauge Coupling Unification with a value of the scalar mass $\tilde{m}$ in the range $10^5$ GeV-$10^{18}$ GeV. We take $M_2 \simeq 2M_1$ as inferred from gaugino mass unification at the GUT scale [2]

### 3.2.2 Gaugino Mass Condition from Anomaly Mediation

Of the possible initial conditions for the Gaugino mass which can have some influence on the upper bound on fermions mass, there is one which is particularly natural, and which is coming from Anomaly Mediated Susy breaking, and according to which the initial conditions for the gaugino masses are:

$$M_i = \frac{\beta_{g_i}}{g_i} m_{3/2} \sim \frac{c_i g_i^2}{16\pi^2} m_{3/2} \tag{3.11}$$

where $\beta_i$ is the beta-function for the gauge coupling, and $c_i$ is an order one number. These initial conditions are not relevant for the Gravitino LSP, as in this case the Neutralinos are lighter than the Gravitinos; but they can be relevant in the case the LSP is given by a fermion in the hidden sector, as we will study later. Further, the study of this case is interesting on its own, as it gives an upper bound on the fermionic superpartners which is higher with respect to the one coming from gaugino mass unification initial conditions.

The study parallels very much what done in the former section, with the only difference being the fact that in this case, as computed in [2], the mass hierarchy between the Gluinos and the Gauginos is higher ( a factor $\sim 10 - 20$ instead of $\sim 3 - 8$). This has the effect of raising the allowed mass for the fermions. We do the same amount of translation as before for the predicted $\alpha_s(M_Z)$. The result is shown in fig.3-5, and gives, as upper limit, $M_2 = 18$ TeV.

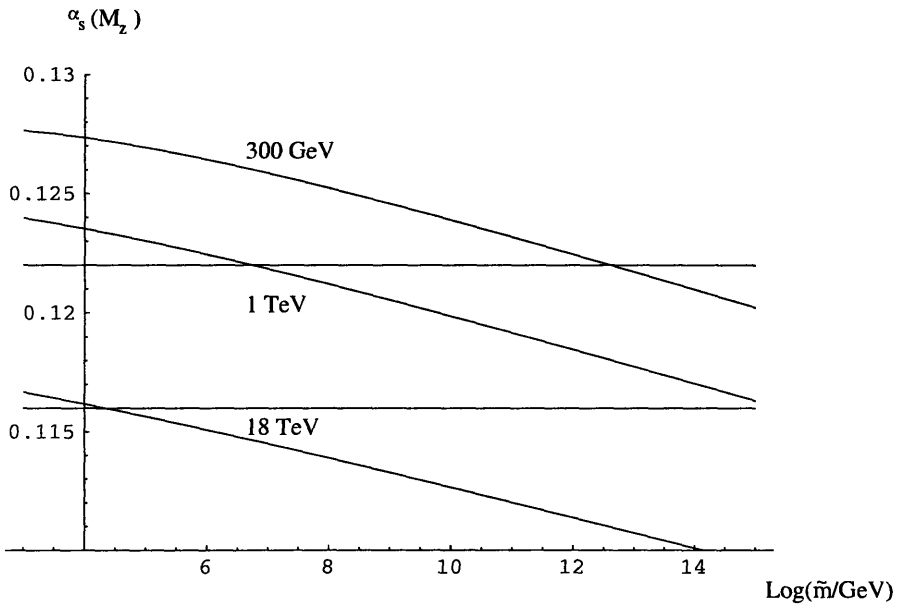


Figure 3-5: In the case of Gaugino mass condition from anomaly mediation at scale $\tilde{m}$, we plot the unification prediction for $\alpha_s(M_Z)$. The results for $M_2 = 300$ GeV, 1 TeV and 18 TeV are shown. The horizontal lines represent the experimental bounds

In fig.3-7, and fig.3-6, we plot the predictions for $\alpha_{GUT}$ and $M_{GUT}$ for the same range of masses, and we see that unification is reached in the perturbative regime,

and that the unification scale is large enough to avoid proton decay limits, but it is getting very close to the experimental bound for large values of the mass $\tilde{m}$.

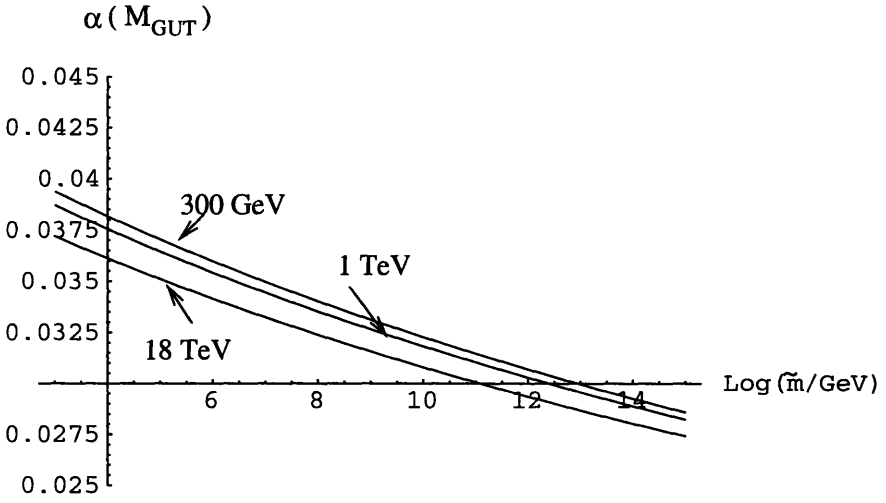


Figure 3-6: In the case of Gaugino mass from Anomaly Mediation, we plot the prediction for $\alpha_{GUT}$. The results for $M_2 = 300$ GeV, 1 TeV and 18 TeV are shown.

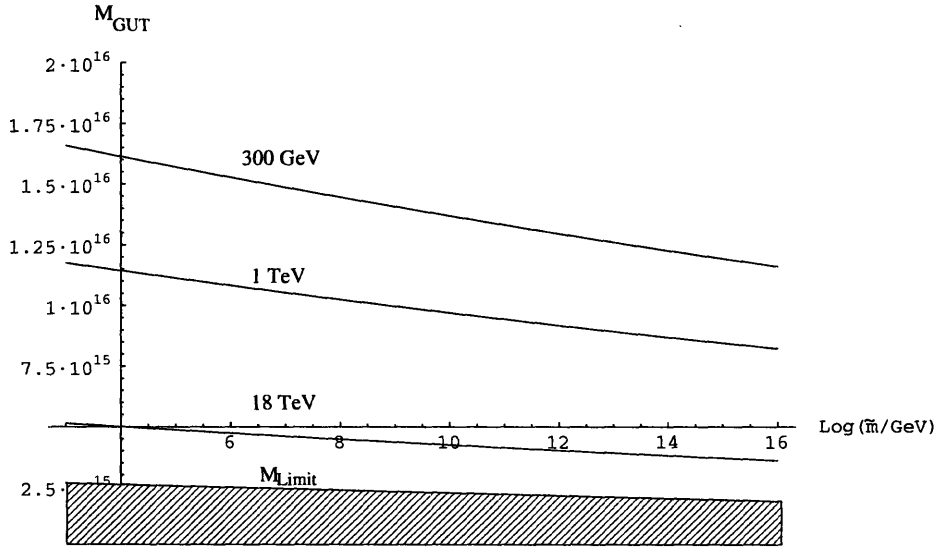


Figure 3-7: In the case of Gaugino mass from Anomaly Mediation, we plot the prediction for $M_{GUT}$. The results for $M_2 = 300$ GeV, 1 TeV and 18 TeV are show, together with the lower bound on $M_{GUT}$ from Proton decay.

As we can see, in the case of Gaugino Mass from Anomaly Mediation, the upper limit on fermion mass is raised to 18 TeV. This last one can be interpreted as a sort

of maximum allowed mass for fermionic superpartners.

It is important to note that, as pointed out in [2], in this case the Bino can not be the NLSP.

## 3.3 Hidden sector LSP and Dark Matter Abundance

An hidden sector LSP which is very weakly interacting can well be the DM from the astrophysical and cosmological point of view. Its present abundance can be given by two different sources: it can be a thermal relic, if in the past the temperature was so high that hidden sector particles were in equilibrium with the thermal bath, or it can be present in the universe just as the result of the decay of the other supersymmetric particles.

We concentrate in the case in which the thermal relic abundance is negligible, which is generically the case for not too large reheating temperatures, and the abundance is given by the decaying of the other supersymmetric particles into the LSP. A discussion on the consequences of a thermal relic abundance of Gravitinos is discussed in [6].

In our case, the relic abundance of the heavier particles is what determines the final abundance of the LSP, and so it is the fundamental quantity to analyze. In the very early universe, the typical time scale of the cosmic evolution $H^{-1}$ is much larger than the time scale of interaction of a weakly interacting particle, and so a weakly interacting particle is in thermal equilibrium. Therefore, its abundance is given by the one of a thermal distribution. As the temperature of the universe drops down, the interaction rate is not able anymore to keep the particle in thermal equilibrium, and so the particle decouples from the thermal bath, and its density begins to dilute, ignoring the rest of the thermal bath. We say in this case that the particle species freezes out.

In the case of weakly interacting particles around the TeV scale, the freeze out

temperature is around decades of GeV, and so they are non relativistic at the moment of freezing out. In this case, the relic abundance of these particles is given by the following formula [7, 8, 9]:

$$\Omega_{NLSP}h^2 \approx 0.1 \left(\frac{10^{-9}\text{GeV}^{-2}}{<\sigma v>}\right)\left(\frac{15}{\sqrt{g_*}}\right)\left(\frac{10^{19}\text{GeV}}{M_{pl}}\right)\left(\frac{x_f}{30}\right)\left(\frac{h^2}{0.5}\right) \tag{3.12}$$

where $< \sigma v >$ is the thermally averaged cross section at the time of freeze out, $x_f = \frac{m_{NLSP}}{Tf}$ where $T_f$ is the freeze out temperature, $g_*$ is the effective number of degrees of freedom at freeze out, and $h$ is the Hubble constant measured in units of 100Km/(sec Mpc). It is immediate to see that, for weakly interacting particle at 1 TeV, the resulting $\Omega$ is of order unity, and this has led to the claim that the Dark Matter bounds some supersymmetric partners to be at TeV scale. In this chapter, we shall check this claim for an LSP in the hidden sector.

Once the weakly interacting particles are freezed out, they will rapidly decay to the NLSP, which, being lighter, will be in general still in thermal equilibrium. So, it will be the NLSP the only one to have a relevant relic abundance, determined by the freeze out mechanism, and so it will be the NLSP that, through its decay, will generate the present abundance of the LSP.

In Split Susy, the NLSP can either be the lightest Neutralino, or the lightest Chargino. The Neutralino is a mixed state of the interaction eigenstates Bino, Wino, and neutral Higgsinos, and is the lightest eigenstate of the following matrix[3]:

$$\begin{pmatrix} M_1 & 0 & -\frac{k_2'v}{\sqrt{8}} & \frac{k_1'v}{\sqrt{8}} \\ 0 & M_2 & \frac{k_2v}{\sqrt{8}} & -\frac{k_1v}{\sqrt{8}} \\ -\frac{k_2'v}{\sqrt{8}} & \frac{k_2v}{\sqrt{8}} & 0 & -\mu \\ \frac{k_1'v}{\sqrt{8}} & -\frac{k_1v}{\sqrt{8}} & \mu & 0 \end{pmatrix} \tag{3.13}$$

which differs from the usual Neutralino matrix in low energy Susy for the Yukawa coupling, which have their Susy value at the Susy breaking scale $\tilde{m}$, but then run differently from that scale to the weak scale.

The Chargino is a mixed eigenstate of charged Higgsino and charged Wino, and

is the lightest eigenstate of the following matrix:

$$\begin{pmatrix} M_2 & \frac{k_1 v}{2} \\ \frac{k_2 v}{2} & \mu \end{pmatrix} \tag{3.14}$$

The actual and precise computation of the thermally averaged cross section of the NLSP at freeze out, which determines the $\Omega_{NLSP}$, is very complicated, because there are many channels to take care of, which depend on the abundance of the particles involved, and on the mixing of states, creating a very complicated system of differential equations. A software called DarkSusy has been developed to reliably compute the relic abundance [10], and, in a couple of recent papers [2, 3], it has been used to compute the relic abundance of the Neutralino NLSP in Split Susy. In this kind of theories, in particular, this computation is a bit simplified, since the absence of the scalar superpartners makes many channels inefficient. Nevertheless, in most cases, the computation is still too complicated to be done analytically.

In the study in this chapter, we consider both the possibility that the NLSP is a Neutralino and a Chargino. In the case of Neutralino NLSP, we modify the Dark Susy code [10] and adapt it to the case of Split Susy. We consider the cases of pure Bino, pure Wino, pure Higgsino, and Photino NLSP. In the case of Chargino NLSP, we consider the case of charged Higgsino and Charged Wino as NLSP, and we estimate their abundance with the most important diagram. We will see, in fact, that in this case a more precise determination of the relic abundance is not necessary.

Once the NLSP has freezed out, it will dilute for a long time, until, at the typical time scale of 1 sec, it will decay gravitationally to the LSP, which will be stable, and will constitute today's Dark Matter. It's present abundance is connected to the NLSP "would be" present abundance by the simple relation:

$$\Omega_{LSP} = \frac{m_{LSP}}{m_{NLSP}} \Omega_{NLSP} \tag{3.15}$$

Already from this formula, we may get some important information on the masses of the particles, just comparing with the case in which the Neutralino or the Chargino

is the LSP. In fact, since $\frac{m_{LSP}}{m_{NLSP}} < 1$, $\Omega_{NLSP}$ has to be greater than what it would have to have if the NLSP was the LSP, in order for the LSP to provide all the DM. The abundance of the NLSP is inversely proportional to $< \sigma v >$, and this means that we need to have a typical cross section smaller than the one we would obtain in the case of a weakly interacting particle at TeV scale. This result can be achieved in two ways: either raising the mass of the particles, since $\sigma \sim \frac{1}{m^2}$, or by choosing some particle which for some reason is very low interacting.

The direction in which the particle become very massive is not very attractive from the LHC detection point of view, but still, in Split Susy, is in principle an acceptable scenario.

The other direction instead immediately lets a new possible candidate to emerge, which could be very attractive from the LHC detection point of view. In fact, in Split Susy, a pure Bino NLSP is almost not interacting, the only annihilation channel being the one into Higgs bosons in which an Higgsino is exchanged. In this case the relic abundance has $\Omega_{NLSP} \gg 1$, and this was the reason why a pure Bino could not be the DM in Split Susy [2, 3]. In the case of a gravitationally interacting LSP, as we are considering, this over abundance would go exactly into the right direction, and it could open a quite interesting region for detection at LHC.

## 3.4 Cosmological Constraints

Since we wish the LSP to be the Dark Matter of the universe, so, we impose its abundance to cope with WMAP data [15, 16].

In general, for low reheating temperature, only the weakly interacting particles are thermally produced, and only the NLSP will remain as a thermal relic in a relevant amount. Later on, it will decay to the LSP. This decay will give the strongest cosmological constraints.

In fact, concentrating on the Gravitino, which interacts only gravitationally, we

can naively estimate its lifetime as:

$$\Gamma \sim \frac{m_{NLSP}^3}{M_{pl}^2} \tag{3.16}$$

where the $m_{NLSP}$ term comes from dimensional analysis. In reality, we can easily do better. In fact, as we have Goldstone bosons associated to spontaneous symmetry breaking, the breaking of supersymmetry leads to the presence of a Goldstino, a massless spinor. Then, as usually occurs in gauge theories, the Goldstino is eaten by the massless Gravitino, which becomes a massive Gravitino with the right number of polarization. Therefore, the coupling of the longitudinal components of the Gravitino to the LSP will be determined by the usual pattern of spontaneous symmetry braking, and in particular will be controlled by the scale of symmetry breaking. This means that the coupling constant may be amplified. In fact, if we concentrate on the Gauginos for simplicity, we can reconstruct their coupling to the Goldstino simply by looking at the symmetry braking term in the lagrangian in unitary gauge, then reintroducing the Goldstino performing a Susy transformation, and promoting the transformation parameter to a new field, the Goldstino. The actual coupling is then obtained after canonical normalization of the Goldstino kinetic term, which is obtained performing a Susy transformation of the mass term of the Gravitino, and remembering that in the case of Sugra, the Susy transformation of the Gravitino contains a piece proportional to the vacuum energy. In formulas, the Gaugino Susy transformation is given by:

$$\delta\lambda = \sigma^{\mu\nu} F_{\mu\nu} \xi \tag{3.17}$$

where $\xi$ is the Goldstino. This implies that the mass term of the Gaugino sources the following coupling between the Gaugino and the Goldstino:

$$\delta(m\lambda\lambda) \supset m_\lambda \lambda \sigma^{\mu\nu} F_{\mu\nu} \xi \tag{3.18}$$

The Goldstino kinetic term cames from the Gravitino tranformation, which is:

$$\delta\psi_\mu = m_{Pl}\partial_\mu\xi + if\sigma_\mu\bar{\xi} \tag{3.19}$$

so, the Gravitino mass term produces the Goldstino kinetic term:

$$\delta(m_{gr}\psi_\mu\sigma^{\mu\nu}\psi_\nu) \supset m_{gr}fm_{pl}\bar{\xi}\sigma^\mu\partial_\mu\xi = f^2\bar{\xi}\sigma^\mu\partial_\mu\xi \tag{3.20}$$

where in the last expression we used that $m_{gr} = f/m_{Pl}$. So, after canonical normalization, we get the following interaction term:

$$L_I = \frac{m_\lambda}{f^2}\lambda\sigma^{\mu\nu}F_{\mu\nu}\xi_c \tag{3.21}$$

where $\xi_c = \xi f$ is the canonically normalized Goldstino. After all this, we get an enhanced decay width like this:

$$\Gamma \sim \frac{1}{M_{pl}^2}\left(\frac{m_{NLSP}}{m_{gr}}\right)^2 m_{NLSP}^3 \tag{3.22}$$

Note that this is independent on the particle species, as it must be by the equivalence principle [17].

Plugging in some number, we immediately see that, for particles around the TeV scale, without introducing a big hierarchy with the Gravitino, the time of decay is approximately $\sim$ 1 sec, and this is right the time of Big Bang Nucleosynthesis (BBN). This is the origin of the main cosmological bound. In fact, the typical decay of the LSP will be into the Gravitino and into its SM partner. The SM particle will be very energetic, especially with respect to a thermal bath which is of the order of 1 MeV, and so it will create showers of particles, which will destroy some of the existent nuclei, and enhance the formation of others, with the final result of alterating the final abundance of the light elements [17].

There is also another quantity which comes into play, and it is what we can call the "destructive power". In fact, the alteration of the light nuclei abundance will

be proportional to the product of the abundance of the decaying particle and to the energy release per decay. This information is synthesized in an upper limit on the variable $\xi$ defined as:

$$\xi = B\epsilon Y \tag{3.23}$$

where $B$ is the branching ratio for hadronic or electromagnetic decays (it turns out that hadronic decays impose constrains a couple of order of magnitude more stringent that electromagnetic decays), $\epsilon$ is the energy release per decay, and finally $Y = \frac{n_\chi}{n_s}$, where $n_s$ is the number of photons per comoving volume, and $n_\chi$ the number of decaying particles per comoving volume. Again, it is easy to see what will be the lower limit on the upper limit on $\xi$. For the moment, we will neglect the dependence on the branching ratio $B$, because, clearly, one of the two branching ratios must be of order one. Then, we understand that the most dangerous particles for BBN will be those particles that decay when BBN has already produced most of the nulcei we have to see today. A particle which decays earlier than this time, will in general have its decay products diluted and thermalized with an efficiency that depends on the kind of decay product of the particle: either baryonic or electromagnetic, and it turns out that the dilution for electromagnetic decays is much more efficient. So, it is clear that the upper limit on the "desctructive power" $\xi$ will be lower for particles which decay after BBN. For these late decaying particles, we can estimate what the upper limit on $\xi$ should be with the following argument. $\xi$ will become dangerous if the energy release is bigger than 1 MeV, in order for the decay product to be able to destroy nuclei, and also if $Y$ is greater than $\frac{n_B}{n_s}$ which represent the number of baryons per comoving volume opportunely normalized. Plugging in the numbers, with, again, $B \sim 1$, we get

$$\xi_{dangerous} \gtrsim 10^{-14}\text{GeV} \tag{3.24}$$

This values of $\xi_{dangerous}$ is more or less where the limit seems to apply in numerical simulations for late decaying particles, and it is in fact independent on the particular kind of decay, as in this case there are not dilution issues [18, 19]. For early decaying particles the limits do depend on the kind of decay, and they get more and more

relaxed as the decay time becomes shorter and shorter, until there is practically no limit on particles which decay earlier than $\sim 10^{-2}$ sec. Notice however that, from the estimates above on the decay time, the particles which we will be interested in will tend to decay right in the region where these limits apply. The limit in eq.(3.24) translates into another useful parameter:

$$\Omega_{dangerous} \gtrsim 10^{-7} \tag{3.25}$$

for the contribution of the NLSP around the time of nucleosynthesis. An easy computation shows that, imposing $\Omega_{DM} \sim 1$ today, we get that the contribution of NLSP goes as:

$$\Omega_{NLSP} \sim 10^{-7} \frac{m_{NLSP}}{m_{gr}} \left(\frac{\text{MeV}}{T}\right) \tag{3.26}$$

This estimates are obviously very rough, but they are useful to give an idea of the physics which is going by, and they are, at the end of the day, quite accurate. They nevertheless tell us that we are really in the region in which these limits are effective, with two possible consequences: on one hand, a big part of the parameter region might be excluded, but also, on the other hand, this tells us that a possible indirect detection through deviations from the standard picture nucleosynthesis might reveal new physics.

In two recent papers [18, 19], numerical simulation were implemented to determine the constraints on $\xi$, both for the hadronic and the electromagnetic decays, and we shall use their data. (See also [20, 21] where a similar discussion is developed.)

Cosmological constraints come also from another observable. A late decaying particle can in fact alter the thermal distribution of the photons which then will form the CMB, introducing a chemical potential in the CMB thermal distribution bigger than the one which is usually expected due to the usual cosmic evolution, or even bigger than the current experimental upper bound [22, 23]. Analytical formulas for the produced effect are given in [24, 25]. Nevertheless, it is useful to notice that the induced chemical potential $\mu$ is mostly and hugely dependent on the time of decay of

the particles. In particular, we see that:

$$\mu \sim e^{-\frac{\tau_{dc}}{\tau_{NLSP}}} \tag{3.27}$$

where $\tau_{NLSP}$ is the lifetime of the NLSP, and $\tau_{dc} \sim 10^6$s is the time at which the double Compton scattering of the photons is no more efficient. The $\xi_{dangerous}$ for this quantity is $\xi_{dangerous} \sim 10^{-9}$ GeV. So, we conclude that basically, for $\tau_{NLSP} < \tau_{dc}$ , there are no limits, while for $\tau_{NLSP} > \tau_{dc}$, the limit from nucleosynthesis is stronger. We easily see that this constraint never comes into play in our work.

From formula (3.22), we can already extract an idea of what will be the final result of the analysis. In fact, we can avoid the limits from nucleosynthesis by decaying early. This means that, according to (3.22), we need to let the ratio $\frac{m_{NLSP}}{m_{LSP}}$ to grow, and consequently $\Omega_{NLSP}$ has to grow as well. This leads to two directions: either a very massive LSP or a a very weakly interacting LSP. The first direction goes in agreement with one of the directions we had found in order to match the constraint from $\Omega_{DM}$, and tells us that, in general, a massive NLSP will be acceptable from the cosmological point of view. However, it will have chanches to encounter the constraints coming from gauge couplings unification. The other direction is to have an NLSP whose main annihilation channel is controlled by another particle, which can be made heavy. As an example, this is the case for the Bino, whose channel is controlled by the Higgsino: so, we might have a light Bino, if the Higgsino will be heavier.

## 3.5 Gravitino LSP

In this section, we concentrate in detail on the possibility that the LSP in Split Susy is the Gravitino, and that it constitute the Dark Matter of the universe. We shall consider the mass of the Gravitino as a free parameter, and we shall try to extract information on the mass and the nature of the NLSP. However, an actual lower limit on the Gravitino mass can be expected in the case Susy is broken directly, as in that case the mass of the Gravitino should be: $m_{gr} \sim \frac{\tilde{m}^2}{M_{pl}}$, where $\tilde{m}$ is the Susy breaking

scale. Since, roughly, in Split Susy $\tilde{m}$ is as light as $\sim 100$ TeV, we get the lower limit $m_{gr} \gtrsim 10^{-8}$ GeV, which, as we will see, is lower than the region we will concentrate on.

As we learnt in the former two sections, there are two fundamental quantities to be computed: the lifetime of the NLSP, and $\Omega_{NLSP}$.

As we said before, we shall consider both the Neutralino and the Chargino as LSP. The decaying amplitude of a Neutralino into Gravitino plus a Standard Model particle was computed in [26, 27, 28].

For decay into Photons:

$$\Gamma(\chi \to \gamma, gr) = \frac{|N_{11}\cos(\theta_w) + N_{12}\sin(\theta_w)|^2}{48\pi M_{pl}^2}\frac{m_\chi^5}{m_{gr}^2}\left(1-\frac{m_{gr}^2}{m_\chi^2}\right)^3\left(1+3\frac{m_{gr}^2}{m_\chi^2}\right) \quad (3.28)$$

where $\chi = N_{11}(-i\tilde{B}) + N_{12}(-i\tilde{W}) + N_{13}\tilde{H}_d + N_{14}\tilde{H}_u$ is the NLSP. As we see, eq.(3.22) reproduces the right behavior in the limit $m_{NLSP}/m_{LSP} \gg 1$ . This decay will contribute only to ElectroMagnetic (EM) energy.

The leading contribution from hadronic decays comes from the decay into $Z, gr$ and $h, gr$. These decays will contribute to EM or Hadronic energy according to the branching ratios of the SM particles. The decay width to Z boson is given by:

$$\begin{aligned}\Gamma(\chi \to Z, gr) = \quad & \frac{|-N_{11}\sin(\theta_w) + N_{12}\cos(\theta_w)|^2}{48\pi M_{pl}^2}\frac{m_\chi^5}{m_{gr}^2}F(m_\chi, m_{gr}, m_z) \quad (3.29)\\ & \left(\left(1-\frac{m_{gr}^2}{m_\chi^2}\right)^2\left(1+3\frac{m_{gr}^2}{m_\chi^2}\right) - \frac{m_Z^2}{m_{gr}^2}G(m_\chi, m_{gr}, m_Z)\right)\end{aligned}$$

where

$$F(m_\chi, m_{gr}, m_z) = \left(\left(1-\left(\frac{m_{gr}+m_Z}{m_\chi}\right)^2\right)\left(1-\left(\frac{m_{gr}-m_Z}{m_\chi}\right)^2\right)\right)^{1/2} \quad (3.30)$$

$$G(m_\chi, m_{gr}, m_z) = 3 + \frac{m_{gr}^3}{m_\chi^3}\left(-12 + \frac{m_{gr}}{m_\chi} + \frac{m_Z^4}{m_\chi^4} - \frac{m_Z^2}{m_\chi^2}\left(3-\frac{m_{gr}^2}{m_\chi^2}\right)\right) \quad (3.31)$$

The decay width to $h$ boson is given by:

$$\Gamma(\chi \to h, gr) = \frac{|-N_{13}\sin(\beta) + N_{14}\cos(\beta)|^2}{48\pi M_{pl}^2}\frac{m_\chi^5}{m_{gr}^2}F(m_\chi, m_{gr}, m_z) \left(\left(1-\frac{m_{gr}^2}{m_\chi^2}\right)^2\left(1+\frac{m_{gr}^2}{m_\chi^2}\right)^4 - \frac{m_h^2}{m_{gr}^2}H(m_\chi, m_{gr}, m_h)\right) \tag{3.32}$$

where $h = -H_d^0 sin(\beta) + H_u^0 Cos(\beta)$ is the fine tuned light Higgs, and

$$H(m_\chi, m_{gr}, m_h) = 3+4\frac{m_{gr}}{m_\chi}+2\frac{m_{gr}^2}{m_\chi^2}+4\frac{m_{gr}^3}{m_\chi^3}+3\frac{m_{gr}^4}{m_\chi^4}+\frac{m_h^4}{m_\chi^4}-\frac{m_h^2}{m_\chi^2}\left(3+2\frac{m_{gr}}{m_\chi}+3\frac{m_{gr}^2}{m_\chi^2}\right) \tag{3.33}$$

We further use the following branching ratios and energy release parameters:

$$B_{EM}^\chi \sim 1 \tag{3.34}$$

$$\epsilon_{EM}^\chi = \frac{m_\chi^2 - m_{gr}^2}{2m_\chi} \tag{3.35}$$

$$B_{Had}^\chi \sim \frac{\Gamma(\chi \to Z, gr)B_{had}^Z + \Gamma(\chi \to h, gr)B_{had}^h + \Gamma(\chi \to q, \bar{q}, gr)}{\Gamma(\chi \to \gamma, gr) + \Gamma(\chi \to h, gr) + \Gamma(\chi \to Z, gr)} \tag{3.36}$$

$$\epsilon_{had}^\chi = \frac{m_\chi^2 - m_{gr}^2 - m_{Z,h}^2}{2m_\chi} \tag{3.37}$$

where $\epsilon_i^\chi$ is the energy release per decay in the EM and in the Hadronic channel, and $B_i^\chi$ is the branching ratio in the EM and Hadronic channel. We use $B_{had}^h \sim 0.9, B_{had}^Z \sim 0.7$. Since it will not play an important role, we just estimate the channel $\Gamma(\chi \to q, \bar{q}, gr)$, and do not perform a complete computation. This channel provides the hadronic decays when $m_{NLSP} - m_{gr}$ is less than the $m_Z$ or $m_h$. The leading diagram in this case is given by the tree level diagram in which there is a virtual $Z$ boson or a virtual Higgs that decays into quarks.

### 3.5.1 Neutral Higgsino, Neutral Wino, and Chargino NLSP

An Higgsino NLSP will be naturally much interacting in Split Susy, quite independently of the other partners mass. In fact, there are gauge interaction and Yukawa

coupling to the other particles. While the coupling to the Z vanishes for $\mu \gg m_Z$, in that case neutral Higgsino and Charged Higgsino are almost degenerate, and so the interaction with the Higgs become relevant. This means that the annihilation rate will never be very weak, and so $\Omega_{NLSP}$ will be large only for large $\mu$. An analytical computation is too complicated for our necessities, even with the simplifications of Split Susy, so, we modify the DarkSusy code [10] to adapt it to the Split Susy case, and we obtain the following relic abundance:

$$\Omega_{\tilde{H}^0} h^2 = 0.09 \left(\frac{\mu}{\text{TeV}}\right)^2 \tag{3.38}$$

In order to avoid nucleosynthesis constraints, we need to decay early. This can be achieved either raising the hierarchy between Higgsino and Gravitino, or raising the mass of the Higgsino. Since $\Omega_{LSP} = \frac{m_{LSP}}{m_{NLSP}} \Omega_{NLSP}$, we can not grow too much with the hierarchy, and so we are forced to raise the mass of the Higgsino.

This is exactly one of the two directions to go in the parameter space we had outlined in the first sections, and it is the one which is less favourable for detection at LHC.

The results of an actual computation are shown in fig.3-8, where we plot the allowed region for the Higgsino NLSP, in the plane $m_{gr}, \delta m = m_{NLSP} - m_{gr}$. The quantity $\delta m$ well represents the available energy for decay, and, obviously, can not be negative. The Hadronic and the Electromagnetic constraints we use come from the numerical simulations done in [18, 19]. There, constraints are given as upper limit on the quantity $\xi = B_{(EM,Had)} \epsilon_{(EM,Had)} Y$ as a function of the time of decay. We then apply this limit to our NLSPs computing both the time of decay and the quantity $\xi$ with the formulas given in the former section.

As we had anticipated, the cosmologically allowed region is given by:

$$m_{gr} \leq 4 \times 10^2 \text{GeV} \tag{3.39}$$

$$m_{\tilde{H}} \geq 20 \text{TeV} \tag{3.40}$$

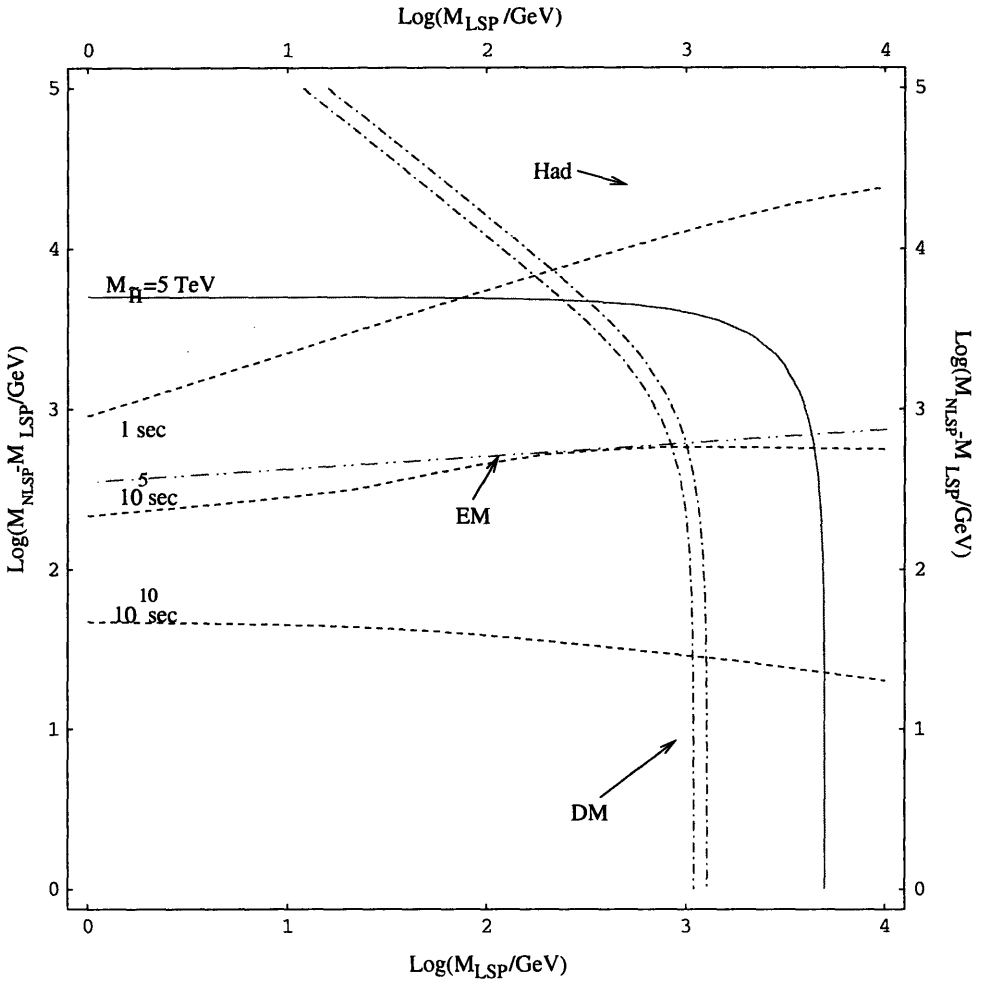


Figure 3-8: Constraints for the Higgsino NLSP, Gravitino LSP. There is no allowed region. The long dashed contour delimitats from above the excluded region by the hadronic constraints from BBN, the dash-dot-dot contour represents the same for EM constraints from BBN, the dash-dot lines represent the region within which $\Omega_{DM}$ is within the experimental limits; finally, we show the short dashed countors where the Higgsino decays to Gravitino at 1 sec, $10^5$ sec, and $10^{10}$ sec, and the solid line where the Higgsino is 5 TeV heavy, which represents the upper bound for Gauge Coupling Unification. For Neutral Wino and Chargino NLSP, the result is very similar.

This mass range is not allowed by gauge coupling unification, as, for Gravitino LSP, we have to use the upper bound on NLSP coming from gaugino mass unification initial conditions. So we conclude that the Higgsino NLSP is excluded. This is a very nice example of how much we can constraint physics combining particle physics data, and cosmological observations.

Finally, note how the hadronic constraints raise the limit on the Higgisino mass

of approximately one order of magnitude.

In the case of the Neutral Wino NLSP, and Chargino NLSP, there are basically no relevant differences with respect to the case of the Neutral Higgsino, the main reason being the fact that the many annihilations channels lead to an high mass for the NLSP, exactly in parallel to the case of the Higgsino. We avoid showing explicitly the results, and simply say that, for all of them, the cosmologically allowed parameter space is very similar in shape and values to the one for Higgsino, with just this slight correction on the numerical values:

$$m_{gr} \leq 5\ 10^2 \text{GeV} \tag{3.41}$$

$$m_{\tilde{W}^0} \geq 30\text{TeV} \tag{3.42}$$

for the Wino case. Notice that the mass is a little higher than in the Higgsino case, as the Wino is naturally more interacting. In fact, its relic abundance is given by (again, using a on porpuse modified version of Dark Susy [10] ):

$$\Omega_{\tilde{W}^0} h^2 = 0.02 \left( \frac{M_2}{\text{TeV}} \right)^2 \tag{3.43}$$

For the Chargino, the mass limit is even higher:

$$m_{gr} \leq 10^3 \text{GeV} \tag{3.44}$$

$$m_{\tilde{W}^+} \geq 40\text{TeV} \tag{3.45}$$

All of these regions are excluded by the requirement of gauge coupling unification.

### 3.5.2 Photino NLSP

As we saw in the former section, hadronic constraints pushed the mass of the NLSP different from a Bino one above the 10 TeV scale, with the resulting conflict with gauge coupling unification. Anyway, just looking at the electromagnetic constraints in fig.3-8 , one can see that a particle that will not decay hadronically at the time

of Nucleosynthesis will be allowed to be one order of magnitude lighter. This makes the photino, $\tilde{A} = \cos(\theta_W)\tilde{B} + \sin(\theta_W)\tilde{W}_3$, a natural candidate to be a NLSP with Gravitino LSP.

Computing the relic abundance of a Photino is rather complicated, even in Split Susy. The reason is that co-hannilation channels with the charged Winos makes a lot of diagrams allowed. In order to estimate the Photino relic abundance, we then observe that, because of the fact that the Bino is very weakly interacting in Split Susy, Photino annihilation channels will be dominated by the contribution of the channels allowed by the Wino component. We then quite reliably estimate the Photino relic abundance starting from the formula for the relic abundance of a pure Wino particle we found before:

$$\Omega_{WinoNLSP}h^2 = 0.02\left(\frac{M_2}{\text{TeV}}\right)^2 \tag{3.46}$$

and consider that the Photino has a Wino component equal to $\sin(\theta_W)$ So, for the Photino case we will have:

$$\Omega_{PhotinoNLSP} \cong \frac{0.02}{\sin(\theta_W)^4}\left(\frac{M_{\tilde{A}}}{\text{TeV}}\right)^2 \cong 0.37\left(\frac{M_{\tilde{A}}}{\text{TeV}}\right)^2 \tag{3.47}$$

We then obtain the allowed region shown in fig.(3-9). The graph is very similar to the Higgsino case, with the difference that the Electromagnetic constraints are less stringent than the Hadronic ones. This allows to have the following region:

$$700 \text{ GeV} \leq M_{\tilde{A}} \leq 5 \text{ TeV} \tag{3.48}$$

the lightest part of which might be reachable at LHC. However, already if we allow an hadronic branching ratio of $10^{-3}$, we see that the Photino NLSP becomes excluded. So, we conclude that a Photino NLSP is in principle allowed, but only if we fine tune it to be extremily close to a pure state of Photino.

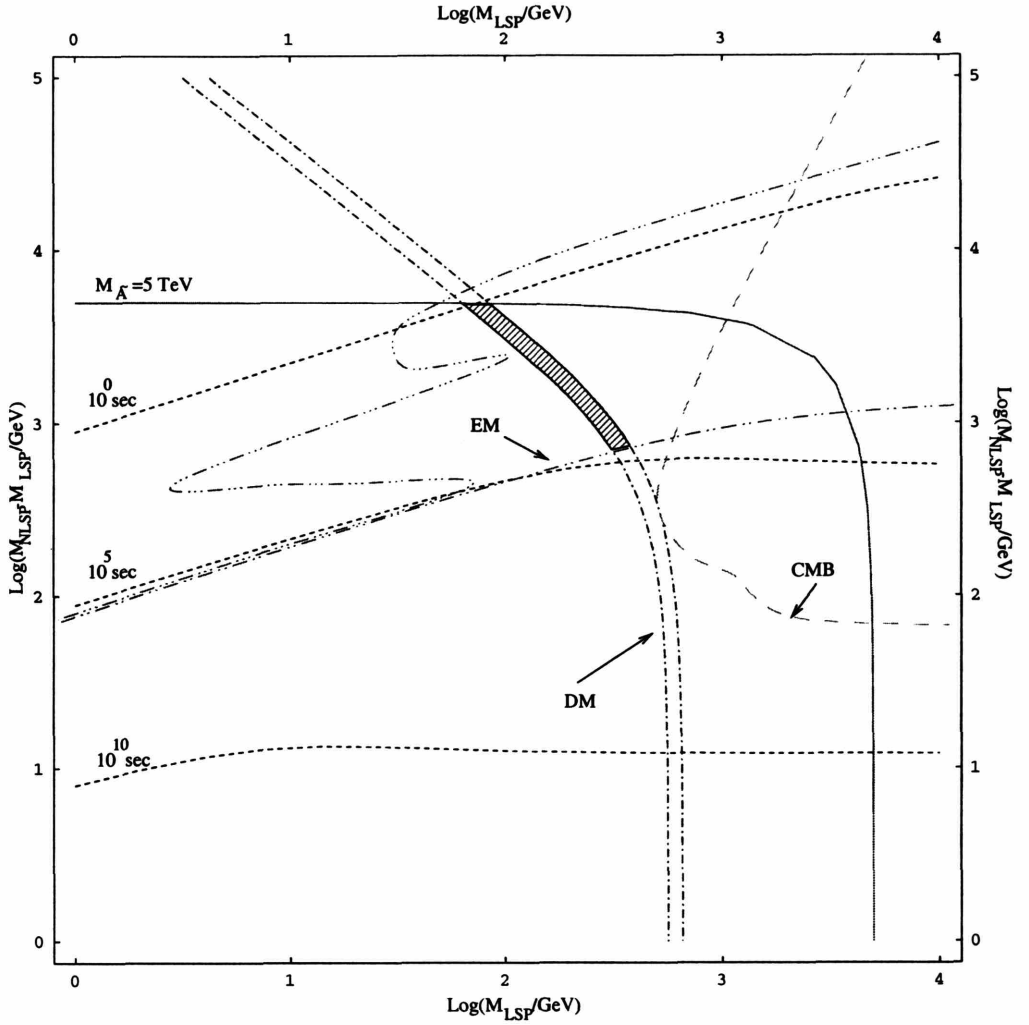


Figure 3-9: Shaded is the allowed region for the Photino NLSP, Gravitino LSP. The long dashed contour delimitates from the left the region excluded by CMB, the dash-dot-dot contour delimitates from above the region excluded by the EM constraints from BBN in the case $B_h \sim 0$, the dashed-dot-dot-dot countor represents the same for $B_h \sim 10^{-3}$. The region within the dash-dot lines represents the region where $\Omega_{DM}$ is within the experimental limits; finally, we show the short dashed contours which represent where the Photino decays to Gravitino at 1 sec, $10^5$ sec, and $10^{10}$ sec, and the solid contour where the Photino is 5 TeV heavy, which represents the upper limit for Gauge Couplig Unification. We see that already for $B_h \sim 10^{-3}$ a Photino NLSP is excluded.

### 3.5.3 Bino NLSP

Bino NLSP is a very good candidate for avoiding all the cosmological constraints. In Split Susy, a Bino NLSP is almost not interacting. For a pure Bino, the only

interaction which determines its relic abundance is the annihilation to Higgs bosons through the exchange of an Higgsino. Since this cross section is naturally very small, by eq.(3.12), $\Omega_{NLSP}$ is very big. This means that, in order to create the right amount of DM (see eq.(3.15)), we need to make the Gravitino very light. And this is exactly what we need to do in order to avoid the nucleosynthesis bounds. We conclude then that, of the two directions to solve the DM and the nucleosynthesis problems that we outlined in the former sections, a Bino NLSP would naturally pick up the one which is the most favorable for LHC detection. However, as we saw in the section on Gauge Coupling Unification (see fig.3-4), the Higgsino can not be much heavier than the Bino. This implies that a Bino like NLSP will have to have some Higgsino component unless it is very heavy and the off diagonal terms in the mass matrix are uniportant. As a consequence, new annihilation channels opens up for the Bino NLSP through its Higgsino component. This has the effect of diminishing the relic abundance of a Bino NLSP with respect to the naive thinking we would have done if we neglected the mixing. As a result, the cosmological constraints begin to play an important role in the region of the spectrum we are interested in, and, at the end, considering the upper limit from gauge coupling unification, exclude a Bino NLSP.

In order to compute the Bino NLSP relic abundance, we again modify the Dark Susy code[10]. The results are shown in fig.3-10. As anticipated, we see that the relic abundance strongly depends on the ratio beteween the Bino and the Higgsino masses $M_1, \mu$. The relic abundance of the Bino NLSP becomes large enough to avoid the cosmological constaints only for so large values of the ratio between $\mu$ and $M_1$ which are not allowed by Gauge Coupling Unification. We conclude, then, that a Bino NLSP is not allowed.

## 3.6 Extradimansional LSP

When we consider generic possibilities to break Susy, we can have, further than the Gravitino, other fermions in a hidden sector which are kept light by an R symmetry. The implications of these fermions as being the LSP can be quite different with respect

to the case of Gravitino LSP, as we will see in this section. Here, we concentrate os Susy breaking in Extra Doimensions, where, as it was shown in [1], it is very generic to expect a light fermion in the hidden sector.

In Susy breaking in Extra Dimension, one can break Susy with a radion field, which gets a VEV. Its fermionic component, the Goldstino, is then eaten by the Gravitino which becomes massive. Even though at tree level there is no potential, one sees that at one loop the Casimir Energy makes the radius instable. One can compensate for this introducing some Bulk Hypermultiplets, finding that, however, the cosmological constant is negative. Then, in order to cancel this, one finds that he has to introduce another source of symmetry breaking, a chiral superfield $X$ localized on the brane (see for example [1]). This represents a sort of minimal set to break Susy in Extra Dimensions. If one protects the $X$ field interactions with a U(1) charge, than one finds that the interactions with the SM particles are all suppressed by the 5 dimensional Plank Mass, of the form:

$$\int d^4\theta \frac{1}{M_5^2} X^\dagger X Q^\dagger Q \tag{3.49}$$

This induces the following mass spectrum [1]:

$$m_{gr} \sim \frac{\pi M_5^3}{M_4^2}; m_S \sim \frac{\pi M_5^5}{M_4^4}; m_i, \mu, m_{\psi_X} \sim \frac{\pi M_5^9}{M_4^8} \tag{3.50}$$

where $M_4^2 \sim r M_5^3$ are the 4 and 5 dimensional Plank constants, and where $M_i$ are the gaugino masses.

It is quite natural to use the extradimension to lower the higher dimensional Plank mass to the GUT scale, a la Horawa-Witten [29], $M_5 \sim M_{GUT} \sim 3 \times 10^{16}$ GeV. We have this range of scales[1]:

$$m_{gr} \sim 10^{13}\text{GeV}; m_S \sim 10^9\text{GeV}; m_{\text{radion}} \sim 10^7\text{GeV}; M, \mu, m_{\psi_X} \sim 100\text{GeV} \tag{3.51}$$

We notice that we have just reached the typical spectrum of Split Susy, in a very

natural way: we break Susy in Extra Dimension, stabilize the moduli, and we introduce a further Susy breaking source to compensate for the cosmological constant. We further notice that there is no much room to move the higher dimensional Plank mass $M_5$ away from the Horawa-Witten value. In fact, the fermion mass scales as $\left(\frac{M_4}{M_5}\right)^8$, so, a slight change of $M_5$ makes the fermions of Split Susy generically either too heavy, making them excluded by gauge coupling unification, or too light, making them conflict with collider bounds.

Concerning the study of the LSP, we notice that the fermionic component of the $X$ field we have to introduce in order to cancel the cosmological constant is naturally light, of the order of the mass of the Gauginos. So, it is worth to investigate the case in which this fermion is the LSP, and how this case differs from the case in which the LSP is the Gravitino.

Concerning the DM abundance, nothing changes with respect to the case of the gravitino LSP, so, we can keep the former results.

Next step it is to evaluate the decay time, to check if the nucleosynthesis and CMB constraints play a role.

To be concrete, let us concentrate on the Higgsino NLSP. When the Higgsino is heavier than the Higgs, the leading contribution to the decay of the Higgsino will come from the tree level diagram mediated by the operator[1]:

$$\int d^2\theta \frac{m^2 X}{M_5^2} H_u H_d \tag{3.52}$$

The decay time is then given by:

$$\tau = \frac{128}{\pi}\left(\frac{M_4}{\pi M_5}\right)^8 \left(1 + \frac{m_{\psi_X}^2}{m_{\tilde{H}}^2} - \frac{m_h^2}{m_{\tilde{H}}^2}\right)^{-1} \left(\frac{(m_{\tilde{H}}^2 + m_{\psi_X}^2 - m_h^2)^2}{4m_{\tilde{H}}^2} - m_{\psi_X}^2\right)^{-1/2} \tag{3.53}$$

In the limit of $m_{\tilde{H}} \gg m_{\psi_X}, m_h$ this expression simplifies to:

$$\tau \sim \frac{128}{\pi^9 m_{\tilde{H}}}\left(\frac{M_4}{M_5}\right)^8 \tag{3.54}$$

Estimating with the number we just used before, we get:

$$\tau \sim 10^{-14} \left( \frac{\text{TeV}}{m_{\tilde{H}}} \right) \text{sec} \tag{3.55}$$

This time is so long before nucleosynthesis, that all the BBN constraints we found in the former case for the Gravitino now disappear. Clearly, this statment is not affected if we vary $M_5$ in the very small window allowed by the restrictions on the fermionic superpartners' spectrum. Basically, in this mass regime, the only constraint which will apply will be the one from $\Omega_{DM}$. As we can see form the formula for the higgsino relic abundance, the region where Higgsino is lighter that Higgs is not relevant, and is excluded by the constraint on Dark Matter abundance.

So, we conclude that nucleosynthesis and CMB constraints do not apply in the case in which the LSP is the field $\psi_X$, and the Higgsino is the NLSP, the only constraints which applies are the one coming from $\Omega_{DM}$ and the one coming from gauge coupling unification. In fig.3-11, we show the allowed region. While the full region is quite large, and covers a rather large phase space, there is a region where the Higgsino is rather light, $\sim 2$ TeV, and the mass of the field $\psi_X$ is constrained quite precisely to be around 2 TeV. The region is bounded from above by the limit on gauge coupling unification at around 18 TeV, as in this case we must allow also for anomaly mediated initial conditions for Gauginos mass at the intermediate scale. This region is not extremely attractive for LHC.

For gaugino NLSP, the situation is very similar, as the decay of the gauginos to the field $\psi_X$ is mediated by the same kind of operator as for the Higgisino case [1]:

$$\int d^2\theta \frac{m^2 X}{M_5^2} WW \tag{3.56}$$

where $W$ is the gaugino vector supermultiplet. Clearly, again in this case, the decay time will be way before the time of BBN. In this cases, the curves that delimitate the allowed region are practically identical to the one of the Higgsino, with the only difference that the region where the NLSP is the lightest and it is practically degenerate with the $\psi_X$, correspont to an higher mass of $\sim 3$ TeV, more difficult to see at

LHC.

Similarly occurs for the Bino NLSP, with the only difference that the region allowed by the Dark Matter constraint is a bit different with respect to the case of Higgsino and Wino. We obtain the allowed region shown in fig.3-12, where we see that the spectrum is very light, with Bino and Higgsino starting at tens of GeV , and gluinos at 200 GeV, with $\psi_X$ in the range $10^1 - 10^3$ GeV . This is a very good region for LHC. Notice that the upper limit on the Bino mass is again 5 TeV, as in the case the Bino is the NLSP, we can not have anomaly mediated initial conditions for Gaugino mass at the intermediate scale.

## 3.7 Conclusions

In Split Susy, the only two motivations to expect new physics at the TeV scale are given by the requirement that gauge coupling unification is achieved, and, mostly, that the stable LSP makes up the Dark Matter of the Universe. This is true in the standard scenario where the LSP is a neutralino. Here we have investigated the other main alternative for the LSP, that is that the LSP is constituted by a hidden sector particle. A natural candidate for this is the Gravitino, which here we studied quite in detail. Nevertheless, it is true that among the different possibilities we have in order to break Susy, one can expect the appearence in the spectrum of another light fermion protected by R symmetry. Here, as an example, we study the case of a light fermion arising in Susy breaking in Extra Dimension.

The requirement to obtain gauge coupling unification limits the masses for the fermions to be less than 5 TeV or 18 TeV, according to the different initial conditions for the Gaugino masses at the the intemediate scale $\tilde{m}$.

In this range of masses, we have seen how constraints from Nucleosynthesis put strong limits on the allowed region. In fact, there are two competing effects: in order to avoid Nuclosynthesis constraints, the NLSP must decay to the LSP early, and this is achieved creating a big hierarchy between the NLSP and the LSP. On the other hand, this hierarchy tends to diminish the produced $\Omega_{LSP}$, and in order to

compensate for it, the NLSP tends to be heavy. This goes against the constraints from gauge coupling unification. This explains why a large fraction of the parameter space is excluded.

The details depend on the particular LSP and NLSP.

### 3.7.1 Gravitino LSP

Gravitino LSP forces us to consider Gaugino Mass Unification at the intermediate scale as initial condition. This implies that we have to live with the more restrictive upper limit on fermionic masses from gauge coupling unification: 5 TeV.

At the same time, the typical decay time of an NLSP to the Gravitino is at around 1 sec, and this goes exactly into the region where constraints from Nucleosynthesis on ElectroMagnetic and Hadronic decays apply.

The final result is that only if the NLSP is very pure Photino like, then the Gravitino can be the LSP, with a Photino between 700 GeV and 5 TeV. If the NLSP is different by this case, then the Gravitino *can not* be the LSP. The reason is that a very Photino like NLSP can avoid the constraints on BBN on hadronic decays, which are much more stringent than the ones coming from electromagnetic decays, and so it can be light enough to avoid the upper limit on its mass coming from gauge coupling unification.

This is very good news for the detactability of Split Susy at LHC. In fact, if the Gravitino was the LSP, than the NLSP could have been much heavier than around 1 TeV, making detection very difficult. In the study in this chapter we show that this possibility is almost excluded.

### 3.7.2 ExtraDimensional LSP

Following the general consideration that in breaking Susy we might expect to have some fermion other than the Gravitino in the hidden sector which is kept light by an R symmetry, we have studied also the possibility that the fermionic component of a chiral field which naturally arises in Extra Dimensional Susy breaking is the LSP. In

this case the time of decay is so early that no Nucleosynthesis bounds apply, so, the only constraints applying are those from Dark Matter and gauge coupling unification.

Concerning gauge coupling unification, in this case we must consider the possibility that the Gaugino Mass initial conditions are also those from anomaly mediation. This implies that we have to give the upper limit of 18 TeV to Fermions' mass.

Having said this, the lower bound on the mass is given by the DM constraint. In fact, it is clear that $\Omega_{NLSP}$ must be greater than $\Omega_{LSP}$. As a consequence, the Mass of the NLSP has to be greater than the one found in [2, 3] for the case in which these particles where the LSP. As a consequence, Charginos and Neutralinos NLSP are in general allowed, but they are restricted to be heavier than 1 TeV. It is quite interesting that, in this cases, the LSP is restricted to be in the range 100-1000 GeV.

Again, there is an exception: the Bino. In this case, the LSP and NLSP are much lighter than in the case of the others Neutralinos NLSP, with an NLSP as light as a few decades of GeV.

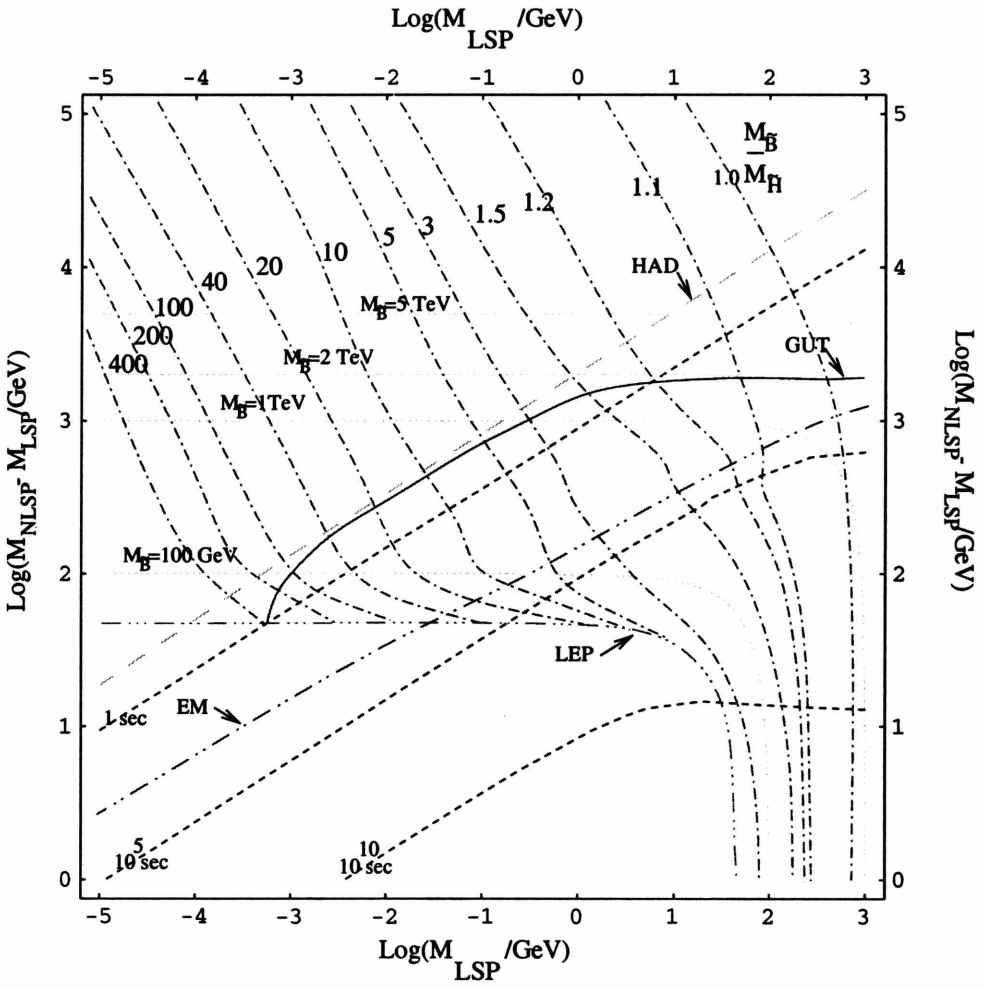


Figure 3-10: Constraints for Bino NLSP. The long dashed countour delimitates from the left the excluded region by the hadronic constraint from BBN, the dash-dot-dot contour represents the same for EM constraints from BBN, the dash-dot lines represents the ratio between the Higgsino mass and the Bino mass necessary for $\Omega_{LSP}$ to be equal to observed DM amount; the solid line represents the upper limit from GUT, while the dash-dot-dot-dot line represents the lower limit from LEP; we also show in short dashed the contours where the Bino decays to Gravitino at 1 sec, $10^5$ sec, and $10^{10}$ sec, and in dotted some characterstic contours for the Bino mass. CMB constraint plays no role here. We take $M_2 \simeq 2M_1$, as inferred from gaugino mass unification at the GUT scale [2], and we see that no allowed region is present.

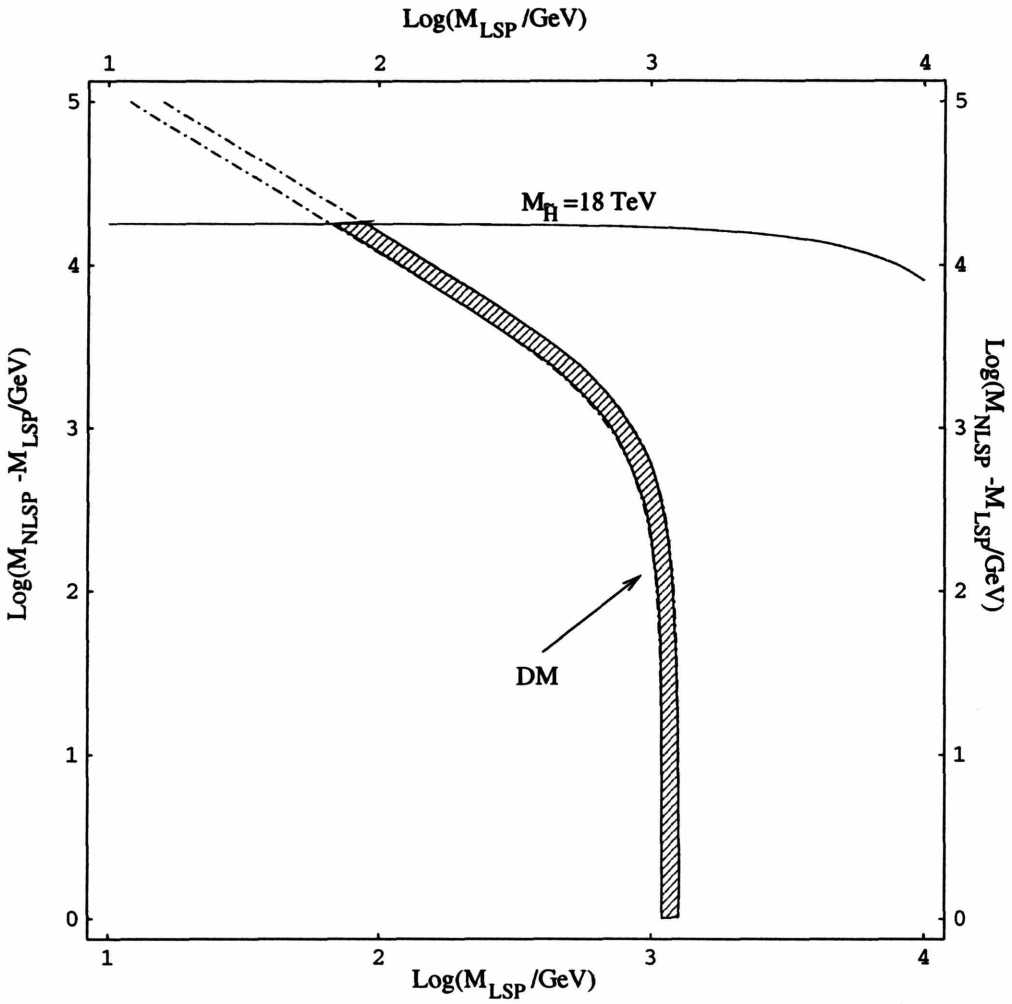


Figure 3-11: Shaded is the allowed region for the Neutral Higgsino NLSP, $\psi_X$ LSP. Since there are no constraints from CMB and BBN, the only constraints come from $\Omega_{DM}$, which delimitates the region within the dash-dot lines, and Gauge Coupling Unification, which set the upper bound of 18 TeV with the solid line. For Neutral Wino and Chargino NLSP the result is very similar.

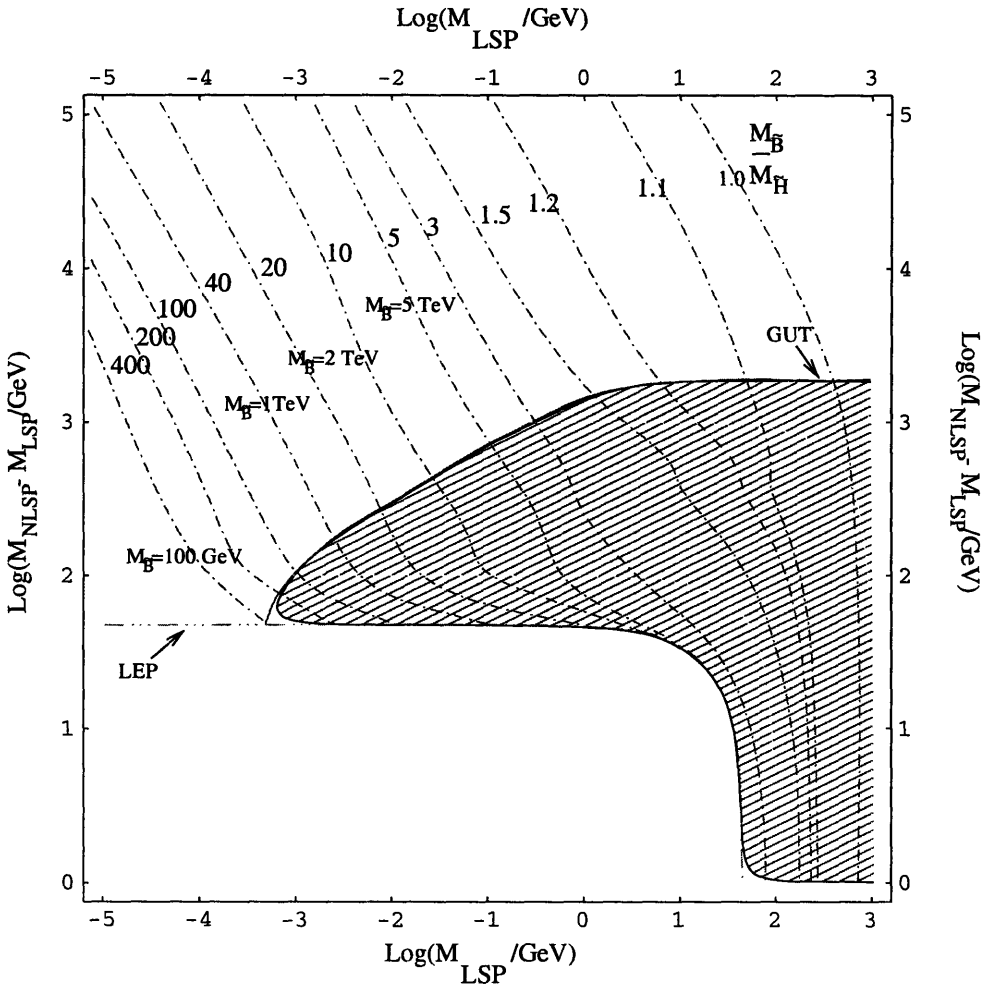


Figure 3-12: Shaded is the allowed region for the Bino NLSP, $\psi_X$ LSP. The dash-dot lines represent the ratio between the Higgsino mass and the Bino mass in order for $\Omega_{LSP}$ to be equal the observed amount of DM. The dotted lines are some characteristic countors for the Bino mass. The solid line is the upper limit from GUT, while the dash-dot-dot-dot line is the lower limit from LEP. We take $M_2 \simeq 2M_1$.

# Bibliography


[1] N. Arkani-Hamed and S. Dimopoulos, arXiv:hep-th/0405159.

[2] G. F. Giudice and A. Romanino, arXiv:hep-ph/0406088.

[3] A. Pierce, arXiv:hep-ph/0406144.

[4] A. Masiero, S. Profumo and P. Ullio, arXiv:hep-ph/0412058.

[5] M. A. Luty and N. Okada, JHEP **0304**, 050 (2003) [arXiv:hep-th/0209178].

[6] N. Arkani-Hamed, S. Dimopoulos, G. F. Giudice and A. Romanino, arXiv:hep-ph/0409232.

[7] J. Bernstein, L. S. Brown and G. Feinberg, Phys. Rev. D **32** (1985) 3261.

[8] R. J. Scherrer and M. S. Turner, Phys. Rev. D **33** (1986) 1585 [Erratum-ibid. D **34** (1986) 3263].

[9] See for example, Kolb and Turner, The Early Universe, Perseus Publishing, 1990

[10] P. Gondolo, J. Edsjo, P. Ullio, L. Bergstrom, M. Schelke and E. A. Baltz, arXiv:astro-ph/0211238.

[11] S. Eidelman *et al.* [Particle Data Group Collaboration], Phys. Lett. B **592** (2004) 1.

[12] G. Altarelli and M. W. Grunewald, arXiv:hep-ph/0404165.

[13] S. Aoki *et al.* [JLQCD Collaboration], Phys. Rev. D **62** (2000) 014506 [arXiv:hep-lat/9911026].

[14] Y. Suzuki *et al.* [TITAND Working Group Collaboration], arXiv:hep-ex/0110005.

[15] C. L. Bennett *et al.*, Astrophys. J. Suppl. **148** (2003) 1 [arXiv:astro-ph/0302207].

[16] D. N. Spergel *et al.* [WMAP Collaboration], Astrophys. J. Suppl. **148** (2003) 175 [arXiv:astro-ph/0302209].

[17] R. H. Cyburt, J. R. Ellis, B. D. Fields and K. A. Olive, Phys. Rev. D **67**, 103521 (2003) [arXiv:astro-ph/0211258].

[18] M. Kawasaki, K. Kohri and T. Moroi, arXiv:astro-ph/0402490.

[19] M. Kawasaki, K. Kohri and T. Moroi, arXiv:astro-ph/0408426.

[20] K. Jedamzik, Phys. Rev. D **70** (2004) 083510 [arXiv:astro-ph/0405583].

[21] K. Jedamzik, Phys. Rev. D **70** (2004) 063524 [arXiv:astro-ph/0402344].

[22] J. Fixsen, E. S. Cheng, J. M. Gales, J. C. Mather, R. A. Shafer and E. L. Wright, Astrophys. J. **473** (1996) 576 [arXiv:astro-ph/9605054].

[23] K. Hagiwara *et al.* [Particle Data Group Collaboration], Phys. Rev. D **66** (2002) 010001.

[24] W. Hu and J. Silk, Phys. Rev. Lett. **70** (1993) 2661.

[25] W. Hu and J. Silk, Phys. Rev. D **48** (1993) 485.

[26] J. L. Feng, S. Su and F. Takayama, arXiv:hep-ph/0404231.

[27] J. L. Feng, A. Rajaraman and F. Takayama, Phys. Rev. Lett. **91** (2003) 011302 [arXiv:hep-ph/0302215].

[28] J. L. Feng, A. Rajaraman and F. Takayama, Phys. Rev. D **68** (2003) 063504 [arXiv:hep-ph/0306024].

[29] P. Horava and E. Witten, Nucl. Phys. B **460** (1996) 506 [arXiv:hep-th/9510209].

# Chapter 4

# Hierarchy from Baryogenesis

We study a recently proposed mechanism to solve the hierarchy problem in the context of the landscape, where the solution of the hierarchy problem is connected to the requirement of having baryons in our universe via Electroweak Baryogenesis. The phase transition is triggered by the fermion condensation of a new gauge sector which becomes strong at a scale $\Lambda$ determined by dimensional transmutation, and it is mediated to the standard model by a new singlet field. In a "friendly" neighborhood of the landscape, where only the relevant operators are "scanned" among the vacua, baryogenesis is effective only if the higgs mass $m_h$ is comparable to this low scale $\Lambda$, forcing $m_h \sim \Lambda$, and solving the hierarchy problem. A new CP violating phase is needed coupling the new singlet and the higgs field to new matter fields. We study the constraints on this model given by baryogenesis and by the electron electric dipole moment (EDM), and we briefly comment on gauge coupling unification and on dark matter relic abundance. We find that next generation experiments on the EDM will be sensitive to essentially the entire viable region of the parameter space, so that absence of a signal would effectively rule out the model.

## 4.1 Introduction

The most problematic characteristic of the Standard Model (SM) seems to be the smallness of its superrenormalizable couplings, the higgs mass $m_h^2$, and the cosmological constant $\Lambda_c$, with respect to the apparent cutoff of the theory, the Planck mass, $M_{pl}$. These give rise respectively to the hierarchy, and cosmological constant problems. According to the naturalness hypothesis, the smallness of these operators should be understood in terms of some dynamical mechanism, and this has been a driving motivation in the last two decades in the high energy theory community.

In the last few years, several things have changed.

Concerning the hierarchy problem, experimental investigation has shown that already many of the theoretically most attractive possibilities for the stability of the weak scale, such as supersymmetry, begins to be disfavored, or present at least some fine tuning issues [1, 2].

Concerning the cosmological constant problem, there was the hope that some symmetry connected to quantum gravity would have forced the cosmological constant to be zero. However, first, cosmological observations have shown evidence for a non zero cosmological constant in our present universe [3, 4]; second, from the string theory point of view, two main things have occurred: on the one hand, consistent solutions with a non zero cosmological constant have been found [5, 6, 7, 8, 9], and, on the other hand, it has been becoming more and more clear that string theory appear to have a huge landscape of vacua, each one with different low energy parameters [10, 12].

If the landscape is revealed to be *real*, it would force a big change in the way physics has to be done, and some deep questions may find a complete new answer. In particular, it is conceivable that some characteristics of our low energy theory are just accidental consequences of the vacua in which we happen to be. This is a very big step from the kind of physics we are used to, and its consequences have been explored recently in [11]. There , it is shown that the presence of a landscape offers a new set of tools to address old questions regarding the low energy effective theory of our universe. On one hand, there are statistical arguments, according to

which we might explore the statistically favored characteristics for a vacuum in the landscape [12, 13, 14, 15, 16, 17, 18, 19, 20, 21, 22]. On the other hand, there are also some selection rules due to anthropic reasoning, which we might have to impose on the vacuum, in order for an observer to be present in it. Pioneering in this, is Weinberg's "structure principle" [23], which predicts the right order of magnitude for the cosmological constant starting from the requirement that structures should have had time to form in our universe in order for life to be present in it.

At this point, it is necessary to speak about predictivity for theories formulated with a lot of different vacua, as it occurs in the landscape. There are two important points that greatly affect the predictivity of the theory. First, we must know how the characteristic of the low energy theory change as we scan among the vacua. Second, we must know also how the probability of populate such a vacuum changes among the vacua, also considering the influence of the cosmological evolution. These are very deep questions whose answer in general requires a full knowledge of the UV theory, and we do not address them here. However, there is still something we can do. In fact, as it was pointed out in [11], theories with a large number of vacua can be described in an effective field theory approach. In such a study, it was shown that it is very natural for parameters not to effectively scan in the landscape, unless their average value in the landscape is null. So, it is reasonable to assume that some parameters in the landscape do scan, and some do not. Among the parameters of the theory, the relevant operators have a particular strong impact on the infrared properties of the theory. But exactly because of this, if they are the only ones to scan, their value can be fixed by environmental arguments. This is however true only if the marginal couplings do not scan. For this reason, a neighborhood of the landscape in which only the relevant parameters are scanning, is called a "friendly neighborhood", because it allows to fix the value of the relevant couplings with environmental reasoning, while the marginal parameters do not scan, and so they are analyzed with the usual instruments of physics, judging them on the basis of their simplicity and of their correlations. We do not know if the true string theory landscape have these properties. However, there is some phenomenological motivation to expect that this could well be. In fact, in the

physics connected to the standard model, we have been able to successfully address question concerning the marginal parameters with dynamical reasoning, deducing some striking features as gauge coupling unification, chiral symmetry breaking, or the weakly interacting dark matter, while, on the contrary, we have been having big troubles concerning the problems connected to the relevant coupling in the standard model, the cosmological constant, and the higgs scale, both of which arise large fine tuning issues. In this chapter, we want to address the hierarchy problem of the electroweak scale assuming we are living in such a "friendly neighborhood" of the landscape. Because of this, we concentrate a little more on the predictivity of a phenomenological model based on this. As it is clear, predictivity in the landscape is very much enhanced if there is an infrared fragile feature [11] which must be realized in the universe in order for it not to be lethal, and which is however difficult to realize in the scanned landscape. Exactly the fact that a necessary fragile feature is difficult to realize gives a lot of constraints on the possible vacua in which we should be, or, in other words, on the parameters of the theory, making then the model predictive. An example of a fragile feature is the presence of structures in the universe. According to Weinberg's argument [23], if we require the fact that in the universe there should be structures, than the value of the cosmological constant is very much tighten to a value close to the observed one. The presence of structures can then also be used to anthropically require the lightness of the higgs field in the case dark matter particles receive mass from electroweak symmetry breaking [11, 24].

In this chapter, we concentrate on another fragile feature which we consider necessary for the development of any sort of possible life in the universe, and which is a necessary completion on Weinberg's structure principle. In the absence of baryons, the dark matter would just form virilized structures, and not clumped structures, which instead are necessary for the development of life. We can construct a model where baryons are explicitly a fragile feature. Then, we can connect the solutions of the problem of baryons to the hierarchy problem with a simple mechanism which imposes a low energy electroweak scale in order for baryons to be present in the universe. This is the line of thought implemented in [11], which is the model on which we

focus in this chapter. As we will explain in detail in the next section, the mechanism is based on the fact that baryogenesis is possible in the model only if the electroweak scale is close to a hierarchical small scale. The hierarchical small scale is naturally introduced setting it equal to the scale at which a new gauge sector of the theory becomes strong through dimensional transmutation. This mechanism naturally provides a small scale. In order to successfully implement baryogenesis, we will also need to add some more CP violation. This will force the presence of new particles and new couplings. The model becomes also predictive: the lightest of these particle will naturally be a weakly interacting particle at the weak scale, and so it will be a very good candidate for dark matter; further, the new CP violating terms will lead to the prediction of a strong electron electric dipole.

The main purpose of the study in this chapter is to investigate in detail the mechanism in which baryogenesis occurs in this model, and the consequent predictions of the model. In particular, we will find that next generation experiments of the electron Electric Dipole Moment (EDM), together with the turning on of LHC, are going to explore the entire viable region of the parameter space, constraining it to such a peculiar region of the parameter space, so that absence of a signal would result in ruling out the model.

The chapter is organized as follows: in sec. 5.2, we explain in detail the model; in sec. 5.3 we study the amount of baryons produced; in sec. 5.4 we determine the electron EDM; in sec. 5.5 we briefly comment on Dark Matter and Gauge Coupling Unification ; and in sec. 5.6, we draw our conclusions.

## 4.2 Hierarchy from Baryogenesis

In this section, following [11], we show how we can connect the electroweak scale to a scale exponentially smaller than the cutoff.

As the presence of baryons is a necessary condition for the formation of clumped structures, it is naturally to require that the vacuum in which we are should allow for the formation of a net baryon number in the universe. This is not a trivial

requirement. In fact, in the early hot phase of the universe, before the electroweak phase transition, baryon number violating interactions through weak sphalerons were unsuppressed, with a rate given approximately by [25]:

$$\Gamma_{ws} = 6k\alpha_w^5 T \tag{4.1}$$

where $k \simeq 20$, with the consequence of erasing all precedently generated baryon asymmetry (if no other macroscopic charges are present). However, at the electroweak phase transition, all the Sakharov's necessary conditions [26] for generating a baryon asymmetry are satisfied, and so it is possible in principle to generate a net baryon number at the electroweak phase transition, through a process known in the literature as electroweak baryogenesis (see [27, 28] for two nice reviews). However, it is known that the SM electroweak phase transition can not, if unmodified, generate the right amount of baryons for two separate reasons. On one hand, CP violating interactions are insufficient [29], and, on the other hand, the phase transition is not enough first order for preventing weak sphalerons to be active also after the phase transition [30]. Since this last point is very important for our discussion, let us review it in detail.

Let us suppose in some early phase of the universe we have produced some initial baryon number $B$ and lepton number $L$, and no other macroscopic charge. In particular $B - L = 0$. The quantum number $B + L$ is anomalous, and the equation for the abundance of particles carrying $B + L$ charge is given by:

$$\frac{d\left(\frac{n_{B+L}}{s}\right)}{dt} = -\Gamma\left(\frac{n_{B+L}}{s}\right) \tag{4.2}$$

where $n_{B+L}$ is the number of baryons and leptons per unit volume, $s$ is the entropy density $\sim T^3$, and $\Gamma$ is related to the sphaleron rate [27], $\Gamma \sim \frac{13}{2} N_f T e^{-(\frac{4\pi}{g_2})(\frac{v(T)}{\sqrt{2}T})}$, where $\frac{v(T)}{\sqrt{2}}$ is the temperature dependent higgs vev ($v(T_0) = 246$ GeV as measured in our vacuum), $N_f$ is the number of fermionic families, and $g_2$ is the SU(2) weak coupling. The reason why reactions destroying baryons are faster than reactions creating them

is due to the fact that the relative reaction rate goes as:

$$\frac{\Gamma_+}{\Gamma_-} \sim e^{-\Delta f} \tag{4.3}$$

where $\Delta f$ is the difference in free energy, and $\Gamma_\pm$ are the sphaleron rates in the two directions. Now, it is easy to see that the free energy grows with the chemical potential $\mu_B$, which then grows with the number of baryons $n_B$. In the limit of small difference, we then get eq.(4.2).

This differential equation can be integrated to give:

$$\left(\frac{n_{B+L}}{s}\right)_{\text{final}} \simeq \left(\frac{n_{B+L}}{s}\right)_{\text{initial}} \text{Exp}\left(-\frac{N_f}{g_*}\frac{\sqrt{2}m_{pl}}{v(T_c)}e^{-\left(\frac{4\pi}{g_2}\frac{v(T_c)}{\sqrt{2}T_c}\right)}\right) \tag{4.4}$$

where $T_c$ is the critical density, and where $g_*$ is the number of effective degrees of freedom ($\sim 55$).

If in the universe there is no macroscopic lepton number, than clearly at present time we would have no baryons left, unless:

$$\frac{N_f}{g_*}\frac{\sqrt{2}m_{pl}}{v(T_c)}e^{-\left(\frac{4\pi}{g_2}\frac{v(T_c)}{\sqrt{2}T_c}\right)} \lesssim 1 \tag{4.5}$$

which roughly implies the constraint:

$$\frac{v(T_c)}{T_c} \gtrsim 1 \tag{4.6}$$

This is the so called "baryons wash out", and the origin of the requirement that the electroweak phase transition should be strongly first order.

Note that this is the same condition we would get if we required sphaleron interactions not to be in thermal equilibrium at the end of the phase transition:

$$\frac{\Gamma}{T_c^3} < H \tag{4.7}$$

implies roughly:

$$T_c \, e^{-\frac{4\pi}{g_2}\frac{v(T_c)}{\sqrt{2}T_c}} < \frac{T_c^2}{M_{pl}} \tag{4.8}$$

and so

$$\frac{v(T_c)}{T_c} \gtrsim 1 \tag{4.9}$$

Also note that the requirement for the sphalerons not to be in thermal equilibrium already just after the phase transition is necessary, as otherwise we would have a baryon symmetric universe, which leads to a far too small residual relic density of baryons.

Later on, when we shall study electroweak baryogenesis, we shall get a number for the baryon number. In order to get then the baryon number at, let us say, Big Bang Nucleosynthesis (BBN), we need to multiply that number by the factor in eq.(4.4). In the next sections, we shall consider the requirement in eq.(4.6) fulfilled, and we will consider completely negligible the wash out from the sphalerons coming from eq.(4.4).

Now, let us go back to the higgs phase transition, and let us assume that in the neighborhood of the landscape in which we are, all the high energy mechanisms for producing baryons have been shut down. This is easy to imagine if, for example, the reheating temperature is smaller than the GUT scale. We are then left with the only mechanism of electroweak baryogenesis. From the former discussion, it appears clear that there should be some physics beyond the SM to help to make the phase transition strong enough.

We may achieve this by coupling the higgs field to a singlet $S$, with the potential equal to:

$$V = \lambda S^4 + \lambda_h (h^\dagger h - \tilde{\lambda} S^2)^2 + \frac{1}{2} m_S^2 S^2 + m_h^2 h^\dagger h \tag{4.10}$$

where we have assumed a symmetry $S \to -S$. We can couple this field to two fermions $\Psi, \Psi^c$, which are charged under a non-Abelian gauge group through the interaction

$$k_S S \Psi \Psi^c \tag{4.11}$$

In order to preserve the symmetry $S \to -S$, we give the fields $\Psi, \Psi^c$ charge $i$. We can then assume that this sector undergos confinement and chiral symmetry breaking at its QCD scale determined by dimensional transmutation

$$< \Psi\Psi^c > \sim \Lambda^3 \tag{4.12}$$

which is naturally exponentially smaller than the cutoff of the theory. We assume that this phase transition is first order, so that departure from thermal equilibrium is guaranteed.

Now, following our discussion in the introduction, suppose that, scanning in the landscape, the only parameters which are effectively scanned are the relevant couplings $m_h$ and $m_S$. If then we must have baryons in our universe so that clumped structures can form, than we need to be in the vacuum in which these two parameters allow for a strong enough first order phase transition in the electroweak sector. So, we have to require that this phase transition triggers the electroweak phase transition. It is clear that this can only be if it triggers a phase transition in the $S$ field, which is possible then only if $m_S$ is of the order of $\Lambda$. Finally, the phase transition in $S$ can trigger a strong first order phase transition in the higgs field only if again $m_h \sim m_S \sim \Lambda$ (for a more detailed discussion, see next subsection). So, summarizing, we see that, the requirement of having baryons in the universe forces the higgs mass to be exponentially smaller than the cutoff, solving in this way the hierarchy problem.

In order to produce baryons, we still need to improve the CP violating interactions, that in the SM are not strong enough. We can minimally extend the introduced model to include a singlet $s$ and 2 SU(2) doublets $\Psi_\pm$, with hypercharge $\pm 1/2$ (notice that they have the same quantum numbers as higgsinos in the Minimal Supersymmetric Standard Model (MSSM)), with the following Yukawa couplings:

$$kSss + k'S\Psi_+\Psi_- + gh^\dagger\Psi_+ s + g'h\Psi_- s \tag{4.13}$$

There is then a reparametrization invariant CP violating phase:

$$\theta = \arg(kk' g^* g'^*) \tag{4.14}$$

The mass terms for this new fields can be prohibited giving proper charges to the fields $s, \Psi_\pm$. This implies that, since at the electroweak phase transition these new fermions get a mass of order of the electroweak scale, and also because of the fact that the lightest fermion is stable, we actually have a nice candidate for dark matter. This last point is a connection between the higgs mass, which, up to this point, we have just assured to be exponentially smaller than the cutoff, and the weak scale, but this connection will come out quite naturally later. So, if this model happens to describe our universe, what we should see at LHC should be the higgs, the two new singlets $S$ and $s$, and the two new doublets $\Psi_\pm$.

Since the model is particularly minimal, it is interesting to explore the possibility for generating the baryon number of the universe in more detail. Before doing so, however, let us see in more detail how the vevs of the higgs and of the singlet $S$ are changed by the phase transition.

### 4.2.1 Phase Transition more in detail

Before going on, here we show more in detail how the requirement of having a strong first order phase transition leads to have $m_S \sim m_h \sim \Lambda$.

In unitary gauge, the equations to minimize the potential are (from here on, we mean by $S$ also the vev of the field $S$; the meaning will be clear by the contest):

$$4\lambda S^3 - 4\lambda_h \tilde{\lambda} S(\frac{v^2}{2} - \tilde{\lambda} S^2) + m_S^2 S + k_S \Lambda^3 \Theta(T_c - T) = 0 \tag{4.15}$$

$$2\lambda_h(\frac{v^2}{2} - \tilde{\lambda} S^2)\frac{v}{\sqrt{2}} + 2m_h^2 \frac{v}{\sqrt{2}} = 0 \tag{4.16}$$

where $T_c$ is the critical temperature. The first equation comes from the derivative with respect to $S$, and we will refer to it as $S$ equation, while for the other we will use the name $h$ equation.

We first consider the case $m_S^2 > 0$ and $m_h^2 > 0$. Before the phase transition, we have the minimum at the symmetric vacua:

$$S = 0,\ v = 0,\ \text{for } T > T_c \tag{4.17}$$

For $T < T_c$, the minimum conditions change, and we can not solve them analytically. We can nevertheless draw some important conclusions. Let us consider the minimum equation for $S$, which is the only equation which changes. Let us first consider the case $m_S \gg \Lambda$. In this case, we can consistently neglect the cubic terms in the $S$ equation, to get:

$$S \simeq -\frac{k_S \Lambda^3}{(m_S^2 - 2\tilde{\lambda}\lambda_h v^2)} \tag{4.18}$$

Then, if $m_S^2 \gg 2\tilde{\lambda}\lambda_h v^2$, we have:

$$S \simeq -\frac{k_S \Lambda^3}{m_S^2} \tag{4.19}$$

$$v = 0 \tag{4.20}$$

while the other solutions are still unphysical, as:

$$\frac{v^2}{2} \simeq -\frac{m_h^2}{\lambda_h} + \tilde{\lambda}\frac{(k_S^2 \Lambda^6)}{m_S^4} < 0 \tag{4.21}$$

If $m_S^2 \ll 2\tilde{\lambda}\lambda_h v^2$, then:

$$S \simeq -\frac{k_S \Lambda^3}{2\tilde{\lambda}\lambda_h v^2} \tag{4.22}$$

For the higgs, the non null solution is:

$$v^2 \simeq -\frac{m_h^2}{\lambda_h} + \tilde{\lambda}\left(\frac{k_S^2 \Lambda^6}{4\tilde{\lambda}^2 \lambda_h^2 v^4}\right) \tag{4.23}$$

which has some relevant effect for the electroweak phase transition only if $m_h \sim \Lambda$. But in that case $v \sim \Lambda$, and from $m_S^2 \ll 2\tilde{\lambda}\lambda_h v^2$ we get that $m_S^2 \ll \Lambda^2$, in contradiction with our initial assumption. Then, if $\frac{m_S^2 - 2\tilde{\lambda}\lambda_h v^2}{S^2} \ll 1$, in the $S$ equation, we can

consistently consider just the cubic term, to get:

$$S \simeq -\frac{k_S^{1/3}\Lambda}{4^{1/3}(\lambda+\tilde{\lambda}\lambda_h)^{1/3}} \tag{4.24}$$

then, the non null solution for $v^2$ becomes:

$$\frac{v^2}{2} \simeq -\frac{m_h^2}{\lambda_h} + \tilde{\lambda}\left(\frac{k_S^{2/3}\Lambda^2}{4^{2/3}(\lambda+\tilde{\lambda}\lambda_h)(\lambda+\tilde{\lambda}\lambda_h)}\right) \tag{4.25}$$

which has some relevant effect only if $m_h^2 \ll \Lambda^2$. However, in this case the condition $\frac{m_S^2-2\tilde{\lambda}\lambda_h v^2}{S^2} \ll 1$ would imply $\frac{m_S}{\Lambda} \ll 1$, again in contradiction with our assumptions.

So, in order to have some effect on the higgs phase transition, we are left with the only possibility of having $m_S \ll \Lambda$.

Restricting to this, consistently, we can neglect the linear term in the $S$ equation, to have:

$$4\lambda S^3 - 4\lambda_h\tilde{\lambda}S\left(\frac{v^2}{2} - \tilde{\lambda}S^2\right) = -k_S\Lambda^3 \tag{4.26}$$

$$2\lambda_h\left(\frac{v^2}{2} - \tilde{\lambda}S^2\right) = -2m_h^2 \tag{4.27}$$

which implies the following equation for $S$:

$$4\lambda S^3 + 4\tilde{\lambda}m_h^2 S = -k_S\Lambda^3 \tag{4.28}$$

For $m_h \gg \Lambda$, we have:

$$S = -\frac{k_S\Lambda^3}{4\tilde{\lambda}m_h^2} \tag{4.29}$$

and the non null solution for $v$ is still not physical:

$$\frac{v^2}{2} = -\frac{m_h^2}{\lambda_h} + \tilde{\lambda}\left(\frac{k_S\Lambda^3}{4\tilde{\lambda}m_h^2}\right)^2 < 0 \tag{4.30}$$

So, finally, we have that in order to have a strong first order phase transition triggered by the new sector, we are forced to have $m_h \ll \Lambda$, which is what we wanted to show. In detail, for $m_h \ll \Lambda$, we implement the following phase transition

$$S:\ 0 \to -\frac{k_S^{1/3}\Lambda}{(4\lambda)^{1/3}} \qquad (4.31)$$
$$v:\ 0 \to 2^{1/3}\frac{\tilde{\lambda}^{1/2}k_S^{1/3}}{\lambda^{1/3}}\Lambda$$

Now, the final step is to show that, not only $m_h \ll \Lambda$ and $m_S \ll \Lambda$, but that actually $m_h \sim \Lambda$ and $m_S \sim \Lambda$. The argument for this is that, scanning in the landscape, it will be generically much more difficult to encounter light scalar masses, as they are fine tuned. So, in the anthropically allowed range, our parameters shall most probably be in the upper part of the allowed range. So, we conclude that this model predicts $m_h \sim m_S \sim \Lambda$, as we wanted to show.

This phase transition must satisfy the requirement that the sphalerons are ineffective ($\frac{v(T_c)}{T_c} \gtrsim 1$), after the phase transition, which occurs at, roughly, the critical temperature $T_c \sim \Lambda$. So:

$$\frac{v(T_c)}{T_c} \simeq \frac{\tilde{\lambda}^{1/2}(2k_S)^{1/3}}{\lambda^{1/3}} \gtrsim 1 \qquad (4.32)$$

which can clearly be satisfied for some choices of the couplings. In order to better understand the natural values of the ratio $v(T_c)/T_c$ in terms of the scalar couplings, it is worth to notice that the coupling $\tilde{\lambda}$ appears in the lagrangian as always multiplied by $\lambda_h$. So, the coupling which naturally tends to be equal to the other ones in the lagrangian is $\lambda_e \equiv \lambda_h\tilde{\lambda}$. With this redefinition, we get the constraint:

$$\frac{v(T_c)}{T_c} \simeq \left(\frac{\lambda_e}{\lambda_h}\right)^{1/2}\left(\frac{2k_S}{\lambda}\right)^{1/3} \gtrsim 1 \qquad (4.33)$$

which can clearly be satisfied with some choice of the parameters. It is also worth to write the ratio of the vevs of $S$ and $h$ after the phase transition:

$$\frac{S}{v} = \left(\frac{\lambda_h}{\lambda_e}\right)^{1/2} \qquad (4.34)$$

We can also analyze the case in which $m_h^2 < 0$. In this case, the electroweak phase transition would occur before the actual strong sector phase transition. However,

since we know that in the SM the phase transition is neither enough first order, nor enough CP violating, we still need, in order to have baryon formation, to require that the strong sector phase transition triggers a phase transition in the higgs sector. It is then easy to see that all the former discussion still applies with tiny changes, and we get the same condition $m_S^2 \sim m_h^2 \sim \Lambda^2$. There is a further check to make, though, which is due to the fact that, in order for baryogenesis to occur, we need an unsuppressed sphaleron rate in the exterior of the bubble. This translates in the requirement, for $m_h^2 < 0$:

$$\frac{|m_h|}{\Lambda} \ll 1 \tag{4.35}$$

which can be satisfied in some vacua.

In the next of this chapter, we will always assume that these conditions are satisfied, and the sphalerons are suppressed in the broken phase.

Now, we are ready to treat baryogenesis in detail.

## 4.3 Electroweak Baryogenesis

During the electroweak phase transition, we have all the necessary conditions to fulfill baryogenesis [27, 28]. We have departure from thermal equilibrium because of the phase transition; we have CP and C violation because of the CP and C violating interactions; and finally we have baryon violation because of the unsuppressed sphaleron rate. The sphaleron rate per unit time per unit volume is in fact unsuppressed in the unbroken phase (see eq.(4.1)).

There are various different effects that contribute to the final production of baryons. For example, CP violation can be due just to some CP violating Yukawa coupling in the mass matrix, or it can be mainly due to the fact that, in the presence of the wall, the mass matrix is diagonalized with space-time dependent rotation matrixes, which induce CP violation. Further, CP violation can be accounted for by some time dependent effective coupling in some interaction terms. Baryon number production as well can be treated differently. In the contest of electroweak baryogenesis which we are dealing with, there are mainly two ways of approaching the problem, one in which

the baryon production occurs locally where the CP violation is taking place, so called local baryogenesis, or one in which it occurs well in the exterior of the bubble, in the unbroken phase, in the so called non local baryogenesis. At the current status of the art, it appears that the non local baryogenesis is the dominant effect, at least for not very large velocity of the wall $v_w$, which however is believed to be not large because the interactions with the plasma tend to slow down the wall considerably [31], and we concentrate on this case (see Appendix A for a brief treatment of baryogenesis in the fast wall approximation).

In order to compute the produced baryon abundance, we follow a semiclassical method developed in [32]. A method based on the quantum Boltzmann equation and the closed time path integral formalism was developed in [33], making a part of the method more precise. However, the corrections given by applying this procedure to our case can be expected to be in general not very important once compared to the uncertainties associated to our poor knowledge of certain parameters of the electroweak phase transition, as it will become clear later, which make the computed final baryon abundance reliable only to approximately one order of magnitude [32]. Further, it is nice to note that our general conclusions will be quite robust under our estimated uncertainty in the computation of the baryon abundance. For these reasons, the method in [32] represents for us the right mixture between accuracy and simplicity which is in the scope of our study.

Since the method is quite contorted, let us see immediately where the basic ingredients for baryogenesis are. Departure from thermal equilibrium obviously occurs because of the crossing of the wall. C violation occurs because of the $V - A$ nature of the interactions. CP violation occurs because the CP violating phases in the mass matrix are rotated away at two different points by two different unitary matrix such that $U(x)^\dagger U(x + dx) \neq 1$. There could be other sources of CP violation, but, in our case, this is the dominant one. Baryon production occurs instead well in the exterior of the wall, in the so called non-local baryogenesis approach, where the weak sphaleron rate is unsuppressed.

Let us anticipate the general logic. The calculation is naturally split into two

part. In the first part, we compute the sources for CP violating charges which are due to the CP violating interactions of the particles with the incoming wall. This calculation will be done restricting ourself to the vicinity of the wall, and solving a set of coupled Dirac-Majorana equations to determine the transmission and reflection coefficients of the particles in the thermal bath when they hit the wall, which are different for particles and antiparticles. In the wall rest frame, the wall is perceived as a space-time dependent mass term. This will give rise to a CP violating current. The non null divergence of this current will be the input of the second part of the calculation. In this second part, we shall move to a larger scale, and describe the plasma in a fluid approximation, where we shall study effective diffusion equations. The key observation is that, once the charges have diffused in the unbroken phase, thermal equilibrium of the sphalerons will force a net baryon number. In fact, in the presence of SU(2) not neutral charges, the equilibrium value of the baryon number is *not* zero:

$$(B+L)_{eq} = \sum_i c_i Q_i \tag{4.36}$$

where $c_i$ are coefficients which depends on the different charges . Once produced, the baryon number will diffuse back in the broken phase, where, due to the suppression of the sphaleron rate, it will be practically conserved up to the present epoch. This will end our calculation.

In the next two subsections, we proceed to the two parts of the outlined calculation.

### 4.3.1 CP violation sources

We begin by computing the source for the CP violating charges, following [32]. We restrict to the region very close the the wall, so that the wall can be considered flat, and we can approximately consider the problem as one dimensional. We consider a set of particles with mass matrix $M(z)$ where $z$ is the coordinate transverse to the wall, moving , in the rest frame of the wall, with energy-momentum $E, \vec{k}$. Taken $z_0$ as the last scattering point, these particles will propagate freely for a mean free time

$\tau_i$, when they will rescatter at the point $z_0+\tau_i v$, where $v$ is the velocity perpendicular to the wall, $k_{tr}/E$. Now, because of the space dependent CP violating mass matrix, these particles will effectively scatter, and the probability of being transmitted and reflected will be different for particles and antiparticles. This will create a current for some charges, whose divergence will then be the source term in the diffusion equations we shall deal with in the next section. The effect will be particularly large for charges which are explicitly violated by the presence of the mass matrix, and we shall restrict to them.

We introduce $J_\pm$ as the average current resulting from particles moving towards the positive and the negative $z$ direction, between $z_0$ and $z_0+\Delta$, where $\Delta=\tau v$, and $\tau$ is the coherence time of the particles due to interactions with the plasma [32]. $J_\pm$ are the CP violating currents associated with each layer of thickness $\Delta$. $J_+$ receives, for example, contributions from particles originating from the thermal bath at $z_0$ with velocity $v$, and propagating until $z_0+\Delta$, as well as from particles originating at $z_0+\Delta$ with velocity $-v$, and being reflected back at $z_0+\Delta$. The formula for $J_\pm$ is given by:

$$J_+ = \left(\mathrm{Tr}\left(\rho_{z_0}\left(T^\dagger Q T - \bar{T}^\dagger Q \bar{T}\right)\right) - \mathrm{Tr}\left(\rho_{z_0+\Delta}\left(\tilde{R}^\dagger Q \tilde{R} - \bar{\tilde{R}}^\dagger Q \bar{\tilde{R}}\right)\right)\right)(1,0,0,\tilde{v}) \quad (4.37)$$

$$J_- = \left(\mathrm{Tr}\left(\rho_{z_0}\left(R^\dagger Q R - \bar{R}^\dagger Q \bar{R}\right)\right) - \mathrm{Tr}\left(\rho_{z_0+\Delta}\left(\tilde{T}^\dagger Q \tilde{T} - \bar{\tilde{T}}^\dagger Q \bar{\tilde{T}}\right)\right)\right)(1,0,0,-v) \quad (4.38)$$

where $R(\bar{R})$ and $T(\bar{T})$ are reflection and transmission matrices of particles (antiparticles) produced at $z_0$ with probability $\rho_{z_0}$, evolving towards positive $z$; while $\tilde{T}$ and $\tilde{R}$ are the correspondent quantities for particles produced at $z_0+\Delta$ with probability $\rho_{z_0+\Delta}$ and evolving towards negative $z$; $v$ is the group velocity perpendicular to the wall at the point $z_0$, and $\tilde{v}$ is the same quantity at $z_0+\Delta$; $Q$ is the operator correspondent to the chosen charge; and the trace is taken over all the relevant degrees of freedom and averaged over location $z_0$ within a layer of thickness $\Delta$. When boosted in the plasma rest frame, these currents will become the building block to construct the CP violating source for the charges that, diffusing into the unbroken phase, will let the production of baryon number possible.

Now, consider a small volume of the plasma, in the plasma rest frame. As the wall crosses it, it leaves a current density equal to $(J_+ + J_-)^\mu_{plasma}$ every time interval $\tau$, where the subscript *plasma* refers to the quantity boosted in the plasma frame. So, at a time $t$, the total current density accumulated will be given by:

$$s^\mu = \int_{t-\tau_R}^{t} dt' \frac{1}{\tau}(J_+(\vec{x},t') + J_-(\vec{x},t')))^\mu_{plasma} \tag{4.39}$$

where $\tau_R$ is the relaxation time due to plasma interaction. From this, the rate of change of the charge $Q$ per unit time is given by:

$$\begin{aligned} \gamma_Q(\vec{x},t) = \quad & \partial_\mu s^\mu = \\ & \frac{1}{\tau}\left(J_+(\vec{x},t) + J_-(\vec{x},t)\right)^0_{plasma} - \frac{1}{\tau}\left(J_+(\vec{x},t-\tau_R) + J_-(\vec{x},t-\tau_R)\right)^0_{plasma} \\ & - \int_{t-\tau_R}^{t} dz \partial_z (J_+ + J_-)^z_{plasma} \end{aligned} \tag{4.40}$$

Since in the SM CP violation is very small, and already proved to be not enough to account for the baryon number of the universe, we can clearly concentrate in the sector of the neutral particles of the new theory, where the mass matrix is given by:

$$M(z) = \begin{pmatrix} kS(z) & \frac{gv}{\sqrt{2}} & \frac{g'v}{\sqrt{2}} \\ \frac{gv}{\sqrt{2}} & 0 & k'S(z) \\ \frac{g'v}{\sqrt{2}} & k'S(z) & 0 \end{pmatrix}$$

The transmission and reflection coefficients can be found by solving the free coupled Dirac-Majorana equations for these particles with the mass matrix given in $M(z)$. We can solve this by a method developed in [32], in a perturbative expansion in mass insertion. As it is explained in [32, 34], the small parameter in the expansion is $m\Delta$, where $m$ is the typical mass of the particles, in the case $w\Delta < 1$, or $m/w$ in the case $w\Delta > 1$. In both cases, the expansion parameter is smaller than one. This can be understood noticing the analogy of our system with the scattering off a diffracting medium with a step potential of order $m$. In that case, reflection and transmission are comparable (and this is the only case in which we produce a net CP violating

charge) only if the wave packet penetrates coherently over a distance of order $1/m$, and has few oscillation over that distance. Suppression of the reflection occurs both if $m\Delta \ll 1$ and if $m/w \ll 1$. In the first case, this is because only a layer of thickness $\Delta$ contributes to the coherent reconstruction of the reflected wave, while in the second case, because fast oscillations tend to attenuate the reconstruction of the reflected wave. Up to sixth order in the mass insertion, we get:

$$\begin{aligned} T = \quad & 1 - \int_0^\Delta dz_1 \int_0^{z_1} dz_2 M_2 M_1^* e^{2iw(z_1-z_2)} + \\ & + \int_0^\Delta dz_1 \int_0^{z_1} dz_2 \int_{z_2}^\Delta dz_3 \int_0^{z_3} dz_4 M_4 M_3^* M_2 M_1^* e^{2iw(z_1-z_2+z_3-z_4)} + \\ & - \int_0^\Delta dz_1 \int_0^{z_1} dz_2 \int_{z_2}^\Delta dz_3 \int_0^{z_3} dz_4 \int_{z_4}^\Delta dz_5 \int_0^{z_5} dz_6 \\ & M_6 M_5^* M_4 M_3^* M_2 M_1^* e^{2iw(z_1-z_2+z_3-z_4+z_5-z_6)} + \\ & + \ldots \end{aligned} \tag{4.41}$$

$$\begin{aligned} \tilde{T} = \quad & 1 - \int_0^\Delta dz_1 \int_{z_1}^\Delta dz_2 M_2^* M_1 e^{-2iw(z_1-z_2)} + \\ & + \int_0^\Delta dz_1 \int_{z_1}^\Delta dz_2 \int_0^{z_2} dz_3 \int_{z_3}^\Delta dz_4 M_4^* M_3 M_2^* M_1 e^{-2iw(z_1-z_2+z_3-z_4)} + \\ & - \int_0^\Delta dz_1 \int_{z_1}^\Delta dz_2 \int_0^{z_2} dz_3 \int_{z_3}^\Delta dz_4 \int_0^{z_4} dz_5 \int_{z_5}^\Delta dz_6 \\ & M_6^* M_5 M_4^* M_3 M_2^* M_1 e^{-2iw(z_1-z_2+z_3-z_4+z_5-z_6)} + \\ & + \ldots \end{aligned} \tag{4.42}$$

$$\begin{aligned} R = \quad & - \int_0^\Delta dz_1 M_1^* e^{2iw(z_1)} + \\ & + \int_0^\Delta dz_1 \int_0^{z_1} dz_2 \int_{z_2}^\Delta dz_3 M_3^* M_2 M_1^* e^{2iw(z_1-z_2+z_3)} + \\ & - \int_0^\Delta dz_1 \int_0^{z_1} dz_2 \int_{z_2}^\Delta dz_3 \int_0^{z_3} dz_4 \int_{z_4}^\Delta dz_5 M_5^* M_4 M_3^* M_2 M_1^* e^{2iw(z_1-z_2+z_3-z_4+z_5)} \\ & + \ldots \end{aligned} \tag{4.43}$$

$$\tilde{R} = \int_0^{\Delta} dz_1 M_1 e^{-2iw(z_1)} + \tag{4.44}$$
$$- \int_0^{\Delta} dz_1 \int_{z_1}^{\Delta} dz_2 \int_0^{z_2} dz_3 M_3 M_2^* M_1 e^{-2iw(z_1 - z_2 + z_3)} +$$
$$+ \int_0^{\Delta} dz_1 \int_{z_1}^{\Delta} dz_2 \int_0^{z_2} dz_3 \int_{z_3}^{\Delta} dz_4 \int_0^{z_4} dz_5 M_5 M_4^* M_3 M_2^* M_1 e^{-2iw(z_1 - z_2 + z_3 - z_4 + z_5)}$$
$$+ \ldots$$

where $M_i = M(z_i)$.The analogous quantities for the antiparticles are obtained replacing $M \rightarrow M^*$ in all the former formulas.

We also need to have the density matrices $\rho_{z_0}$ and $\rho_{z_0+\Delta}$.We can choose these densities as describing thermal equilibrium densities in eigenstates of the unbroken phase:

$$\rho_{z_0} = \mathrm{Diag}\left(n_s(E,\tilde{v}), n_{\psi_+}(E,\tilde{v}), n_{\psi_-}(E,\tilde{v})\right) \tag{4.45}$$

where $n(E,v)$ is the Fermi-dirac distribution, boosted in the wall frame:

$$n = \frac{1}{e^{\frac{\gamma_w(E - v_w k_{tr})}{T_c}} + 1} \tag{4.46}$$

and $\rho_{z_0+\Delta} = \rho_{z_0}(\tilde{v} \rightarrow -v)$. The motivation of this is that particles are produced in interaction eigenstates which differ from mass eigenstates by a unitary rotation; ignoring this, amounts at ignoring small corrections of order $(M(z)/T_c)^2$. The choice of thermal distribution is particularly good in the small velocity $v_w$ regime, in which we have restricted, where the non thermal contribution is of order $v_w$, and it induces corrections of order $v_w^2$ in the final baryon density [32].

Finally, we have to consider the charges which can play a role in generating the baryon number. When choosing such charges, one has to consider that the most important charges are those which are approximately conserved in the unbroken phase, as these are the ones which can efficiently diffuse in the unbroken phase, and induce a large generation of baryon number. Keeping this in mind, it is easy to see that the only relevant charge in our model is the "higgs number" charge, which in the same basis in which we expressed the mass matrix, for the new CP violating sector

particles, is given by:

$$Q_h = \mathrm{Diag}\,(0,0,1,-1) \tag{4.47}$$

The name "higgs number" just comes from the fact that the fields $\Psi_\pm$ have the same quantum numbers as higgsinos in the MSSM. Now, we can substitute in the formulas for $J_+$ and $J_-$. In order to keep some analytical expression, we decide to do a derivative expansion $M(z) = M(z_0)+M'(z_0)(z-z_0)+\mathcal{O}(\tau/w)^2$ and $v = \tilde{v}+\mathcal{O}(\tau/w)^2$. This expansion is justified in the parameter range $\tau \ll w$, which is expected to be approximately fulfilled [34].

Unlike in the case of the analogous calculation for the MSSM [32] where the leading effect occurs at fourth order in mass insertion, here the leading contribution occurs at sixth order. We will explain later the reason of this. For the moment, we get:

$$\begin{aligned}
&J_+ = (1,0,0,v) \times \Big( \\
&+4 \int_0^\Delta dz_1 \int_0^{z_1} dz_2 \int_{z_2}^\Delta dz_3 \int_0^{z_3} dz_4 \int_{z_4}^\Delta dz_5 \int_0^{z_5} dz_6 \\
&\sin(2w(z_1 - z_2 + z_3 - z_4 + z_5 - z_6))\mathrm{Im}\,(\rho_{z_0} Q_h M_6 M_5^* M_4 M_3^* M_2 M_1^*) + \\
&-4 \int_0^\Delta dz_1 \int_0^{z_1} dz_2 \int_0^\Delta dz_3 \int_0^{z_3} dz_4 \int_{z_4}^\Delta dz_5 \int_0^{z_5} dz_6 \\
&\sin(2w(z_1 - z_2 - z_3 + z_4 - z_5 + z_6))\mathrm{Im}\,(\rho_{z_0} Q_h M_1 M_2^* M_6 M_5^* M_4 M_3^*) + \\
&+4 \int_0^\Delta dz_1 \int_0^\Delta dz_2 \int_{z_2}^\Delta dz_3 \int_0^{z_3} dz_4 \int_{z_4}^\Delta dz_5 \int_0^{z_5} dz_6 \\
&\sin(2w(z_1 - z_2 + z_3 - z_4 + z_5 - z_6))\mathrm{Im}\,(\rho_{z_0+\Delta} Q_h M_1^* M_6 M_5^* M_4 M_3^* M_2) \Big)
\end{aligned} \tag{4.48}$$

$$
\begin{aligned}
J_- = (1,0,0,-v) \times \Big( & \qquad (4.49)\\
-4 \int_0^{\Delta} dz_1 \int_{z_1}^{\Delta} dz_2 \int_0^{z_2} dz_3 \int_{z_3}^{\Delta} dz_4 \int_0^{z_4} dz_5 \int_{z_5}^{\Delta} dz_6 & \\
\sin(2w(z_1 - z_2 + z_3 - z_4 + z_5 - z_6)) \mathrm{Im}\left(\rho_{z_0+\Delta} Q_h M_6 M_5^* M_4 M_3^* M_2 M_1^*\right) + & \\
+4 \int_0^{\Delta} dz_1 \int_{z_1}^{\Delta} dz_2 \int_0^{\Delta} dz_3 \int_{z_3}^{\Delta} dz_4 \int_0^{z_4} dz_5 \int_{z_5}^{\Delta} dz_6 & \\
\sin(2w(z_1 - z_2 - z_3 + z_4 - z_5 + z_6)) \mathrm{Im}\left(\rho_{z_0+\Delta} Q_h M_1 M_2^* M_6 M_5^* M_4 M_3^*\right) + & \\
-4 \int_0^{\Delta} dz_1 \int_0^{\Delta} dz_2 \int_0^{z_2} dz_3 \int_{z_3}^{\Delta} dz_4 \int_0^{z_4} dz_5 \int_{z_5}^{\Delta} dz_6 & \\
\sin(2w(z_1 - z_2 + z_3 - z_4 + z_5 - z_6)) \mathrm{Im}\left(\rho_{z_0} Q_h M_1^* M_6 M_5^* M_4 M_3^* M_2\right) \Big) &
\end{aligned}
$$

where the $z$ dependence in each mass matrix $M_i$ is to be understood at linearized level.

We can substitute the results in eq.(4.40), to get an expression for the higgs charge source. In reality, if we take the relaxation time large enough, and if we keep performing a derivative expansion, only the first term in eq.(4.40) is relevant. At first order in the wall velocity, we get:

$$
\begin{aligned}
\gamma_Q = \quad & \frac{\gamma_w v_w}{\tau} T_c^7 \mathcal{J} \times \qquad (4.50)\\
& \Big( \sum_{i=\psi,s} \int \frac{d^3k}{2\pi^3} \frac{f(w_i \Delta)}{w^7} v_i \frac{e^{E_i/T_c}}{(1+e^{E_i/T_c})^2} \frac{E_i}{T_c} \Big)
\end{aligned}
$$

where $\mathcal{J}$ is a CP violating invariant:

$$
\mathcal{J} = \frac{1}{4} g g' k k' (g^2 - g'^2) \sin(\theta) \qquad (4.51)
$$

and $f_i(w\Delta)$ is:

$$f_\Psi(w\Delta) = \frac{v(z_0)^3 S(z_0)}{24T_c^7}((S'(z_0)(9 - 24w^2\Delta^2 - 14w^4\Delta^4)v(z_0) - 9v'(z_0)S(z_0) \quad (4.52)$$
$$-2w^2\Delta(11v'(z_0)\Delta(3 + w^2\Delta^2) + 3(5 + 2w^2\Delta^2)v(z_0))S(z_0) +$$
$$6\cos(6w\Delta)(-S'(z_0)v(z_0) + v'(z_0)S(z_0)) + 6\cos(4w\Delta)(2S'(z_0)(-1 + 3w^2\Delta^2)v(z_0)$$
$$+2v'(z_0)S(z_0) + w^2\Delta(-3v'(z_0)\Delta + v(z_0))S(z_0)) +$$
$$3\cos(2w\Delta)(3S'(z_0)(1 + 6w^2\Delta^2)v(z_0)$$
$$-3v'(z_0)S(z_0) + 2w^2\Delta(3v'(z_0)\Delta + 4v(z_0))S(z_0))$$
$$+2w(2S'(z_0)\Delta(-3 + 14w^2\Delta^2)v(z_0) + (5v'(z_0)\Delta(3 + 7w^2\Delta^2) +$$
$$3(1 + 7w^2\Delta^2)v(z_0))S(z_0))\sin(2w\Delta)3w(16S'(z_0)\Delta v(z_0)$$
$$+(-13v'(z_0)\Delta + v(z_0))S(z_0))\sin(4w\Delta) + 6w\Delta)$$
$$(-S'(z_0)v(z_0) + v'(z_0)S(z_0))\sin(6w\Delta))))$$

$$f_s(w\Delta) = \frac{v(z_0)^3 S(z_0)}{48T_c^7}(S'(z_0)(15 + 12w^2\Delta^2 - 28w^4\Delta^4)v(z_0) \quad (4.53)$$
$$-15v'(z_0)S(z_0) - 4w^2\Delta(v'(z_0)\Delta(48 + 11w^2\Delta^2) +$$
$$3(5 + 2w^2\Delta^2)v(z_0))S(z_0) + 12\cos(6w\Delta)(S'(z_0)v(z_0)$$
$$-v'(z_0)S(z_0)) + 3\cos(4w\Delta)(S'(z_0)$$
$$(1 - 12w^2\Delta^2)v(z_0) - v'(z_0)S(z_0) + 4w^2\Delta(6v'(z_0)\Delta + v(z_0))S(z_00) +$$
$$6\cos(2w\Delta(S'(z_0)(-5 + 14w^2\Delta^2)v(z_0) + 5v'(z_0)S(z_0) + 2w^2\Delta(5\ v'(z_0)\Delta +$$
$$4v(z_0))S(z_0)) + 12w(S'(z_0)\Delta(-7 + 6w^2\Delta^2)v(z_0) + (v(z_0) +$$
$$\Delta(5v'(z_0)(2 + 3w^2\Delta^2) + 7w^2\Delta v(z_0))S(z_0))\sin(2w\Delta)$$
$$-6w(-9S'(z_0)\Delta v(z_0) + (12v'(z_0)\Delta + v(z_0))S(z_0))\sin(4w\Delta) + 12w\Delta(S'(z_0)v(z_0)$$
$$-v'(z_0)S(z_0))\sin(6w\Delta)))$$

where $z_0$ here is a typical point in the middle of the wall. We can estimate the coherence time as $\tau \sim (g_w T_c)^{-1}$, and so we can take, roughly, the typical interval which is valid also in the MSSM [32]: $15 \leq \tau T_c \leq 35$, and in the approximation

of making the particles massless, which is still consistent with our approximations, we can integrate numerically the integral, and fit it linearly in $\tau$ (which is a good approximation in the range of interest), to obtain:

$$\gamma_Q(\vec{x},t) \simeq 24 v_w \gamma_w \left(gg'kk'(g^2-g'^2)\sin(\theta)\right) \times \frac{\left(1+\frac{1}{8}(\tau T_c - 25)\right)}{\tau T_c} \frac{v^3 S}{T_c^3} \left(S'v - v'S\right) \tag{4.54}$$

Even though the reparametrization invariant CP violating phase $\theta$ requires only 4 Yukawa couplings to be present in the theory, it is somewhat puzzling that the leading effect appears at sixth order in the couplings. The reason is as follows. In the case $g = g'$, there is an approximate $Z_2$ symmetry which exchanges the $\Psi_\pm$ fields. This is only an approximate symmetry, because $\Psi_\pm$ differ by their hypercharge. However, the hypercharge is considered a subleading effect here, and never comes into play in our computation, and so we do not see the breaking of this symmetry. The $Z_2$ symmetry has, in the basis we have been using up to now, the matrix form:

$$Z_2 = \begin{pmatrix} 1 & 0 & 0 \\ 0 & 0 & 1 \\ 0 & 1 & 0 \end{pmatrix}$$

We clearly see that:

$$[M(z), Z_2] = 0, \ [\rho(z), Z_2] = 0, \ \{Q, Z_2\} = 0 \tag{4.55}$$

which then implies that:

$$Tr\left(\rho_{z_0} T Q T^\dagger\right) = 0 \tag{4.56}$$

and similar for the others terms in $J_+$ and $J_-$. So, in the limit in which $g = g'$, the baryon asymmetry should vanish. Then, since each particle needs to have an even number of mass insertions to be transmitted or reflected, and since the CP violation requires at least 4 mass insertion, we finally obtain that the coupling dependence in the CP violating source must be of the form present in eq.(4.54). From this discussion,

it is clear that in the case $g = g'$ the baryon production will be heavily suppressed, and, from what we will see later, it will be clear that the couplings in this case will have to be so large to necessarily hit a Landau pole at very low energies, making the model badly defined. We shall neglect this degeneracy of the couplings for the next of the chapter.

Now, we are ready to begin the second part of the computation.

### 4.3.2 Diffusion Equations

Here, we begin the second part of the calculation, still following [32]. We turn to analyze the system at a larger scale, and approximate it to a fluid. We then study the evolution of the CP violating charges due to the presence of the sources and of the diffusion effects in the plasma. To this purpose, we shall write a set of coupled differential equations which include the effects of diffusion, particle number changing reactions, and CP violating source terms, and we shall solve them to find the various densities. We shall be interested in the evolution of particles which carry some charges which are approximately conserved in the unbroken phase. Near thermal equilibrium, which is a good approximation for small velocities, we can approximate the number density as:

$$n_i = k_i \mu_i T_c^2 / 6 \tag{4.57}$$

where $\mu_i$ is the chemical potential, and $k_i$ is a statistical factor which is equal to 2 for each bosonic degree of freedom, and 1 for each fermionic.

The system of differential equations simplifies a lot if we neglect all couplings except the gauge couplings, the top quark Yukawa coupling, and the Yukawa couplings in the new CP violating sector. From the beginning, we take the interactions mediated from these last ones to be fast with respect to the typical timescale of the fluid. We include the effect of strong sphaleron, but neglect the one of the weak sphalerons until almost the end of the computation. This allows us to forget about leptons. We need only to keep track of the following populations: the top left doublet: $Q = (t_L + b_L)$, the right top: $T = t_R$, the Higgs particle plus our new fields $\Psi_\pm$:$H = h_0 + \Psi_+ + \Psi_-$

Strong sphalerons will be basically the only process to generate the right bottom quarks $B = b_R$, and the quarks of the first two generations $Q_{(1,2)L}, U_R, C_R, S_R, D_R$. This implies that all these abundance can be expressed in terms of the one of $B$:

$$Q_{1L} = Q_{2L} = -2U_R = -2D_R = -2S_R = -2C_R = -2B = 2(Q+T) \tag{4.58}$$

The rate of top Yukawa interaction, Higgs violating process, and axial top number violation are indicated as $\Gamma_y, \Gamma_h, \Gamma_m$, respectively. We take all the quarks to have the same diffusion equation, and the same for the higgs and the $\Psi$s. The charge abundances are then described by the following set of differential equations:

$$\begin{aligned}
\dot{Q} = \quad & D_q\nabla^2 Q - \Gamma_y(Q/k_Q - H/k_H - T/k_T) - \Gamma_m(Q/k_Q - T/k_T) \\
& -6\Gamma_{ss}(2Q/k_Q - T/k_T + 9(Q+T)/k_B) \\
\dot{T} = \quad & D_q\nabla^2 T - \Gamma_y(-Q/k_Q + H/k_H + T/k_T) \\
& -\Gamma_m(-Q/k_Q + T/k_T) + 3\Gamma_{ss}(2Q/k_Q - T/k_T + 9(Q+T)/k_B) \\
\dot{H} = \quad & D_h\nabla^2 H - \Gamma_y(-Q/k_Q + T/k_T + H/k_H) - \Gamma_h H/k_h + \gamma_Q
\end{aligned} \tag{4.59}$$

We can restrict ourselves to the vicinity of the wall, so that we can neglect the curvature of the surface, and assume we can express everything in a variable $\bar{z} = |\vec{r} + \vec{v}_w t|$. The resulting equations of motions become:

$$\begin{aligned}
v_w Q' = \quad & D_q Q'' - \Gamma_y(Q/k_Q - H/k_H - T/k_T) - \Gamma_m(Q/k_Q - T/k_T) \\
& -6\Gamma_{ss}(2Q/k_Q - T/k_T + 9(Q+T)/k_B) \\
v_w T' = \quad & D_q T'' - \Gamma_y(-Q/k_Q + H/k_H + T/k_T) \\
& -\Gamma_m(-Q/k_Q + T/k_T) + 3\Gamma_{ss}(2Q/k_Q - T/k_T + 9(Q+T)/k_B) \\
v_w H' = \quad & D_h H'' - \Gamma_y(-Q/k_Q + T/k_T + H/k_H) - \Gamma_h H/k_h + \gamma_Q
\end{aligned} \tag{4.60}$$

We now assume that $\Gamma_y$ and $\Gamma_{ss}$ are very fast, and we develop the result at $\mathcal{O}(1/\Gamma_y, 1/\Gamma_{ss})$. This allows to algebraically express $Q$ and $T$ in terms of $H$, to get the following re-

lationships:

$$Q = H\left(\frac{k_Q(9k_T - k_B)}{k_H(k_B + 9k_Q + 9k_T)}\right) \tag{4.61}$$

$$T = -H\left(\frac{k_T(2k_B + 9k_Q)}{k_H(k_B + 9k_Q + 9k_T)}\right) \tag{4.62}$$

and, substituting back, we find the following effective differential equation for $H$:

$$v_w H' = \bar{D}H'' - \bar{\Gamma}H + \bar{\gamma} \tag{4.63}$$

where the effective couplings are given by:

$$\bar{D} = \frac{D_q(9k_Qk_T - 2k_Qk_B - 2k_Bk_T) + D_hk_H(9k_Q + 9k_T + k_B)}{9k_Qk_T - 2k_Qk_B - 2k_Bk_T + k_H(9k_Q + 9k_T + k_B)} \tag{4.64}$$

$$\bar{\gamma} = \gamma_Q\left(\frac{k_H(9k_Q + 9k_T + k_B)}{9k_Qk_T - 2k_Qk_B - 2k_Bk_T + k_H(9k_Q + 9k_T + k_B}\right) \tag{4.65}$$

$$\bar{\Gamma} = (\Gamma_m + \Gamma_h)\left(\frac{(9k_Q + 9k_T + k_B)}{9k_Qk_T - 2k_Qk_B - 2k_Bk_T + k_H(9k_Q + 9k_T + k_B)}\right) \tag{4.66}$$

We can estimate the relaxation rates for the higgs number and the axial quark number as [32]:

$$(\Gamma_m + \Gamma_h) \sim \frac{4M_W^2(T_c, z)}{21g^2T_c}\lambda_t^2 \tag{4.67}$$

where $\lambda_t$ is the top Yukawa coupling, and $M_W$ is the $W$ boson mass, and, in order to keep analytical control, we approximate the source term and the relaxation term as step functions:

$$\bar{\gamma} = \tilde{\gamma},\ w > \bar{z} > 0 \tag{4.68}$$

$$\bar{\gamma} = 0,\ \text{otherwise}$$

and

$$\bar{\Gamma} = \tilde{\Gamma},\ \bar{z} > 0 \tag{4.69}$$

$$\bar{\Gamma} = 0,\ \bar{z} < 0$$

For the source term $\bar{\gamma}$, we can take the avaraged value of expression (4.54). However, due to our lack of knowledge of the details of the profiles of the fields during the phase transition, we can just approximate that expression with:

$$\tilde{\gamma}_Q = \quad 24 v_w \gamma_w \left(g g' k k' (g^2 - g'^2) \sin(\theta)\right) \times \frac{\left(1 + \frac{1}{8}(\tau T_c - 25)\right)}{\tau T_c} \frac{v^4 S^2}{T_c^3 \, W} \tag{4.70}$$

where we have taken $S' \sim S/W$ and $v' \sim v/W$, with $W$ the wall width, and we have assumed, as expected, that no cancellation is occurring. Here $S$ and $v$ are taken to be of the order they are today. In the approximation that $\bar{D}$ is constant, and with the boundary conditions given by $H(\pm\infty) = 0$, we have an analytical solution in the unbroken phase [32]:

$$H = \mathcal{A} e^{\bar{z} v_w / \bar{D}} \tag{4.71}$$

where, in the limit that $\bar{D}\tilde{\Gamma} \ll v_w^2$, which is in general applicable,

$$\mathcal{A} \simeq \frac{\bar{\gamma}}{\bar{\Gamma}} \left(1 - e^{-2W\sqrt{\bar{\Gamma}/\bar{D}}}\right) \tag{4.72}$$

Note that diffusion of the higgs field, and so of the other charges, in the unbroken phase, occurs for a distance of order $z \sim \bar{D}/v_w$.

We now turn on the weak sphaleron rate, which is the responsible for the baryon generation. The baryon density follows the following equation of motion:

$$v_w \rho_B = D_q \rho_B'' - \Theta(-\bar{z}) 3 \Gamma_{ws} n_L(\bar{z}) \tag{4.73}$$

where we have assumed that the weak sphaleron operates only in the unbroken phase, and where $n_L$ is the total number density of left fermions. The solution to this equation is given by, at first order in $v_w$:

$$\rho_B = -\frac{3\Gamma_{ws}}{v_w} \int_{-\infty}^{0} d\bar{z} \; n_L(\bar{z}) \tag{4.74}$$

Now, in the approximation in which all the particles in our theory are light, we have:

$$k_Q = 6,\ k_T = 3,\ k_B = 3,\ k_H = 8 \tag{4.75}$$

and in the limit as $\Gamma_{ss} \to \infty$, the resulting baryon abundance is zero [32]. This means that we have to go to the next order in the strong sphaleron rate expansion. Note also that, with this particle content, using the SM quark and higgs diffusion equation $D_q \sim 6/T_c$, $D_h \sim 110/T_c$ [35], we have $\bar{D} \sim 96/T_c$ and $\bar{D}\Gamma_y/v_w^2 \gg 2/v_w^2$, so that the assumption that the Yukawa interaction is fast is self-consistent, since $\Gamma_y \sim (27/2)\lambda_t^2 \alpha_s T_c$ [32]. Finally, we take:

$$\Gamma_{ws} = 6k\alpha_w^5 T_c,\ \Gamma_{ss} = 6k'\frac{8}{3}\alpha_s^4 T_c \tag{4.76}$$

where $k'$ is an order one parameter and $k \sim 20$ [25]. To go to next order in the expansion in large $\Gamma_{ss}$, we write:

$$Q = H\left(\frac{k_Q(9k_T - k_B)}{k_H(k_B + 9k_Q + 9k_T)}\right) + \delta_Q \tag{4.77}$$

$$T = -H\left(\frac{k_T(2k_B + 9k_Q)}{k_H(k_B + 9k_Q + 9k_T)}\right) + \frac{k_T}{k_Q}\delta_Q \tag{4.78}$$

Substituting in (4.60), we get:

$$\delta_Q = \left(\frac{D_q H'' - v_w H'}{\Gamma_{ss}}\right)\left(\frac{-k_B^2 k_Q(k_Q + 2k_T)}{3k_H(9k_Q + 9k_t + k_B)^2}\right) + \mathcal{O}(1/\Gamma_{ss}^2, 1/\Gamma_y) \tag{4.79}$$

Using $n_L = Q + Q_{1L} + Q_{2L} = 5Q + 4T = \left(\frac{5k_Q + 4k_T}{k_Q}\right)\delta_Q$, we get:

$$n_L = 7\delta_Q = -\frac{3}{112}\left(\frac{D_q H'' - v_w H'}{\Gamma_{ss}}\right) \tag{4.80}$$

Substituting the solution for the Higgs field, we finally get:

$$\frac{\rho_B}{s} = -\left(\frac{9\mathcal{A}\Gamma_{ws}}{112\ s\ \Gamma_{ss}}\right)\left(1 - \frac{D_q}{\bar{D}}\right) \tag{4.81}$$

where $s = (2\pi^2 g_*/45)T_c^3 \simeq 55 T_c^3$. Substituting our parameters, we get:

$$\frac{\rho_B}{s} \simeq 5 \times 10^{-5} \left(\frac{k_{sp}/20}{k'_{sp}}\right) v_w \gamma_w \frac{\left(1 + \frac{1}{8}(T_c\tau - 25)\right)}{(T_c\tau/25)} \\ \left(gg'(g^2 - g'^2)kk' \sin(\theta)\right) \left(\frac{v}{T_c}\right)^3 \left(\frac{S}{T_c}\right)^2 \tag{4.82}$$

It is worth to make a couple of small comments on the parametric dependence of this expression. The dependence of the coupling terms, and therefore on the vevs of $h$ and $S$, was explained in the former section. The wall width $W$ has simplified away because the exponential in eq.(4.72) is small and can be Taylor expanded. The presence of $\Gamma_{ss}$ in the denominator is due to the particular particle content of this model, for which the leading term in the expansion in $1/\Gamma_{ss}$ is zero. The factor $10^{-5}$ is mainly due to the factor of $\sim 10^{-2}$ from the entropy density, and the ratio $20\ \alpha_w^5/\alpha_s^4$, times some other factors coming from the diffusion terms. For typical values of the wall velocity, we can take approximately the SM range: $v_w \sim 0.05 - 0.3$, while the mean free time is $\tau \sim 20/T_c - 30/T_c$. With these values, the produced baryon number ranges in the regime:

$$\frac{\rho_B}{s} \simeq \left(2 \times 10^{-7} - 3 \times 10^{-6}\right) \left(gg'(g^2 - g'^2)kk' \sin(\theta)\right) \left(\frac{v}{T_c}\right)^3 \left(\frac{S}{T_c}\right)^2 \tag{4.83}$$

This is the number which has to be equal to the baryon density at BBN:

$$\left(\frac{\rho_B}{s}\right)_{\text{BBN}} = 9 \times 10^{-11} \tag{4.84}$$

For the moment, let us try do draw some preliminary conclusions on what this does imply on the parameters of the model. Clearly, there are still too many parameters which could be varied, so, as a beginning, we can set all the Yukawa couplings in the new CP violating sector to be roughly equal to each other $k \sim k' \sim g \sim g'$, and $v/T_c \sim 1$, we then get:

$$\frac{\rho_B}{s} \sim \left(2 \times 10^{-7} - 4 \times 10^{-6}\right) \left(g^6 \sin(\theta)\right) \left(\frac{S}{v}\right)^2 \simeq 10^{-10} \tag{4.85}$$

We then get the following constraint:

$$g^6 \left(\frac{S}{v}\right)^2 \sin(\theta) \sim 10^{-4} \tag{4.86}$$

It is natural, in this theory, to take the CP violating phase to be of order 1. In this case:

$$g \sim g' \sim k \sim k' \sim 0.21 \left(\frac{v}{S}\right)^{1/3} \tag{4.87}$$

From this we see that the assumption of considering the interactions mediated by these Yukawa couplings to be fast is justified for a large fraction of the parameter space. These values become lower bounds for the couplings if we allow for the CP violating phase to be smaller than order 1 (see eq.(4.86)).

## 4.4 Electric Dipole Moment

The same CP violating phase which is responsible for baryogenesis, induces an electric dipole moment through the 2-loop diagram shown in fig.4-1.

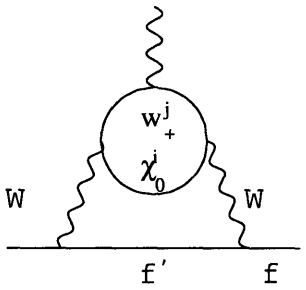


Figure 4-1: 2 loops diagram contributing to fermion EDM, where $\chi_0^i$ are the neutral mass eigenstates, and $\omega_+$ is the charged one.

The situation here is much different than in the MSSM, where a CP violating phase in general introduces EDM at one loop level, the constraints on which generically force very small CP violating phases in the MSSM. It is instead much more similar to the case of split supersymmetry [44, 45, 47], where all the one loop diagrams contributing to the EDM are decoupled. Here the leading diagram is at two loops level, and, as we will soon see, it will induce electron EDM naturally just a little beyond the present

constraints, and on the edge of detection by future experiments.

The induced EDM is (see [38]):

$$\frac{d_f^W}{e} = \pm\frac{\alpha^2 m_f}{8\pi^2 s_W^4 M_W^2}\sum_{i=1}^{3}\frac{m_{\chi_i} m_\omega}{M_W^2}\ \mathrm{Im}\ (O_i^L O_i^{R*})\mathcal{G}\left(r_i^0, r^\pm, r_{f'}\right)\ , \tag{4.88}$$

$$\mathcal{G}\left(r_i^0, r^\pm, r_{f'}\right) = \int_0^\infty dz \int_0^1 \frac{d\gamma}{\gamma}\int_0^1 dy\ \frac{y\,z\,(y+z/2)}{(z+R)^3(z+K_i)} \tag{4.89}$$

$$= \int_0^1 \frac{d\gamma}{\gamma}\int_0^1 dy\, y\left[\frac{(R-3K_i)R+2(K_i+R)y}{4R(K_i-R)^2} + \frac{K_i(K_i-2y)}{2(K_i-R)^3}\ln\frac{K_i}{R}\right]\ .$$

with

$$R = y+(1-y)r_{f'}\ ,\ K_i = \frac{r_i^0}{1-\gamma}+\frac{r^\pm}{\gamma}\ ,\ r^\pm \equiv \frac{m_\omega^2}{M_W^2}\ ,\ r_i^0 \equiv \frac{m_{\chi_i}^2}{M_W^2}\ ,\ r_{f'} \equiv \frac{m_{f'}^2}{M_W^2}\ . \tag{4.90}$$

$$O_i^R = N_{3i}^*,\ O_i^L = -N_{4i}C^R \tag{4.91}$$

where $C^R = e^{-i\theta}$ and $N^T M_N N = \mathrm{diag}\{\mathrm{m}_{\chi_1}, \mathrm{m}_{\chi_2}, \mathrm{m}_{\chi_3}\}$ with real and positive diagonal elements. The plus(minus) sign on the right-hand side of eq.(6.2) corresponds to the fermion $f$ with weak isospin $+(-)1/2$. and $f'$ is its electroweak partner. We mean by $\omega$ the charged mass eigenstate, and with $\chi_i$, $i = 1,2,3$, the neutral mass eigenstates in order of increasing mass.

Diagonalizing the $3\times 3$ mass matrix numerically, we see that generically the model predicts EDM very close to detection. The induced EDM for some generic parameters are shown in fig.4-2.

It is clear then that improvements of the determination of the EDM are going to explore the most interesting region of the parameter space. Ongoing and next generation experiments plan to improve the EDM sensitivity by several orders of magnitude within a few years. For example, DeMille and his Yale group [39] will use the molecule PbO to improve the sensitivity of the electron EDM to $10^{-29}$ $e$ cm within three years, and possibly to $10^{-31}$ $e$ cm within five years. Lamoreaux and his Los Alamos group [40] developed a solid state technique that can improve the sensitivity

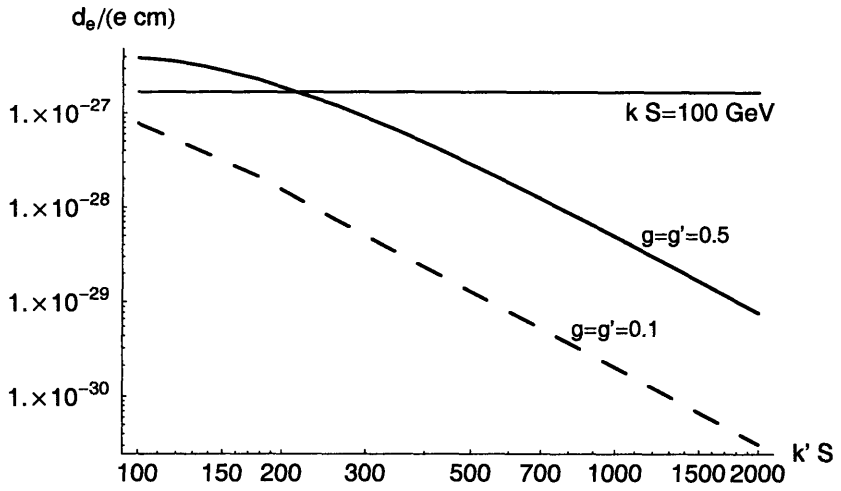


Figure 4-2: The predicted EDM in this model. We plot the induced electron EDM as a function of $k'S$. The solid line represents the induced EDM with $g = g' = 1/2$ and $kS = 100$ GeV, while the dashed line represents $g = g' = 1/10$ and $kS = 100$ GeV, and we take maximal CP violating phase. The horizontal line represents the present electron EDM constraint $d_e < 1.7 \times 10^{-27} e$ cm at 95% CL [37].

to the electron EDM by $10^4$ to reach $10^{-31}$ $e$ cm. By operating at a lower temperature it is feasible to eventually reach a sensitivity of $10^{-35}$ $e$ cm, an improvement of eight orders of magnitude over the present sensitivity. The time scale for these is uncertain, as it is tied to funding prospects. Semertzidis and his Brookhaven group [41] plan to trap muons in storage rings and increase the sensitivity of their EDM measurement by five orders of magnitude. A new measurement has been presented by the Sussex group [42]. A number of other experiments aim for an improvement in sensitivity by one or two orders of magnitude, and involve nuclear EDMs.

In order to understand the current and future constraints on the model, we can study what is the induced electron EDM, once we have satisfied the constraint from baryogenesis in eq.(4.83):

$$gg'(g^2 - g'^2)kk'\frac{v^3 S^2}{T_c^5} \sim 10^{-4} \tag{4.92}$$

The way we proceed is as follows. First, we fix $g' = g/\sqrt{2}$. This is a good representative of the possible ratios between $g$ and $g'$, as it is quite far from the region where

the approximate symmetry in the case $g = g'$ suppresses baryogenesis, and $g'$ is not too small to suppress baryogenesis on its own. Later on we shall relax this condition. Having done this, we invert eq.(4.92), to get an expression for $g$ in terms of the other parameters of the model. Now, the couplings $g, g'$ are expressed in terms of $T_c$, and in terms of $kS$ and $k'S$ which, as it will be useful, in the case of small mixing, can be thought of as respectively the singlet and the doublet mass. We shall impose the constraint on the couplings $g, g', k, k'$ to be less than $\sim 1$, in order for these Yukawa couplings not to hit a Landau pole before the unification scale $\sim 10^{15}$ GeV.

We decide to restrict our analysis to the case in which the possible ratios between the marginal couplings of the same sector of the theory are smaller than 2 orders of magnitude. Here, by same sector of the theory we mean either the CP violating sector, or the sector of the scalar potential and the strong gauge group. The justification of this relies in the fact that we wish to explore the most natural region of the parameter space. For this reason, we expect that there is no large hierarchy between the marginal couplings of the same sector. We think that 2 order of magnitudes is a threshold large enough to delimitate this natural region. However, since marginal couplings are radiatively relatively stable, and large hierarchies among them does not give rise to fine tuning issues, in principle, large hierarchies among the marginal couplings are acceptable. We think that, however, such a hierarchy would require the addition of further structure to the model to justify its presence, and we decide to restrict to the simplest realization of the model. As a consequence of this, the most important restrictions we apply are: $10^{-2} \lesssim k/k' \lesssim 10^2$, and $10^{-2} \lesssim k_S/\lambda \lesssim 10^2$. In particular, using eq.(4.33) and eq.(4.34), this implies $\frac{1}{5}\ T_c \lesssim S \lesssim 5\ T_c$, which, using the limit $k, k' \lesssim 1$, implies that the largest of $kS$ and $k'S$ must be smaller than $5\ T_c$.

The upper bound on the CP violating sector particles tells us that there is a small part of the parameter space which we are going to explore, in which the particles responsible for the production of baryons are non relativistic. In that case, we can approximately extend the result found in eq.(4.92), with the purpose of having order of magnitude estimates, in the following way. From eq.(4.50), it is clear that baryon production is Boltzmann suppressed if the particles are non relativistic. In that case,

the CP violating charge will be generated by the scattering of these particle in the region where the induced mass on the particles is of the order of the critical temperature, as this is the condition of maximum CP violating interaction compatible with not being Boltzmann suppressed. Having observed this, it is easy to approximately extend the result of eq.(4.92) to the non relativistic case, by taking the vevs of the fields at the a value such that the induced mass is of the order of the critical temperature.

In fig.3, we show the induced EDM as a function of $kS$, for several values of the critical temperature $T_c$, for $k'S = 100$, on top, and $k'S = 500$, at the bottom, with the couplings $g, g'$ chosen as explained above, in order to fulfil the baryogenesis requirement. Notice that 500 GeV is roughly the limit that LHC will put on SU(2) doublets. We choose the maximum CP violating phase. The horizontal lines represent the present constraint on EDM $d_e < 1.7 \times 10^{-27} e$ cm at 95% CL [37], and the future expected one [39, 40, 41] of order $10^{-31} e$ cm. A few features are worth to be noted. We see that, for fixed $T_c$, the EDM decreases as we decrease $kS$, for $kS$ light enough. This is due the fact that, reducing $kS$, we reduce both the EDM and the produced quantity of baryons. However, the loss in the production of baryons is compensated with a much smaller, compared to the decrease in $kS$, increase in the couplings $g, g'$, so that, the baryon abundance can remain constant, while the EDM decreases. For large $kS$, the EDM decreases both because the mass of the particles in the loops becomes heavier and heavier, and also because the mixing becomes more and more suppressed. The maximum is located at the point where $kS \sim k'S$. In that case, in fact, the mass matrix has a diagonal piece roughly proportional to the identity, so, even though the diagonal elements are much larger than the off diagonal ones, mixing is much enhanced, and so is the EDM, which is proportional to the mixing. The lower and upper limit on the value of $kS$, as well as the minimum temperature, are dictated by the restrictions $k'S \lesssim 5\ T_c$, $kS \lesssim 5\ T_c$, and $k/k' \gtrsim 10^{-2}$. Now, as we decrease the critical temperature, the resulting EDM tends to decrease. In fact, decreasing the temperature much enhances the baryon production. This allows to decrease the couplings $g, g'$, which explains why the induced EDM decreases. We

verify that increasing the hierarchy between $g$ and $g'$ does not change the results a lot, as the decrease in baryons production requires to make the other couplings large. Increasing the value of $k'S$ up to the maximum allowed value of 1.1 TeV (since $T_c^{\max} \simeq v$) does not produce any relevant change in the result, because this raises the minimum temperature, so that baryogenesis requires larger couplings, which forces the EDM not to decrease relevantly. It is only once the CP violating phase is lowered to less than $10^{-2}$ that a small experimentally unreachable region is opened up around $k'S = 500$ GeV and $kS \lesssim 1$ GeV. The same region is opened also enlarging the allowed hierarchy between the couplings to above $5 \times 10^2$. However, clearly, the presence at the same time of a large hierarchy and of a very small CP phase requires some additional structure on the model to explain the reason for their presence.

The main conclusion we can draw from combining the analysis on baryogenesis and EDM is that, at present, the most natural region of the parameter space is perfectly allowed, however, improvements in the determination of the EDM, are going to explore the entire viable region of the parameter space, so that absence of signal, would result in effectively ruling out the model, at least if no further structure is added.

## 4.5 Comments on Dark Matter and Gauge Coupling Unification

The proposed model finds its main motivation in stabilizing the weak scale through the requirement of attaining baryons in our universe. However, further than this, it is clear that the model provides two other interesting phenomenological aspects: gauge coupling unification and dark matter. Here, we just briefly introduce these aspects, and we postpone a more detailed discussion to future work.

Thanks to the two doublets we have inserted in our model, which have the same quantum numbers as higgsinos in the MSSM, gauge coupling unification works much better than in the standard model. As it was shown in [11], gauge coupling unification

with the standard model plus higgsinos works roughly as well as the MSSM at two loops level, with the only possible problem being the fact that the unification scale is a bit low at around $\sim 10^{15}$ GeV. The problem from proton decay can however be avoided with some particular model at the GUT scale [11, 43]. We expect that 2-loop gauge coupling unification works quite well also in this model, with only small corrections coming from the presence of the singlet scalar $S$.

Concerning the Dark Matter relic abundance, the lightest of the newly introduced particles is stable, and so it provides a natural candidate for Dark Matter. Estimating the relic abundance is quite complex, as it depends on the composition of the particle, and on its annihilation and coannihilations rate. However, if our newly introduced Yukawa couplings are not very close to their upper limit (of order one), and if the lightest particle is mostly composed of the two doublets, then its relic abundance is very similar to the one of pure higgsino dark matter in split supersymmetry [44, 45, 46, 47, 48, 49], requiring the doublets to be around the TeV scale. In the case of singlet dark matter, we expect the singlet to give the right abundance for a much lighter mass, as it is naturally much less interacting. However, estimates become much more difficult, and we postpone the precise determination of the relic abundance to future work.

## 4.6 Conclusions

In this study, we have addressed the solution to the electroweak hierarchy problem in the context of the landscape, following a recent model proposed in [11].

We have shown that it is possible to connect the electroweak scale to a hierarchically small scale at which a gauge group becomes strong by dimensional transmutation. The assumption is that we are in a "friendly neighborhood" of the landscape in which only the relevant parameters of the low energy theory are effectively scanned. We then realize the model in such a way that there is a fragile, though necessary, feature of the universe which needs to be realized in our universe in order to sustain any sort of life. As a natural continuation of Weinberg's "structure principle", the fragile

feature is the presence of baryons in the universe, which are a necessary ingredient for the formation of clumped structures. We assume that, in the friendly neighborhood of the landscape in which we should be, baryogenesis is possible only through the mechanism of electroweak baryogenesis. Then, in order to produce a first order phase transition strong enough so that sphalerons do not wash out the produced baryon density, we develop a new mechanism to implement the electroweak phase transition. We introduce a new gauge sector which becomes strong at an exponentially small scale through dimensional transmutation. We couple this new sector to a singlet $S$ which is then coupled to the higgs field. The electroweak phase transition occurs as the new gauge sector becomes strong, and produces a chiral condensation. This triggers a phase transition for the singlet $S$, which then triggers the phase transition for the higgs fields. In order to preserve baryon number, we need the phase transition to be strong enough, and this is true only if the higgs mass is comparable to the QCD scale of the strong sector. This solves the hierarchy problem. In order to provide the necessary CP violation, we introduce 2 SU(2) doublets $\Psi_{\pm}$ with hypercharge $\pm 1/2$, and a gauge singlet $s$.

When we require the model to describe our world, the model leads to falsifiable predictions.

The main result of the study in this chapter is the computation of the produced baryon number, for which we obtain:

$$\frac{\rho_B}{s} \simeq \left(2 \times 10^{-7} - 3 \times 10^{-6}\right) \left(g g' (g^2 - g'^2) k k' \sin(\theta)\right) \left(\frac{v}{T_c}\right)^3 \left(\frac{S}{T_c}\right)^2 \qquad (4.93)$$

The requirement that this baryon abundance should cope with the observed one leads to a lower bound on a combination of the product of the CP violating phase, the new couplings, the $S$ vev, and the critical temperature $T_c$.

We infer that Gauge Coupling Unification, and the right amount of Dark Matter relic abundance are easily achieved in this model.

We study in detail the induced electron Electric Dipole Moment (EDM), and we find that, at present, the most natural region of the parameter space of the theory is

allowed. However, soon in the future improvement in the EDM experiments will be sensitive the entire viable region of the parameter space of the model, so that absence of a signal would result in practically ruling out the model.

## 4.7 Appendix: Baryogenesis in the Large Velocity Approximation

The method we have used in the main part of this work is based on some approximations that fail in limit of very fast wall speed: $v_w \sim 1$. Even though this regime seems to be disfavored by actual computations of the wall speed[31], it is worth to try to estimate the result even in this case. In this appendix we are going to do an approximate computation in the large wall velocity approximation. In this new regime, calculations become much more complicated, as the assumption of local thermodynamical equilibrium begins to fail, and the baryon number tends to be produced in the region of the wall, in the so called local baryogenesis scenario.

We follow the treatment of [51]. In this approach, the phase transition is treated from an effective field theory point of view. A good way of looking at the high temperature phase of the unbroken phase is imagining it as discretized in a lot of cells, whose side is given by the typical size of the weak sphaleron barrier crossing configuration of the gauge field: $\zeta \sim (\alpha_W T_c)^{-1}$. Concentrating on each cell, we have that the thermal energy in a cell is in general much larger than the energy necessary to create a gauge field oscillation capable of crossing the barrier, and this means that most of the energy is in oscillations with smaller wavelength than $\zeta$. So, these configurations cross the barrier at energy far above the one of the sphaleron configuration, and so their rate has nothing to do with the sphaleron rate, and this explain why their rate per unit volume is of order $\zeta^4$ (In the case $m_h^2 < 0$, electroweak symmetry breaking has already occurred outside the bubble, but this discussion still roughly applies). We can parameterize the configuration in one cell with one variable $\tau$, which depends only on time. Obviously, this is a very rough approximation, but

this is at least a beginning. We try to describe the dynamics of the configuration near crossing the barrier, at a maximum of the energy, that we fixe to be at $\tau = 0$. Near this point, we can write the following Lagrangian, which is very similar to the one in [51]:

$$L(\tau, \dot{\tau}) = \frac{c_1}{2\zeta}\dot{\tau}^2 + \frac{c_2}{2\zeta^3}\tau^2 + \frac{c_3}{\zeta}b\phi\dot{\tau} \tag{4.94}$$

where $c_i$ are dimensionless parameters depending on the different possible barrier crossing trajectories, while $b$ will be determined shortly. Since the point $\tau = 0$ is a maximum of the energy, no odd powers of $\tau$ can appear. The appearance of the odd power in $\dot{\tau}$ can be understood because, at one loop level, the CP violating mass matrix of the particles in the CP violating sector induces an operator which contains the term $\mathrm{Tr}F_{\mu\nu}\tilde{F}^{\mu\nu}$. This can be seen in the following way, in an argument similar to the one shown in [47]. We can imagine to do a chiral rotation on these field of amplitude equal to the CP violating phase. Because of the anomaly, this will induce the operator:

$$\mathcal{O} = \frac{g_2^2}{16\pi^2}\phi\mathrm{Tr}F_{\mu\nu}\tilde{F}^{\mu\nu} \tag{4.95}$$

where $g_2$ is the SU(2) weak coupling, and $F_{\mu\nu}$ is the SU(2) field strength, and where

$$\phi = \mathrm{Arg}(\mathrm{Det}(M)) = \mathrm{Arcsin}\left(\frac{kk'S^2\sin(\theta)}{kk'S^2\sin(\theta)^2 + (gg'v^2 + kk'S^2\cos(\theta))^2}\right) \tag{4.96}$$

Promoting the vevs of $h$ and $S$ to the actual fields, we find the operator we were looking for. Now, the term $\mathrm{Tr}F_{\mu\nu}\tilde{F}^{\mu\nu}$ contains a term proportional to the time derivative of the Chern Simons number, and so the operator $\mathcal{O}$ must contribute to the effective action (4.94) with a term proportional to $b\phi\dot{\tau}$, with $b = \frac{g_2^2}{16\pi^2}$, explaining the reason for the presence of the term in $\dot{\tau}$

The equation of motion for $\tau$ is:

$$\ddot{\tau} = \frac{c_2}{c_1\zeta^2}\tau - \frac{c_3}{c_1}\frac{g_2^2}{16\pi^2}\dot{\phi} \tag{4.97}$$

If the wall is fast enough,we can solve it in the impulse approximation, to get:

$$\Delta\dot{\tau} = -\frac{c_3}{c_1}\frac{g_2^2}{16\pi^2}\Delta\phi \tag{4.98}$$

This kick to $\Delta\dot{\tau}$ makes the distribution of velocities of barrier crossing configurations asymmetric, leading to a production of baryons with respect to antibaryons.

Now, this kick will be very inefficient in changing the distribution of baryons, unless the kick is larger than the typical speed $\dot{\tau}_0$ a generic configuration would have if it crossed the barrier in the absence of the wall. So, we require: $\Delta\dot{\tau} > \dot{\tau}_0$. The fraction of configurations which satisfy this requirement is proportional to $\Delta\dot{\tau}$, but is very difficult to estimate. Following [51], we just say that it is equal to $f\Delta\dot{\tau}$, where $f$ is our "ignorance" coefficient. So, we finally get:

$$n_B \sim f\Delta\dot{\tau}\zeta^{-3} \tag{4.99}$$

where we have reabsorbed the constants $c_i$ into $f$. We finally get:

$$\frac{\rho_B}{s} \sim f\frac{\alpha_W^3}{45}\frac{g_2^2}{16\pi^2}\Delta\phi \tag{4.100}$$

There are a lot of heavy approximations which suggest that this estimate is very rough [51]: from the value of the coefficient $c_i$, to the approximation of restricting to one degree of freedom, to the impulse approximation in solving the differential equation, and to the estimate of the fraction of configurations influenced by the kick. All these suggests that we should take eq.(4.100) with $f \sim 1$, as at most an upper limit on the baryon production, as the authors of [51] suggest.

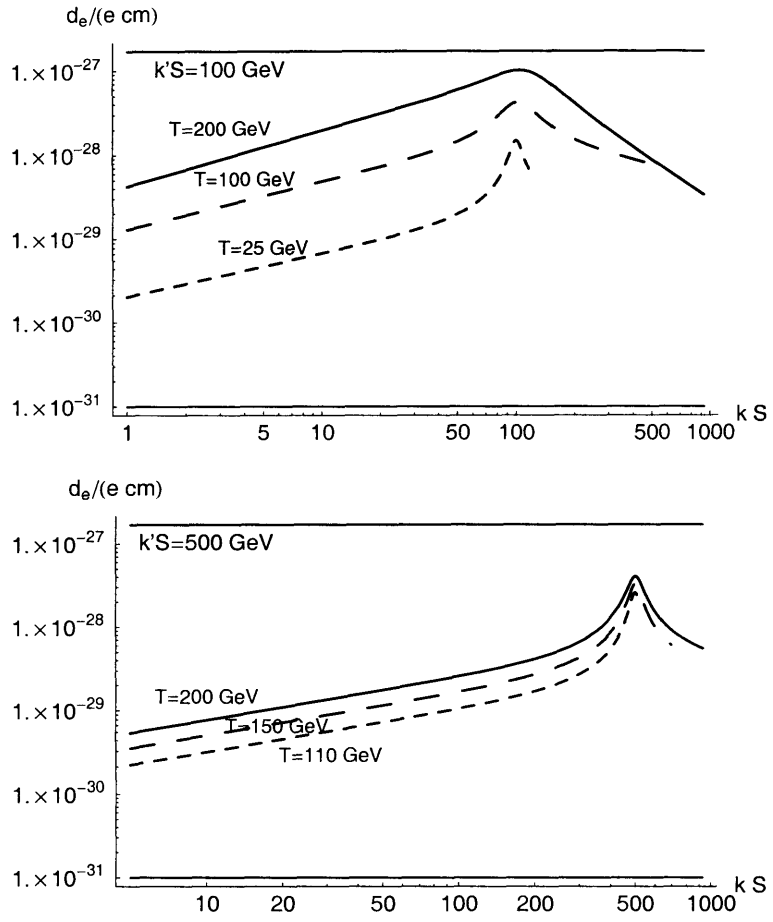


Figure 4-3: Top, the predicted EDM given the constraint from Baryogenesis satisfied, as a function of $kS$ for $k'S = 100$ GeV, $g' = g/\sqrt{2}$, maximum CP violating phase, and $T_c = 200$ GeV (solid line), 100 GeV (long dashed), 25 GeV (short dashed). Bottom, the same for $k'S = 500$ GeV, and $T_c = 200$ GeV (solid line), 150 GeV (long dashed), 110 GeV (short dashed). The horizontal lines represent the present electron EDM constraint $d_e < 1.7 \times 10^{-27} e$ cm at 95% CL [37], and the expected improvement up to $d_e < 10^{31} e$ cm [39, 40, 41] .

# Bibliography


[1] R. Barbieri and A. Strumia, "What is the limit on the Higgs mass?," Phys. Lett. B **462** (1999) 144, hep-ph/9905281.

[2] L. Giusti, A. Romanino and A. Strumia, "Natural ranges of supersymmetric signals," Nucl. Phys. B **550** (1999) 3, hep-ph/9811386.

[3] D. N. Spergel *et al.* [WMAP Collaboration], "First Year Wilkinson Microwave Anisotropy Probe (WMAP) Observations: Determination of Cosmological Parameters," Astrophys. J. Suppl. **148** (2003) 175, astro-ph/0302209.

[4] S. Perlmutter *et al.* [Supernova Cosmology Project Collaboration], "Measurements of Omega and Lambda from 42 High-Redshift Supernovae," Astrophys. J. **517** (1999) 565, astro-ph/9812133.

[5] R. Bousso and J. Polchinski, "Quantization of four-form fluxes and dynamical neutralization of the cosmological constant," JHEP **0006** (2000) 006, hep-th/0004134.

[6] S. B. Giddings, S. Kachru and J. Polchinski, "Hierarchies from fluxes in string compactifications," Phys. Rev. D **66** (2002) 106006, hep-th/0105097.

[7] G. Curio and A. Krause, "G-fluxes and non-perturbative stabilisation of heterotic M-theory," Nucl. Phys. B **643** (2002) 131, hep-th/0108220.

[8] A. Maloney, E. Silverstein and A. Strominger, "De Sitter space in noncritical string theory," hep-th/0205316.

[9] S. Kachru, R. Kallosh, A. Linde and S. P. Trivedi, "De Sitter vacua in string theory," Phys. Rev. D **68**, 046005 (2003), hep-th/0301240.

[10] L. Susskind, "The anthropic landscape of string theory," hep-th/0302219.

[11] N. Arkani-Hamed, S. Dimopoulos and S. Kachru, "Predictive landscapes and new physics at a TeV," hep-th/0501082.

[12] M. R. Douglas, "The statistics of string / M theory vacua," JHEP **0305** (2003) 046, hep-th/0303194.

[13] G. Dvali and A. Vilenkin, "Cosmic attractors and gauge hierarchy," Phys. Rev. D **70** (2004) 063501, hep-th/0304043.

[14] S. Ashok and M. R. Douglas, "Counting flux vacua," JHEP **0401** (2004) 060, hep-th/0307049.

[15] F. Denef and M. R. Douglas, "Distributions of flux vacua," JHEP **0405** (2004) 072, hep-th/0404116.

[16] A. Giryavets, S. Kachru and P. K. Tripathy, "On the taxonomy of flux vacua," JHEP **0408** (2004) 002, hep-th/0404243.

[17] J. P. Conlon and F. Quevedo, "On the explicit construction and statistics of Calabi-Yau flux vacua," JHEP **0410** (2004) 039, hep-th/0409215.

[18] O. DeWolfe, A. Giryavets, S. Kachru and W. Taylor, "Enumerating flux vacua with enhanced symmetries," JHEP **0502** (2005) 037, hep-th/0411061.

[19] J. Kumar and J. D. Wells, "Landscape cartography: A coarse survey of gauge group rank and stabilization of the proton," Phys. Rev. D **71** (2005) 026009, hep-th/0409218.

[20] G. Dvali, "Large hierarchies from attractor vacua," hep-th/0410286.

[21] R. Blumenhagen, F. Gmeiner, G. Honecker, D. Lust and T. Weigand, "The statistics of supersymmetric D-brane models," Nucl. Phys. B **713** (2005) 83, hep-th/0411173.

[22] F. Denef and M. R. Douglas, "Distributions of nonsupersymmetric flux vacua," JHEP **0503** (2005) 061, hep-th/0411183.

[23] S. Weinberg, "Anthropic Bound On The Cosmological Constant," Phys. Rev. Lett. **59** (1987) 2607.

[24] P. C. Schuster and N. Toro, "Is dark matter heavy because of electroweak symmetry breaking? Revisiting heavy neutrinos," hep-ph/0506079.

[25] D. Bodeker, *Phys. Lett.* **B426** (1998) 351, hep-ph/9801430; P. Arnold and L.G. Yaffe, hep-ph/9912306; P. Arnold, *Phys. Rev.* **D62** (2000) 036003; G.D. Moore and K. Rummukainen, *Phys. Rev.* **D61** (2000) 105008; G.D. Moore, *Phys. Rev.* **D62** (2000) 085011.

[26] A. D. Sakharov, "Violation Of CP Invariance, C Asymmetry, And Baryon Asymmetry Of The Universe," Pisma Zh. Eksp. Teor. Fiz. **5** (1967) 32 [JETP Lett. **5** (1967 SOPUA,34,392-393.1991 UFNAA,161,61-64.1991) 24].

[27] A. Riotto, "Theories of baryogenesis," hep-ph/9807454.

[28] A. Riotto and M. Trodden, "Recent progress in baryogenesis," Ann. Rev. Nucl. Part. Sci. **49** (1999) 35, hep-ph/9901362.

[29] M. B. Gavela, P. Hernandez, J. Orloff, O. Pene and C. Quimbay, "Standard model CP violation and baryon asymmetry. Part 2: Finite temperature," Nucl. Phys. B **430**, 382 (1994), hep-ph/9406289.

[30] K. Rummukainen, M. Tsypin, K. Kajantie, M. Laine and M. E. Shaposhnikov, "The universality class of the electroweak theory," Nucl. Phys. B **532**, 283 (1998), hep-lat/9805013.

[31] M. Dine, R. G. Leigh, P. Y. Huet, A. D. Linde and D. A. Linde, "Towards the theory of the electroweak phase transition," Phys. Rev. D **46** (1992) 550, hep-ph/9203203.

[32] P. Huet and A. E. Nelson, "Electroweak baryogenesis in supersymmetric models," Phys. Rev. D **53** (1996) 4578, hep-ph/9506477.

[33] A. Riotto, "Towards a Nonequilibrium Quantum Field Theory Approach to Electroweak Baryogenesis," Phys. Rev. D **53** (1996) 5834, hep-ph/9510271; A. Riotto, "Supersymmetric electroweak baryogenesis, nonequilibrium field theory and quantum Boltzmann equations," Nucl. Phys. B **518** (1998) 339, hep-ph/9712221; A. Riotto, "The more relaxed supersymmetric electroweak baryogenesis," Phys. Rev. D **58** (1998) 095009, hep-ph/9803357.

[34] P. Huet and E. Sather, "Electroweak baryogenesis and standard model CP violation," Phys. Rev. D **51**, 379 (1995), hep-ph/9404302.

[35] M. Joyce, T. Prokopec and N. Turok, "Nonlocal electroweak baryogenesis. Part 1: Thin wall regime," Phys. Rev. D **53** (1996) 2930, hep-ph/9410281.

[36] X. Zhang and B. L. Young, "Effective Lagrangian approach to electroweak baryogenesis: Higgs mass limit and electric dipole moments of fermion," Phys. Rev. D **49** (1994) 563, hep-ph/9309269;

[37] B. C. Regan, E. D. Commins, C. J. Schmidt and D. DeMille, "New limit on the electron electric dipole moment," Phys. Rev. Lett. **88** (2002) 071805.

[38] D. Chang, W. F. Chang and W. Y. Keung, "Electric dipole moment in the split supersymmetry models," Phys. Rev. D **71** (2005) 076006, hep-ph/0503055.

[39] D. Kawall, F. Bay, S. Bickman, Y. Jiang and D. DeMille, "Progress towards measuring the electric dipole moment of the electron in metastable PbO," AIP Conf. Proc. **698** (2004) 192.

[40] S. K. Lamoreaux, "Solid state systems for electron electric dipole moment and other fundamental measurements," nucl-ex/0109014.

[41] Y. K. Semertzidis, "Electric dipole moments of fundamental particles," hep-ex/0401016.

[42] J. J. Hudson, B. E. Sauer, M. R. Tarbutt and E. A. Hinds, "Measurement of the electron electric dipole moment using YbF molecules," Phys. Rev. Lett. **89** (2002) 023003, hep-ex/0202014.

[43] R. Mahbubani, L. Senatore, in preparation

[44] N. Arkani-Hamed and S. Dimopoulos, "Supersymmetric unification without low energy supersymmetry and signatures for fine-tuning at the LHC," hep-th/0405159.

[45] G. F. Giudice and A. Romanino, "Split supersymmetry," Nucl. Phys. B **699** (2004) 65 [Erratum-ibid. B **706** (2005) 65], hep-ph/0406088.

[46] A. Pierce, "Dark matter in the finely tuned minimal supersymmetric standard model," Phys. Rev. D **70** (2004) 075006, hep-ph/0406144.

[47] N. Arkani-Hamed, S. Dimopoulos, G. F. Giudice and A. Romanino, "Aspects of split supersymmetry," Nucl. Phys. B **709** (2005) 3, hep-ph/0409232.

[48] L. Senatore, "How heavy can the fermions in split SUSY be? A study on gravitino and extradimensional LSP," Phys. Rev. D **71**, 103510 (2005), hep-ph/0412103.

[49] A. Masiero, S. Profumo and P. Ullio, "Neutralino dark matter detection in split supersymmetry scenarios," Nucl. Phys. B **712** (2005) 86 [arXiv:hep-ph/0412058].

[50] see for example E. W. Kolb and M. S. Turner, The Early Universe, Perseus Publishing, 1990

[51] A. Lue, K. Rajagopal and M. Trodden, "Semi-analytical approaches to local electroweak baryogenesis," Phys. Rev. D **56** (1997) 1250, hep-ph/9612282.

# Chapter 5

# Limits on non-Gaussianities from WMAP data

We develop a method to constrain the level of non-Gaussianity of density perturbations when the 3-point function is of the "equilateral" type. Departures from Gaussianity of this form are produced by single field models such as ghost or DBI inflation and in general by the presence of higher order derivative operators in the effective Lagrangian of the inflaton. We show that the induced shape of the 3-point function can be very well approximated by a factorizable form, making the analysis practical. We also show that, unless one has a full sky map with uniform noise, in order to saturate the Cramer-Rao bound for the error on the amplitude of the 3-point function, the estimator must contain a piece that is linear in the data. We apply our technique to the WMAP data obtaining a constraint on the amplitude $f_{\rm NL}^{\rm equil.}$ of "equilateral" non-Gaussianity: $-366 < f_{\rm NL}^{\rm equil.} < 238$ at 95% C.L. We also apply our technique to constrain the so-called "local" shape, which is predicted for example by the curvaton and variable decay width models. We show that the inclusion of the linear piece in the estimator improves the constraint over those obtained by the WMAP team, to $-27 < f_{\rm NL}^{\rm local} < 121$ at 95% C.L.

## 5.1 Introduction

Despite major improvements in the quality of cosmological data over the last few years, there are very few observables that can characterize the early phases of the Universe, when density perturbations were generated. Deviations from a purely Gaussian statistics of density perturbations would be a very important constraint on models of early cosmology. In single field slow-roll inflation, the level of non-Gaussianity is sharply predicted [1, 2] to be very small, less than $10^{-6}$. This is quite far from the present experimental sensitivity. On the other hand, many models have recently been proposed with a much higher level of non-Gaussianity, within reach of present or forthcoming data. For nearly Gaussian fluctuations, the quantity most sensitive to departures from perfect Gaussianity is the 3-point correlation function. In general, each model will give a different correlation between the Newtonian potential modes[1]:

$$\langle \Phi(\mathbf{k}_1)\Phi(\mathbf{k}_2)\Phi(\mathbf{k}_3)\rangle = (2\pi)^3\delta^3\big(\mathbf{k}_1+\mathbf{k}_2+\mathbf{k}_3\big)F(k_1,k_2,k_3)\ . \tag{5.1}$$

The function $F$ describes the correlation as a function of the triangle shape in momentum space.

The predictions for the function $F$ in different models divide quite sharply into two qualitatively different classes as a consequence of qualitatively different ways of producing correlations among modes [4]. The first possibility is that the source of density perturbations is not the inflaton but a second light scalar field $\sigma$. In this case non-Gaussianities are generated by the non-linear relation between the fluctuation $\delta\sigma$ of this field and the final perturbation $\Phi$ we observe. This non-linearity is *local* as it acts when the modes are much outside the horizon; schematically we have $\Phi(\mathbf{x}) = A\,\delta\sigma(\mathbf{x}) + B(\delta\sigma^2(\mathbf{x}) - \langle\delta\sigma^2\rangle) + \ldots$ . Even starting from a purely Gaussian

[1]Even with perfectly Gaussian primordial fluctuations, the observables, *e.g.* the temperature anisotropy, will not be perfectly Gaussian as a consequence of the non-linear relation between primordial perturbations and what we will eventually observe. These effects are usually of order $10^{-5}$ (see for example [3]) and thus beyond (but not much) present sensitivity. In the following we will disregard these contributions.

$\delta\sigma$, the quadratic piece introduces a 3-point function for $\Phi$ of the form

$$F(k_1, k_2, k_3) = f_{\rm NL}^{\rm local} \cdot 2\Delta_\Phi^2 \cdot \left( \frac{1}{k_1^3 k_2^3} + \frac{1}{k_1^3 k_3^3} + \frac{1}{k_2^3 k_3^3} \right) , \tag{5.2}$$

where $\Delta_\Phi$ is the power spectrum normalization, $\langle \Phi(\mathbf{k}_1)\Phi(\mathbf{k}_2)\rangle = (2\pi)^3\delta^3(\mathbf{k}_1+\mathbf{k}_2)\Delta_\Phi \cdot k_1^{-3}$, which for the moment has been taken as exactly scale invariant, and where $f_{\rm NL}^{\rm local}$ is proportional to $B$. Examples of this mechanism are the curvaton scenario [5] and the variable decay width model [6], which naturally give rise to $f_{\rm NL}^{\rm local}$ greater than 10 and 5, respectively.

The second class of models are single field models with a non-minimal Lagrangian, where the correlation among modes is created by higher derivative operators [7, 8, 9, 10]. In this case, the correlation is strong among modes with comparable wavelength and it decays when we take one of $k$'s to zero keeping the other two fixed. Although different models of this class give a different function $F$, all these functions are qualitatively very similar. We will call this kind of functions *equilateral*: as we will see, the signal is maximal for equilateral configurations in Fourier space, whereas for the local form (5.2) the most relevant configurations are the *squeezed* triangles with one side much smaller than the others.

The strongest constraint on the level of non-Gaussianity comes from the WMAP experiment. The collaboration analyzed their data searching for non-Gaussianity of the *local* form (5.2), finding the data to be consistent with purely Gaussian statistics and placing limits on the parameter $f_{\rm NL}^{\rm local}$ [11]:

$$-58 < f_{\rm NL}^{\rm local} < 134 \quad \text{at } 95\% \text{ C.L.} \tag{5.3}$$

The main purpose of the study in this chapter is to perform a similar analysis searching for non-Gaussianities of the equilateral form. We can extend the definition of $f_{\rm NL}^{\rm local}$ in eq. (5.2) to a generic function $F$ by setting the overall normalization on equilateral configurations:

$$F(k, k, k) = f_{\rm NL} \cdot \frac{6\Delta_\Phi^2}{k^6} . \tag{5.4}$$

In this way, two different models with the same $f_{\rm NL}$ will give the same 3-point function for equilateral configurations. For equilateral models in particular, the overall amplitude will be characterized by $f_{\rm NL}^{\rm equil.}$. Indirect constraints on $f_{\rm NL}^{\rm equil.}$ have been obtained starting from the limit of eq. (5.3) in [4], resulting in $|f_{\rm NL}^{\rm equil.}| \lesssim 800$; we will see that a dedicated analysis is, as expected, much more sensitive. Many of the equilateral models naturally predict sizeable values of the parameter $f_{\rm NL}^{\rm equil.}$: ghost inflation and DBI inflation [8, 9] tend to have $f_{\rm NL}^{\rm equil.} \sim 100$, tilted ghost inflation $f_{\rm NL}^{\rm equil.} \gtrsim 1$ [10], while slow roll inflation with higher derivative coupling typically give $f_{\rm NL}^{\rm equil.} \lesssim 1$ [7].

In Section 5.2 we discuss the main idea of the analysis. We will see that an optimal analysis is numerically very challenging for a generic form of the function $F$, but simplifies dramatically if the function $F$ is factorizable in a sense that will be defined below. As all the equilateral forms predicted in different models are (qualitatively and quantitatively) very similar, our approach will be to choose a factorizable function that well approximates this class. The analysis is further complicated by the breaking of rotational invariance: a portion of the sky is fully masked by the presence of the galaxy and moreover each point is observed a different number of times. In Section 5.3 we look for an optimal estimator for $f_{\rm NL}$. We discover that, unlike the rotationally invariant case, the minimum variance estimator contains not only terms which are cubic in the temperature fluctuations, but also linear pieces. These techniques are used to analyze the WMAP data in Section 5.4. The result is that the data are compatible with Gaussian statistics. The limit for the equilateral models is

$$-366 < f_{\rm NL}^{\rm equil.} < 238 \quad \text{at } 95\% \text{ C.L.} \tag{5.5}$$

We also obtain a limit on $f_{\rm NL}^{\rm local}$

$$-27 < f_{\rm NL}^{\rm local} < 121 \quad \text{at } 95\% \text{ C.L.} \tag{5.6}$$

which is a slight improvement with respect to (5.3) as a consequence of the above-mentioned additional linear piece in the estimator.

## 5.2 A factorizable equilateral shape

It is in principle straightforward to generalize the analysis for non-Gaussianities from the local model to another one. We start assuming that the experimental noise on the temperature maps is isotropic and that the entire sky is observed (no Galactic and bright source mask); we will relax these assumptions in the next Section. In this case it can be proved that an optimal estimator $\mathcal{E}$ for $f_{\rm NL}$ exists [12, 13], that is an estimator which saturates the Cramer-Rao inequality and thus gives the strongest possible constraint on the amplitude of the non-Gaussian signal. The estimator $\mathcal{E}$ is a sum of terms cubic in the temperature fluctuations, each term weighted by its signal to noise ratio:

$$\mathcal{E} = \frac{1}{N} \cdot \sum_{l_i m_i} \frac{\langle a_{l_1 m_1} a_{l_2 m_2} a_{l_3 m_3} \rangle}{C_{l_1} C_{l_2} C_{l_3}} \, a_{l_1 m_1} a_{l_2 m_2} a_{l_3 m_3} \, . \tag{5.7}$$

Given the assumptions, the power spectrum $C_l$ (which is the sum of the CMB signal and noise) is diagonal in Fourier space; $N$ is a normalization factor which makes the estimator unbiased. From rotational invariance we can simplify the expression introducing the Wigner $3j$ symbols to

$$\mathcal{E} = \frac{1}{N} \cdot \sum_{l_i m_i} \begin{pmatrix} l_1 & l_2 & l_3 \\ m_1 & m_2 & m_3 \end{pmatrix} \frac{B_{l_1 l_2 l_3}}{C_{l_1} C_{l_2} C_{l_3}} \, a_{l_1 m_1} a_{l_2 m_2} a_{l_3 m_3} \, , \tag{5.8}$$

where $B_{l_1 l_2 l_3}$ is the angle-averaged bispectrum which contains all the information about the model of non-Gaussianity we are considering. If $B_{l_1 l_2 l_3}$ is calculated for $f_{\rm NL} = 1$, then the normalization factor $N$ is given by

$$N = \sum_{l_1 l_2 l_3} \frac{(B_{l_1 l_2 l_3})^2}{C_{l_1} C_{l_2} C_{l_3}} \, . \tag{5.9}$$

We now have to relate the angle-averaged bispectrum to the underlying correlation among 3d modes $F(k_1, k_2, k_3)$. After some manipulations following [14], the estimator

takes the form

$$\mathcal{E} = \tag{5.10}$$
$$\frac{1}{N}\cdot\sum_{l_i m_i}\int d^2\hat{n}\, Y_{l_1m_1}(\hat{n})Y_{l_2m_2}(\hat{n})Y_{l_3m_3}(\hat{n})\int_0^\infty r^2dr\; j_{l_1}(k_1r)j_{l_2}(k_2r)j_{l_3}(k_3r)\; C_{l_1}^{-1}C_{l_2}^{-1}C_{l_3}^{-1}$$
$$\int\frac{2k_1^2dk_1}{\pi}\frac{2k_2^2dk_2}{\pi}\frac{2k_3^2dk_3}{\pi}F(k_1,k_2,k_3)\Delta_{l_1}^T(k_1)\Delta_{l_2}^T(k_2)\Delta_{l_3}^T(k_3)\; a_{l_1m_1}a_{l_2m_2}a_{l_3m_3}\;,$$

where $\Delta_l^T(k)$ is the CMB transfer function which relates the $a_{lm}$ to the Newtonian potential $\Phi(k)$:

$$a_{lm} = 4\pi i^l\int\frac{d^3k}{(2\pi)^3}\Delta_l^T(k)\Phi(k)Y_{lm}^*(\hat{k})\;. \tag{5.11}$$

Equation (5.10) is valid for any shape of the 3-point function $F$. Unfortunately this expression is computationally very challenging. The sums over $m$ can be taken inside the integrals and factorized, but we are still left with a triple sum over $l$ of an integral over the sphere. The calculation time grows as $N_{\rm pixels}^{5/2}$, where the number of pixels $N_{\rm pixels}$ is of order $3\times10^6$ for WMAP. This approach is therefore numerically too demanding.

As noted in [14], a crucial simplification is possible if the function $F$ is factorizable as a product of functions of $k_1$, $k_2$ and $k_3$ or can be written as a sum of a small number of terms with this property. In this case the second line of (5.10) becomes factored as the product of functions of each $l$ separately, so that now also the sum over $l$ can be done before integrating over the sphere. For example if we assume that $F(k_1,k_2,k_3) = f_1(k_1)f_2(k_2)f_3(k_3)$, the estimator simplifies to

$$\mathcal{E} = \frac{1}{N}\cdot\int d^2\hat{n}\int_0^\infty r^2dr\;\prod_{i=1}^3\sum_{l_im_i}\int\frac{2k^2dk}{\pi}j_{l_i}(kr)f_i(k)\Delta_{l_i}^T(k)C_{l_i}^{-1}a_{l_im_i}Y_{l_im_i}(\hat{n})\;. \tag{5.12}$$

The calculation is obviously much faster now: it now scales like $N_{\rm pixels}^{3/2}$ and it is dominated by going back and forth between real and spherical harmonics space. From expression (5.2) we see that this simplification is possible for the local shape, and it was indeed used for the analysis of the WMAP data in [11, ?].

Unfortunately, none of the "equilateral models" discussed in the Introduction predicts a function $F$ which is factorizable (see some explicit expressions in [4]), so that it is not easy to perform an optimal analysis for a particular given model. However, all these models give 3-point functions which are quite similar, so that it is a very good approximation to take a factorizable shape function $F$ which is close to the class of functions we are interested in and perform the analysis for this shape. In the limit $k_1 \to 0$ with $k_2$ and $k_3$ fixed, all the equilateral functions diverge as $k_1^{-1}$ [4] (while the local form eq. (5.2) goes as $k_1^{-3}$). An example of a function which has this behavior, is symmetric in $k_1$, $k_2$ and $k_3$, and is a sum of factorizable functions (and is homogeneous of order $k^{-6}$, see below) is [2]

$$F(k_1,k_2,k_3) = f_{\rm NL}^{\rm equil.}\cdot 6\Delta_\Phi^2\cdot\left(-\frac{1}{k_1^3k_2^3}-\frac{1}{k_1^3k_3^3}-\frac{1}{k_2^3k_3^3}-\frac{2}{k_1^2k_2^2k_3^2}+\frac{1}{k_1k_2^2k_3^3}+(5\ perm.)\right), \tag{5.14}$$

where the permutations act only on the last term in parentheses. The mild divergence for $k_1 \to 0$ is achieved through a cancellation among the various terms.

In figure 5-1, we compare this function with the local shape. The dependence of both functions under a common rescaling of all $k$'s is fixed to be $\propto k^{-6}$ by scale invariance, so that we can factor out $k_1^{-6}$ for example. Everything will now depend only on the ratios $k_2/k_1$ and $k_3/k_1$, which fix the shape of the triangle in momentum space. For each shape we plot $F(1,k_2/k_1,k_3/k_1)(k_2/k_1)^2(k_3/k_1)^2$; this is the relevant quantity if we are interested in the relative importance of different triangular shapes. The square of this function in fact gives the signal to noise contribution of a particular shape in momentum space [4]. We see that for the function (5.14), the signal to noise

[2] Eq. (5.14) can be derived as follows. In order to make the divergence of $F$ mild in the squeezed limit we can use at the numerator a quantity which goes to zero in the same limit. The area of the triangle does the job, going like $k_1$ for $k_1 \to 0$. The area can be expressed purely in terms of the sides through Heron's formula [16], $A = \sqrt{s(s-k_1)(s-k_2)(s-k_3)}$, where $s = \frac{1}{2}(k_1+k_2+k_3)$ is the semiperimeter. The first $s$ in the square root is irrelevant for our purposes, since it goes to a constant in the squeezed limit; we will therefore omit it. Also we want a sum of factorizable functions, so we get rid of the square root by considering $A^2$. In conclusion, a function with all the features stated above is

$$F(k_1,k_2,k_3) \propto \frac{(s-k_1)(s-k_2)(s-k_3)}{k_1^3\,k_2^3\,k_3^3}, \tag{5.13}$$

which, once expanded, reduces exactly to eq. (5.14).

is concentrated on equilateral configurations, while squeezed triangles with one side much smaller than the others are the most relevant for the local shape.

In figure 5-2 we study the equilateral function predicted both in the presence of higher-derivative terms [7] and in DBI inflation [9]. In the second part of the figure we show the difference between this function and the factorizable one used in our analysis. We see that the relative difference is quite small. The same remains true for other equilateral shapes (see [4] for the analogous plots for other models).

In [4], a "cosine" between different shapes was defined which quantifies how different is the signal given by two distributions. The cosine is calculated from the scalar product of the functions in fig. 5-1. We can think about this cosine as a sort of correlation coefficient: if the cosine is close to 1 the two shapes are very difficult to distinguish experimentally and an optimal analysis for one of them is very good also for the other. On the other hand, a small cosine means that, once non-Gaussianities are detected, there is a good chance to distinguish the two functions and that an optimal analysis for one shape is not very good for the other. The cosine between our template shape and the functions predicted by equilateral models is very close to one (0.98 with the ghost inflation [8] prediction and 0.99 for higher derivative/DBI models [7, 9]). This means that the error introduced in the analysis by the use of the factorizable shape instead of the correct prediction for a given equilateral model is at the percent level. On the other hand, as evident from figure 5-1, our template shape is quite different from the local model — the cosine is merely 0.41.

All these numbers are obtained in 3 dimensions assuming that we can directly measure the fluctuations with a 3d experiment like a galaxy survey. The CMB anisotropies are a complicated projection from the 3d modes. This makes it more difficult to distinguish different shapes, although the picture remains qualitatively the same.

Let us proceed with the study of our template shape. To further simplify the

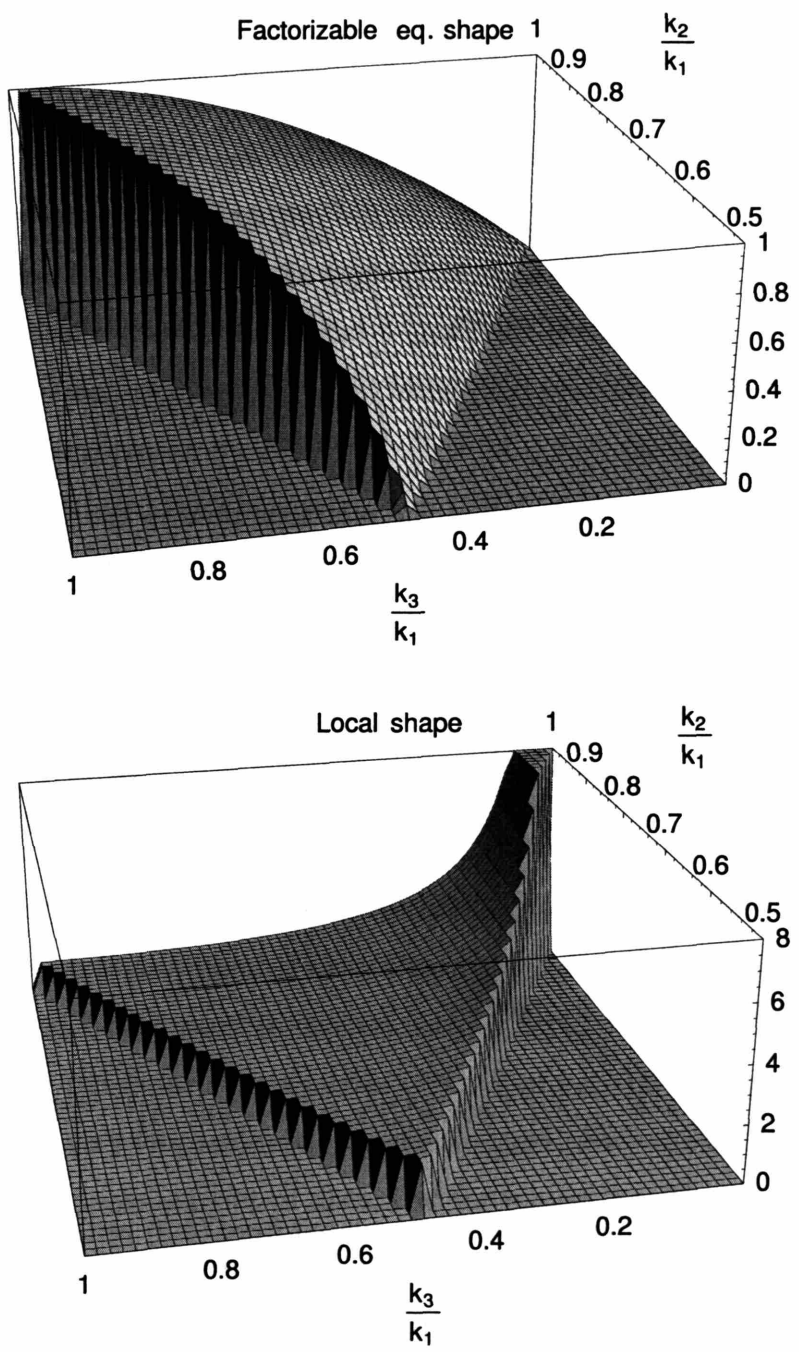


Figure 5-1: Plot of the function $F(1, k_2/k_1, k_3/k_1)(k_2/k_1)^2(k_3/k_1)^2$ for the equilateral shape used in the analysis (top) and for the local shape (bottom). The functions are both normalized to unity for equilateral configurations $\frac{k_2}{k_1} = \frac{k_3}{k_1} = 1$. Since $F(k_1, k_2, k_3)$ is symmetric in its three arguments, it is sufficient to specify it for $k_1 \geq k_2 \geq k_3$, so $\frac{k_3}{k_1} \leq \frac{k_2}{k_1} \leq 1$ above. Moreover, the triangle inequality says that no side can be longer than the sum of the other two, so we only plot $F$ in the triangular region $1 - \frac{k_2}{k_1} \leq \frac{k_3}{k_1} \leq \frac{k_2}{k_1} \leq 1$ above, setting it to zero elsewhere.

estimator in eq. (5.10), we define the functions

$$\alpha_l(r) \equiv \frac{2}{\pi}\int_0^{+\infty} dk\, k^2\, \Delta_l^T(k) j_l(kr) \tag{5.15}$$

$$\beta_l(r) \equiv \frac{2}{\pi}\int_0^{+\infty} dk\, k^{-1}\, \Delta_l^T(k) j_l(kr) \Delta_\Phi \tag{5.16}$$

$$\gamma_l(r) \equiv \frac{2}{\pi}\int_0^{+\infty} dk\, k\, \Delta_l^T(k) j_l(kr) \Delta_\Phi^{1/3} \tag{5.17}$$

$$\delta_l(r) \equiv \frac{2}{\pi}\int_0^{+\infty} dk\, \Delta_l^T(k) j_l(kr) \Delta_\Phi^{2/3}\,. \tag{5.18}$$

We use this strange ordering of the functions to keep the notation compatible with [11, ?], where the functions $\alpha$ and $\beta$ were introduced for the analysis of the local shape. To evaluate $\mathcal{E}$, we start from the spherical harmonic coefficients of the map $a_{lm}$ and calculate the four maps

$$A(r,\hat{n}) \equiv \sum_{lm} \frac{\alpha_l(r)}{C_l} Y_{lm}(\hat{n}) a_{lm}\,, \qquad B(r,\hat{n}) \equiv \sum_{lm} \frac{\beta_l(r)}{C_l} Y_{lm}(\hat{n}) a_{lm}\,, \tag{5.19}$$

$$C(r,\hat{n}) \equiv \sum_{lm} \frac{\gamma_l(r)}{C_l} Y_{lm}(\hat{n}) a_{lm}\,, \qquad D(r,\hat{n}) \equiv \sum_{lm} \frac{\delta_l(r)}{C_l} Y_{lm}(\hat{n}) a_{lm}\,. \tag{5.20}$$

Now the estimator $\mathcal{E}$ is given by

$$\mathcal{E} = -\frac{18}{N}\int r^2 dr \int d^2\hat{n}\, \left[A(r,\hat{n})B(r,\hat{n})^2 + \frac{2}{3}D(r,\hat{n})^3 - 2B(r,\hat{n})C(r,\hat{n})D(r,\hat{n})\right] \tag{5.21}$$

and the normalization $N$ can be calculated from (5.9) using the explicit form

$$B_{l_1 l_2 l_3} = \sqrt{\frac{(2l_1+1)(2l_2+1)(2l_3+1)}{4\pi}} \begin{pmatrix} l_1 & l_2 & l_3 \\ 0 & 0 & 0 \end{pmatrix} \times \tag{5.22}$$

$$6\int_0^\infty r^2 dr\, [-\alpha_{l_1}(r)\beta_{l_2}(r)\beta_{l_1}(r) + (2\ perm.) \tag{5.23}$$

$$-2\delta_{l_1}(r)\delta_{l_2}(r)\delta_{l_3}(r) + \beta_{l_1}(r)\gamma_{l_2}(r)\delta_{l_3}(r) + (5\ perm.)]\,.$$

The functions $\alpha$, $\beta$, $\gamma$ and $\delta$ used in the analysis can be obtained numerically starting from the transfer functions $\Delta_l^T(k)$, which can be computed given a particu-

lar cosmological model with publicly available software as CMBFAST [17]. Some plots of these functions are given in fig. 5-3, where we choose values of $r$ close to $\tau_0 - \tau_R$ (conformal time difference between recombination and the present), as these give the largest contribution to the estimator. The oscillatory behavior induced by the transfer function $\Delta_l^T(k)$ is evident, with a peak at $l \sim 200$. The factors of $l(l+1)$ and $(2l+1)$ in the $\beta$ and $\delta$ functions, respectively, can be understood from the behavior at low $l$'s, in the Sachs-Wolfe regime. Here the transfer function can be approximated by $\Delta_l^T(k) = -j_l\left(k(\tau_0 - \tau_R)\right)/3$, and we then see that $\beta_l(\tau_0 - \tau_R) \propto \int_0^\infty dk\ k^{-1}\ j_l^2(k(\tau_0 - \tau_R)) \propto 1/\left(l(l+1)\right)$ and $\delta_l(\tau_0 - \tau_R) \propto \int_0^\infty dk\ j_l^2(k(\tau_0 - \tau_R)) \propto 1/(2l+1)$. From these expressions we also see that the function $\beta$ (the only one which is dimensionless) is very similar to the $C_l^{\rm cmb}$'s as, in the Sachs-Wolfe regime, $C_l^{\rm cmb} \simeq \frac{2}{9\pi} \int_0^\infty dk\, k^{-1}\, \Delta_\Phi\, j_l^2(k(\tau_0 - \tau_R))$.

## 5.3 Optimal estimator for $f_{\rm NL}$

There are two quite general experimental complications that make the estimator $\mathcal{E}$ defined in the last Section non-optimal. First, foreground emission from the Galactic plane and from isolated bright sources contaminates a substantial fraction of sky, which must be masked out before the analysis [18]. This projection which can be accomplished by giving very large noise to regions that are affected by foregrounds, besides reducing the available amount of data, has the important effect of breaking rotational invariance, so that the signal covariance matrix $C^{\rm cmb}_{l_1 m_1, l_2 m_2}$ of the masked sky becomes non-diagonal in multipole space. Second, the noise level is not the same in different regions of the sky, because the experiment looks at different regions for different amounts of time. This implies that also the noise covariance matrix $C^{\rm noise}_{l_1 m_1, l_2 m_2}$ is non-diagonal in multipole space. The importance of the anisotropy of the noise was pointed out in [11], as it caused an increase of the variance of the estimator $\mathcal{E}$ at high $l$'s.

For these reasons, it is worth trying to generalize the estimator $\mathcal{E}$. We consider estimators for $f_{\rm NL}$ (for a given shape of non-Gaussianities) which contain both trilinear

and linear terms in the $a_{lm}$'s. In the rotationally invariant case, a linear piece in the estimator can only be proportional to the monopole, which is unobservable. However, in the absence of rotational invariance, linear terms can be relevant. In this class, it is straightforward to prove that the unbiased estimator with the smallest variance is given by

$$\begin{aligned}\mathcal{E}_{\rm lin}(a) \;=\; & \frac{1}{N}\sum_{l_i m_i}\Big(\langle a_{l_1m_1}a_{l_2m_2}a_{l_3m_3}\rangle_1\, C^{-1}_{l_1m_1,l_4m_4}C^{-1}_{l_2m_2,l_5m_5}C^{-1}_{l_3m_3,l_6m_6}a_{l_4m_4}a_{l_5m_5}a_{l_6m_6} \\ & -3\,\langle a_{l_1m_1}a_{l_2m_2}a_{l_3m_3}\rangle_1\, C^{-1}_{l_1m_1,l_2m_2}C^{-1}_{l_3m_3,l_4m_4}a_{l_4m_4}\Big)\,,\end{aligned} \tag{5.24}$$

where $N$ is a normalization factor:

$$N=\sum_{l_i m_i}\langle a_{l_1m_1}a_{l_2m_2}a_{l_3m_3}\rangle_1\, C^{-1}_{l_1m_1,l_4m_4}C^{-1}_{l_2m_2,l_5m_5}C^{-1}_{l_3m_3,l_6m_6}\langle a_{l_4m_4}a_{l_5m_5}a_{l_6m_6}\rangle_1\,. \tag{5.25}$$

The averages $\langle\ldots\rangle_1$ are taken with $f_{\rm NL}=1$. As we stressed, the covariance matrix $C = C^{\rm cmb} + C^{\rm noise}$ contains the effects of the mask projection and the anisotropic noise and it is thus non-diagonal in multipole space.

It turns out that the estimator $\mathcal{E}_{\rm lin}$ saturates the Cramer-Rao bound, *i.e.* it is not only optimal in its class, but it is also the minimum variance unbiased estimator among all the possible ones. To prove this, we expand the probability distribution in the limit of weak non-Gaussianity (which is surely a good approximation for the CMB) using the Edgeworth expansion [19, 20, 21].

$$P(a|f_{\rm NL})=\Big(1-f_{\rm NL}\sum_{l_i m_i}\langle a_{l_1m_1}a_{l_2m_2}a_{l_3m_3}\rangle_1\frac{\partial}{\partial a_{l_1m_1}}\frac{\partial}{\partial a_{l_2m_2}}\frac{\partial}{\partial a_{l_3m_3}}\Big)\frac{e^{-\frac{1}{2}\sum a^*_{l_4m_4}C^{-1}_{l_4m_4,l_5m_5}a_{l_5m_5}}}{\sqrt{(2\pi)^N\det(C)}}\,. \tag{5.26}$$

Now, following the same arguments of [13] which considered the same problem in the rotationally invariant case, the estimator is optimal (in the sense that its variance saturates the Cramer-Rao bound), if and only if the following condition is satisfied:

$$\frac{d\log P(a|f_{\rm NL})}{d\,f_{\rm NL}}=F(f_{\rm NL})\,(\mathcal{E}_{\rm lin}(a)-f_{\rm NL})\,, \tag{5.27}$$

where $F(f_{\rm NL})$ is a generic function[3] of the parameter $f_{\rm NL}$. From the probability distribution (5.26) it is easy to check that the estimator $\mathcal{E}_{\rm lin}$ is proportional to $d\log P(a|f_{\rm NL})/d\,f_{\rm NL}$ in the limit of small $f_{\rm NL}$. We conclude that $\mathcal{E}_{\rm lin}$ is an optimal estimator for a nearly Gaussian distribution.

We now want to make some approximations to the optimal estimator $\mathcal{E}_{\rm lin}$ to make it numerically easier to evaluate. The full inversion of the covariance matrix is computationally rather cumbersome (although doable as the matrix is with good approximation block diagonal [22]). We therefore approximate $C^{-1}a$ in the trilinear term of eq. (5.24) by masking out the sky before computing the $a_{lm}$'s and taking $C$ as diagonal:

$$\text{trilinear} \rightarrow \frac{1}{N}\sum_{l_i m_i} \frac{\langle a_{l_1 m_1} a_{l_2 m_2} a_{l_3 m_3}\rangle_1}{C_{l_1} C_{l_2} C_{l_3}}\, a_{l_1 m_1} a_{l_2 m_2} a_{l_3 m_3}\ , \tag{5.28}$$

where $\langle a_{l_1 m_1} a_{l_2 m_2} a_{l_3 m_3}\rangle_1$ is still given by the full sky expressions of the last Section. Once we have made this approximation for the trilinear term it is easy to prove that the choice for the linear term which minimizes the variance is

$$\text{linear} \rightarrow -\frac{3}{N}\sum_{l_i m_i} \frac{\langle a_{l_1 m_1} a_{l_2 m_2} a_{l_3 m_3}\rangle_1}{C_{l_1} C_{l_2} C_{l_3}}\, C_{l_1 m_1, l_2 m_2}\, a_{l_3 m_3}\ . \tag{5.29}$$

Note that we must not approximate the covariance matrix $C$ in the numerator as diagonal. This would leave only a term proportional to the monopole $a_{00}$ (which is unobservable), as in the rotationally invariant case.

The normalization factor $N$ is given by

$$N = f_{\rm sky} \sum_{l_1 l_2 l_3} \frac{(B_{l_1 l_2 l_3})^2}{C_{l_1} C_{l_2} C_{l_3}}\ , \tag{5.30}$$

where $f_{\rm sky}$ is the fraction of the sky actually observed. As shown in [23], this correctly takes into account the reduction of data introduced by the mask for multipoles much higher than the inverse angular scale of the mask. The accuracy of this approximation has been checked on non-Gaussian simulations for the local shape in [11].

[3]When eq. (5.27) is satisfied, the function $F$ turns out to be the Fisher information for the parameter $f_{\rm NL}$, $F(f_{\rm NL}) = \langle (d\log P(a|f_{\rm NL})/df_{\rm NL})^2\rangle$.

Let us try to understand qualitatively the effect of the linear correction. Take a large region of the sky that has been observed many times so that its noise level is low. This region will therefore have a small-scale power lower than average. Now, in a given realization depending on how the large scale modes look like, this long-wavelength modulation of the small-scale power spectrum may be "misinterpreted" by the trilinear estimator as a non-Gaussian signal. Indeed, for the local shape, most of the signal comes precisely from the correlation between long wavelength modes and the small scale power [4]. On the other hand, for equilateral shapes, as we noted, the signal is quite low on squeezed configurations so that we expect this effect to be small. The linear term measures the correlation between a given map and the anisotropies in the power spectrum, thus correcting for this spurious signal. Clearly the spurious correlation is zero on average, but the effect increases the variance of the estimator.

We will apply the linear correction of the estimator only for the local shape, since, as we will verify later, it gives a very small effect for equilateral shapes. Following the same steps as in the last Section to factorize the trilinear term in the estimator, we get an explicit expression for the linear piece in the local case:

$$-\frac{3}{N}\int r^2 dr \int d^2\hat{n} \sum_{l_3 m_3} \left( 2S_{AB}(\hat{n},r)\frac{\beta_{l_3}(r)}{C_{l_3}}Y_{l_3,m_3}(\hat{n}) + S_{BB}(\hat{n},r)\frac{\alpha_{l_3}(r)}{C_{l_3}}Y_{l_3,m_3}(\hat{n}) \right) a_{l_3 m_3} \,, \tag{5.31}$$

where the two maps $S_{AB}(\hat{n},r)$ and $S_{BB}(\hat{n},r)$ are defined as

$$S_{AB}(\hat{n},r) = \sum_{l_i m_i} \frac{\alpha_{l_1}(r)}{C_{l_1}}Y_{l_1,m_1}(\hat{n})\frac{\beta_{l_2}(r)}{C_{l_2}}Y_{l_2,m_2}(\hat{n})\langle a_{l_1 m_1} a_{l_2 m_2}\rangle \,, \tag{5.32}$$

$$S_{BB}(\hat{n},r) = \sum_{l_i m_i} \frac{\beta_{l_1}(r)}{C_{l_1}}Y_{l_1,m_1}(\hat{n})\frac{\beta_{l_2}(r)}{C_{l_2}}Y_{l_2,m_2}(\hat{n})\langle a_{l_1 m_1} a_{l_2 m_2}\rangle \,. \tag{5.33}$$

As discussed above, it is only the anisotropic part of the matrix $\langle a_{l_1 m_1} a_{l_2 m_2}\rangle$ that gives a contribution to the linear part of the estimator. This matrix can be decomposed as

$$\langle a_{l_1 m_1} a_{l_2 m_2}\rangle = \langle a^{\rm cmb}_{l_1 m_1} a^{\rm cmb}_{l_2 m_2}\rangle + \langle a^{\rm noise}_{l_1 m_1} a^{\rm noise}_{l_2 m_2}\rangle, \tag{5.34}$$

where $a_{lm}^{\rm cmb}$ are the $a_{lm}$'s of a map generated with CMB signal only and then performing the mask projection, and $a_{lm}^{\rm noise}$ are the ones associated with a map generated with noise only and then performing the mask projection. Both of these two matrices have an anisotropic component. For the map $\langle a_{l_1m_1}^{\rm cmb} a_{l_2m_2}^{\rm cmb} \rangle$, this arises only because of the sky cut, while for the map $\langle a_{l_1m_1}^{\rm noise} a_{l_2m_2}^{\rm noise} \rangle$, it is generated both by the sky cut and by the anisotropy of the noise power. We already discussed about the effect of the anisotropy of the noise in the previous paragraph; this effect turns out to be the most relevant. The sky cut gives a much smaller effect because, as we will explain more in detail in the next Section, it is mainly associated with the average value of the temperature outside of the sky cut, and this average value is subtracted out before the analysis.

## 5.4 Analysis of WMAP 1-year data

We keep our methodology quite similar to the one used by the WMAP collaboration for their analysis of the local shape [11] in order to have a useful consistency check. We compare WMAP data with Gaussian Monte-Carlo realizations, which are used to estimate the variance of the estimator. We generate with HEALPix[4] a random CMB realization, with fixed cosmological parameters, at resolution *nside*=256 (786,432 pixels). The parameters are fixed to the WMAP best fit for a ΛCDM cosmology with power-law spectrum [24]: $\Omega_b h^2 = 0.024$, $\Omega_m h^2 = 0.14$, $h = 0.72$, $\tau = 0.17$, $n_s = 0.99$. With these parameters, the present conformal time $\tau_0$ is 13.24 Gpc and the recombination time is $\tau_R = 0.27$ Gpc. A given realization is smoothed with the WMAP window functions for the Q1, Q2, V1, V2, W1, W2, W3 and W4 bands [25]. To each of these 8 maps we add an independent noise realization: for every pixel the noise is a Gaussian random variable with variance $\sigma_0^2/N_{\rm obs}$, where $N_{\rm obs}$ is the number of observations of the pixel and $\sigma_0$ is a band dependent constant [26]. The maps are then combined to give a single map: we make a pixel by pixel average of the 8 maps weighted by the noise $\sigma_0^2/N_{\rm obs}$. We use this procedure because it is identical to that

[4]See HEALPix website: http://www.eso.org/science/healpix/

used in [11], thereby allowing direct comparisons between our results and those of the WMAP team. In future work, it can in principle be improved in two ways. First of all, for the window function to be strictly rather than approximately uniform across the sky, the weights of the eight input maps should be constant rather than variable from pixel to pixel. This is a very small effect in practice, since the eight $N_{\rm obs}$-maps are very similar, making the weights close to constant. Second, the sensitivity on small scales can be improved by using $l$-dependent weights [27]: for instance, at very high $l$, most of the weight should be given to the $W$ bands, since they have the narrowest beam. This would also have a small effect for our particular application, since our estimator uses only the first few hundred multipoles. We explicitly checked that this would not reduce the variance of our estimator appreciably.

We apply the $Kp0$ mask to the final map, to cut out the Galactic plane and the known point sources [18]: this mask leaves the 76.8% of the pixels, $f_{\rm sky} = 0.768$. The average temperature outside the mask is then subtracted.

On the resulting map we calculate the estimators defined in the preceding Sections. For the local shape we performed the analysis both with and without the linear piece discussed in Section 5.3. The quadratic maps of equations (5.32) and (5.33) used for the linear correction are calculated by averaging many ($\simeq 600$) Monte-Carlo maps obtained with the same procedure above. We use HEALPix to generate and analyze maps at resolution level *nside*=256 (786,432 pixels). The integration over $r$ is performed from $\tau_0 - 0.025\,\tau_R$ up to $\tau_0 - 2.5\,\tau_R$ with $\sim 200$ equidistant points, and then with another logarithmically spaced $\sim 60$ points up to the present epoch. Such a high resolution both in $r$ spacing and in *nside* is necessary in order to reproduce the cancellation on squeezed triangles which occurs among the various terms in the equilateral shape (5.14). The computation of each $f_{\rm NL}$ on a 2.0 GHz Opteron processor with 2 GB of RAM takes about 60 minutes for the local shape, and 100 minutes for the equilateral shape.

We then apply exactly the same procedure to WMAP data. These maps are analyzed after template foreground corrections are applied, in order to reduce foreground signal leaking outside the mask, as described in [18].

A useful analytic bound on the variance of the estimators for $f_{\rm NL}^{\rm local}$ and $f_{\rm NL}^{\rm equil.}$ is obtained from the variance of the full sky estimator (with homogeneous noise) (5.8) with an $f_{\rm sky}$-correction which takes into account the reduction in available information from not observing the whole sky. Taking into account the normalization factor, one readily obtains

$$\sigma_{\rm an}^{-2} = f_{\rm sky} \sum_{l_1<l_2<l_3} \frac{B_{l_1 l_2 l_3}^2}{C_{l_1} C_{l_2} C_{l_3}} \,, \tag{5.35}$$

where $B_{l_1 l_2 l_3}$ must be evaluated for $f_{\rm NL}^{\rm local}$ or $f_{\rm NL}^{\rm equil.}$ equal to 1. As we discussed, our approach is not strictly optimal as we are not inverting the full covariance matrix, so we expect $\sigma_{\rm an}$ to be smaller than the actual standard deviation that we measure from our Monte-Carlos.

In figure 5-4, we show the standard deviation of estimators for the local shape parameter $f_{\rm NL}^{\rm local}$ as a function of the maximum multipole analyzed. We compare the results of our Monte-Carlo simulations (with and without the linear correction) with the analytic bound discussed above. The results without linear correction are compatible with the analysis in [11]. We see that the addition of the linear piece reduces the variance divergence at high $l$'s. The residual divergence is probably associated with the fact that we did not invert the full covariance matrix. The estimator with the smallest variance is the one with linear correction at $l_{\rm max} = 335$, with a standard deviation of 37. The analytic approximation has an asymptotic value of 30 which should be considered the best possible limit with the present data. Our estimator thus extracts about $(37/30)^{-2} \approx 66\%$ of the $f_{\rm NL}^{\rm local}$-information (inverse variance) from the WMAP data. The analysis of the data with $l_{\rm max} = 335$ gives 47, so there is no evidence of deviation from pure Gaussianity and we can set a $2\sigma$ limit of

$$-27 < f_{\rm NL}^{\rm local} < 121 \quad \text{at } 95\% \text{ C.L.} \tag{5.36}$$

In fig. 5-5, we show a map $S_{AB}(\hat{n}, r)$ for a radius around recombination calculated with noise only and for $l_{\rm max} = 370$, as an illustrative example of the role of the linear piece. As we will clarify below, it is in fact the anisotropy of the noise that causes most of the contribution to the linear piece. The companion map $S_{BB}(\hat{n}, r)$ is qualitatively

very similar to the map $S_{AB}$. It is the anisotropy of the noise that gives rise to a non-trivial (*i.e.* non-uniform) $S_{AB}$ map, as is clear from the comparison in the same figure with a plot of the number of observations per pixel. This can help us in understanding the contribution of the linear piece associated with the anisotropy of the noise to the estimator. Let us consider a particular Gaussian Monte Carlo realization with a long wavelength mode crossing one of the regions with a high number of observations. The trilinear piece of the estimator will then detect a spurious non-Gaussian signal associated with the correlation between this long wavelength mode and the small short scale power of the noise ([5]). The maps $S_{AB}$ and $S_{BB}$, because of their particular shape, will have a non-zero dot product with precisely the same long wavelength mode of the Monte Carlo map, and with an amplitude proportional to the anisotropy of the two point function of the noise, thus effectively subtracting the spurious signal detected by the trilinear piece and reducing the variance of the estimator.

As the mask breaks rotational invariance, the CMB signal also gives non-uniform $S$-maps. However, the breaking of rotational invariance can be neglected far from the galaxy mask, so we expect that the contribution to the $S$-maps from the CMB is to first approximation constant outside the mask (and zero inside). In this approximation, the linear contribution of the estimator would be sensitive only to the average value outside the mask. However, given that we are constraining the statistical properties of temperature fluctuations, the average temperature in the region outside the mask has to be subtracted before performing the analysis; therefore we expect the linear correction associated with the CMB signal to be rather small. These expectations are in fact verified by our simulations. We checked that the maps $S$ coming from the CMB signal are to first approximation constant outside the mask, with additional features coming from the patches used to mask out bright sources outside the Galactic plane. We then verified that if the average value of the temperature is not subtracted, the linear term coming from the CMB signal gives a very important reduction of the estimator variance, while its effect is almost negligible when the mean temperature is

[5]The effect of this spurious signal obviously averages to zero among many Monte Carlo realizations but it increases the variance of the estimator.

subtracted, as we do in the analysis.

In figure 5-6, we study the standard deviation of the estimators for $f_{\rm NL}^{\rm equil.}$. The estimator without linear corrections is quite close to the information-theoretical limit, so we did not add the linear corrections (which would require many averages analogous to the maps $S_{AB}$ and $S_{BB}$). The reason why we have such a good behavior is that, as mentioned, here most of the signal comes from equilateral configurations. Thus the estimator is not very sensitive to the correlation between the short scale power and the (long wavelength) number of observations. Moreover the inversion of the covariance matrix is important only for the low multipoles, which give only a small fraction of the signal for $f_{\rm NL}^{\rm equil.}$. We find that the estimator with smallest standard deviation is at $l_{\rm max} = 405$, with a standard deviation of 151. The analysis of the data with the same $l_{\rm max}$ gives $-64$. We deduce a $2\sigma$ limit

$$-366 < f_{\rm NL}^{\rm equil.} < 238 \quad \text{at } 95\% \text{ C.L.} \tag{5.37}$$

The given limit is approximately 2 times stronger than the limit obtained in [4], indirectly obtained starting from the limit on $f_{\rm NL}^{\rm local}$. The limit appears weaker than for the local case because, for the same $f_{\rm NL}$, the local distribution has larger signal to noise ratio than an equilateral one, as evident from fig. 5-1. This is not a physical difference but merely a consequence of our defining $f_{\rm NL}$ at the equilateral configuration.

To check that the two limits correspond approximately to the same "level of non-Gaussianity" we can define a quantity which is sensitive to the 3-point function integrated over all possible shapes of the triangle in momentum space. In this way it will be independent of which point we choose for normalization. We define this quantity, which we will call NG, directly in 3d as an integral of the square of the functions in fig. 5-1

$$\mathrm{NG} \equiv \left( \int_{\triangle} \frac{x_2 dx_2\, x_3 dx_3}{(2\pi)^2} \frac{F(1, x_2, x_3)^2}{\Delta_\Phi^3\, x_2^{-3} x_3^{-3}} \right)^{1/2} . \tag{5.38}$$

The integration is restricted to the same triangular region as in fig.s 5-1 and 5-2:

$1 - x_2 \leq x_3 \leq x_2 \leq 1$. The measure of integration comes from the change of variables from the 3d wavevectors to the ratios $x_2 = k_2/k_1$ and $x_3 = k_3/k_1$. NG is parametrically of order $\Delta_\Phi^{1/2} \cdot f_{\rm NL}$ (where $\Delta_\Phi \simeq 1.9 \cdot 10^{-8}$ [24, 28]), which is the correct order of magnitude of the non-Gaussianity, analogous to the skewness for a single random variable. To better understand the meaning of the defined quantity, note that if we integrate inside the parentheses in eq. (5.38) over the remaining wavevector we get the total signal to noise ratio (or better the non-Gaussian to Gaussian ratio). This further integration would approximately multiply NG by the square root of the number of data. This means that to detect a given value of NG we need a number of data of order $\mathrm{NG}^{-2}$, in order to have a signal to noise ratio of order 1. This is clearly a good way to quantify the deviation of the statistics from pure Gaussianity. The $2\sigma$ windows for $f_{\rm NL}$ can be converted to constraints on NG (we define NG to have the same sign of $f_{\rm NL}$) [6]

$$-0.006 < \mathrm{NG}^{\rm local} < 0.025 \quad \text{at } 95\% \text{ C.L.} \tag{5.39}$$

$$-0.016 < \mathrm{NG}^{\rm equil.} < 0.010 \quad \text{at } 95\% \text{ C.L.} \tag{5.40}$$

Contrary to what one might think from a naive look at the limits on $f_{\rm NL}$, the maximum tolerated amount of non-Gaussian signal in a map is thus very similar for both shapes.

So far in this chapter, we have neglected any possible dependence on the cosmological parameters. A proper analysis would marginalize over our uncertainties in parameters and this would increase the allowed range of $f_{\rm NL}$. In order to estimate what the effect of these uncertainties is, let us imagine that the real cosmological parameters are not exactly equal to the best fit ones. The cosmological parameters are determined mainly from the 2-point function of the CMB, $C_l^{\rm cmb}$, therefore the largest error bars are associated to those combinations of parameters which leave $C_l^{\rm cmb}$ unchanged. In the limit in which the $C_l^{\rm cmb}$'s remain the same, also the variance of our estimator (which is computed with the best fit cosmological parameters for

[6] Note that for the local model the integration in eq. (5.38) diverges like the log of the ratio of the minimum to the maximum scales in the integral. For the quoted numbers we chose a ratio of 1000.

a ΛCDM cosmology with power-law spectrum [24]) remains the same: in the weak non-Gaussian limit the variance just depends on the 2-point function. However, the combination of parameters which leave unchanged the $C_l^{\rm cmb}$'s does not necessarily leave unchanged the bispectrum, therefore uncertainties in the determination of the cosmological parameters will have an influence on the expectation value of the estimator. The expectation value of the estimator would be:

$$\langle \mathcal{E} \rangle = \frac{1}{N} \sum_{l_1<l_2<l_3} \frac{B_{l_1 l_2 l_3} \widetilde{B}_{l_1 l_2 l_3}}{C_{l_1} C_{l_2} C_{l_3}} \,, \tag{5.41}$$

where $N$, $B_{l_1 l_2 l_3}$ and $C_l$ are the same as in our analysis, computed with the best fit cosmological parameters, while $\widetilde{B}_{l_1 l_2 l_3}$ is the true bispectrum. Thus when varying parameters, the normalization $N$ needs to be changed to make the estimator unbiased.

The most relevant uncertainty is the reionization optical depth $\tau$, which is correlated with the uncertainty in the amplitude of the power spectrum $\Delta_\Phi$. With the purpose of having a rough estimate, we can approximate the effect of reionization by a multiplicative factor $e^{-\tau}$ in front of the transfer function $\Delta_l^T(k)$ for $l$ corresponding to scales smaller than the horizon at reionization. In order to keep the $C_l^{\rm cmb}$'s unchanged, at least at high $l$'s, we then multiply $\Delta_\Phi$ by $e^{2\tau}$. The bispectrum is proportional to $\Delta_\Phi^2\ \Delta_l^T(k)^3$ and thus changes even if the $C_l$'s do not. For the equilateral shape most of the signal comes from equilateral configurations with all the 3 modes inside the horizon at reionization; in this case $\langle \mathcal{E} \rangle$ scales roughly as $e^\tau$. For the local shape the signal comes from squeezed configurations with one mode of much smaller wavelength than the others. Taking only 2 modes inside the horizon at reionization we get $\langle \mathcal{E} \rangle \propto e^{2\tau}$.

If we consider the $1\sigma$ error, $\tau = 0.166^{+0.076}_{-0.071}$ [24], we find that the uncertainty in the reionization depth should correspond to an error on $f_{\rm NL}$ of order 8% for the equilateral shape, and 15% for the local shape. These numbers translate directly into uncertainties in the allowed ranges we quote. In the future, if the error induced by the uncertainty in the cosmological parameters will become comparable to the variance of the estimator, a more detailed analysis will be required; however, at the moment

an analysis with fixed cosmological parameters is certainly good enough.

## 5.5 Conclusions

We have developed a method to constrain the level of non-Gaussianity when the induced 3-point function is of the "equilateral" type. We showed that the induced shape of the 3-point function can be very well approximated by a factorizable form making the analysis practical. Applying our technique to the WMAP first year data we obtained

$$-366 < f_{\rm NL}^{\rm equil.} < 238 \quad \text{at } 95\% \text{ C.L.} \tag{5.42}$$

The natural expectation for this amplitude for ghost or DBI inflation is $f_{\rm NL}^{\rm equil.} \sim 100$, below the current constraints but at a level that should be attainable in the future. The limit an experiment can set on $f_{\rm NL}$ just scales as the inverse of the maximum $l$ the experiment can detect. As a result, in the case of WMAP, increased observing time will approximately decrease the error bars by 30% and 60% for 4 years and 8 years of observation. The increased angular resolution and smaller noise of Planck pushes the point where noise dominates over signal to $l \sim 1500$. This should result in a factor of 4 improvement on the present constraints. In addition polarization measurements by Planck can further reduce the range by an additional factor of 1.6 [29].

We also constrained the presence of a 3-point function of the "local" type, predicted for example by the curvaton and variable decay width inflation models, obtaining

$$-27 < f_{\rm NL}^{\rm local} < 121 \quad \text{at } 95\% \text{ C.L.} \tag{5.43}$$

We defined a quantity NG, which quantifies for any shape the level of non-Gaussianity of the data, analogously to the skewness for a single random variable. The limits on NG are very similar for the two shapes, approximately $|\text{NG}| < 0.02$ at 95% C.L. .

We showed that unless one has a full sky map with uniform noise, the estimator

must contain a piece that is linear on the data in order to extract all the relevant information from the data and saturate the Cramer-Rao bound for the 3-point function measurement uncertainty. This correction is particularly important for the local shape and accounts for the improvement of our limits over that from the WMAP team. Moreover this correction goes a long way towards reducing the divergence in the variance of the estimator as $l_{\max}$ is increased.

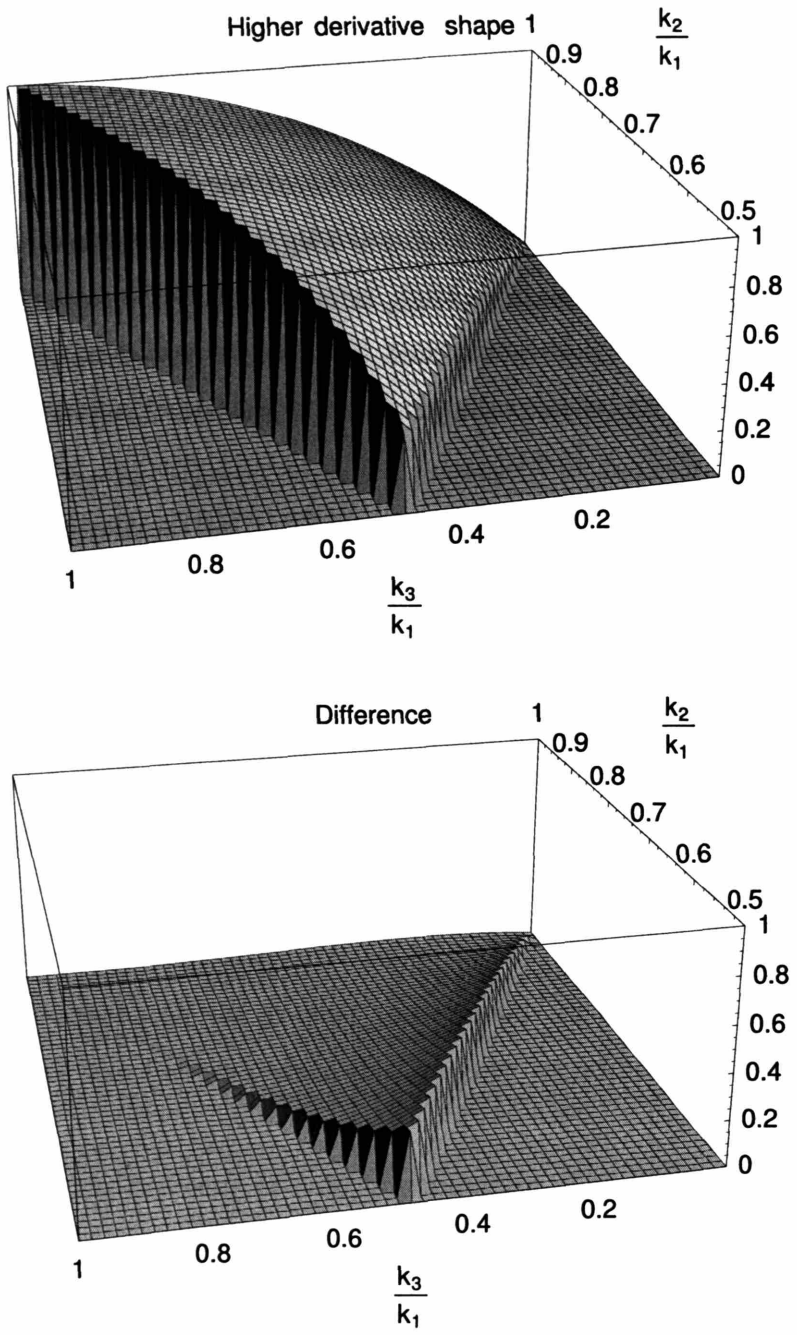


Figure 5-2: Top. Plot of the function $F(1, k_2/k_1, k_3/k_1)(k_2/k_1)^2(k_3/k_1)^2$ predicted by the higher-derivative [7] and the DBI models [9]. Bottom. Difference between the above plot and the analogous one (top of fig. 5-1) for the factorizable equilateral shape used in the analysis.

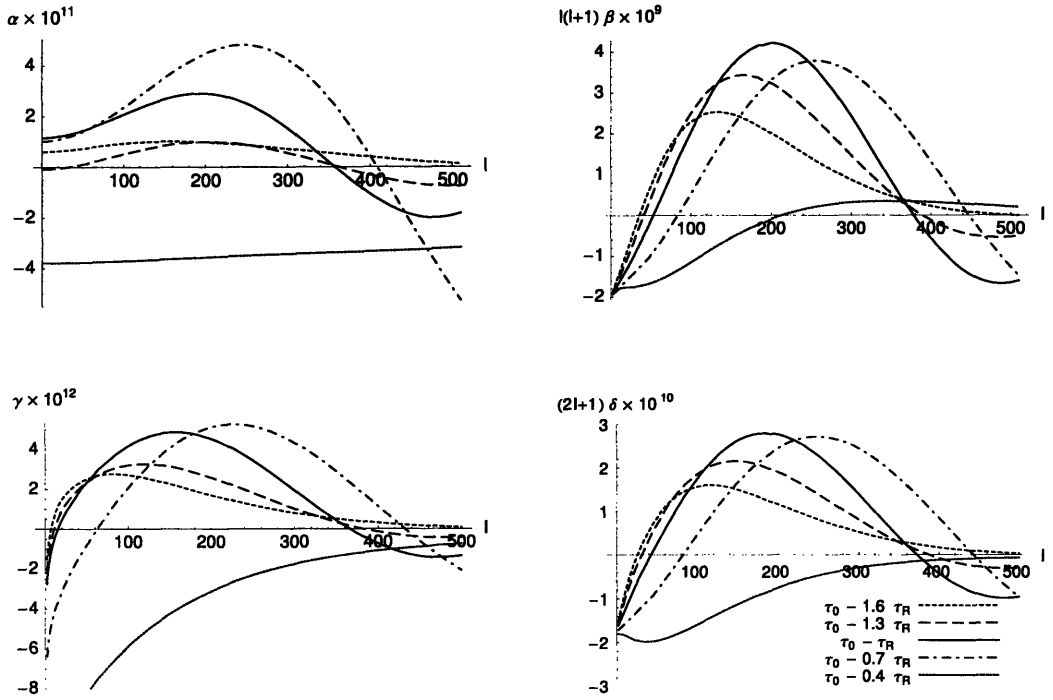


Figure 5-3: The functions $\alpha_l(r)$ (in units of $\mathrm{Mpc}^{-3}$), $\beta_l(r)$ (dimensionless), $\gamma_l(r)$ (in units of $\mathrm{Mpc}^{-2}$), and $\delta_l(r)$ (in units of $\mathrm{Mpc}^{-1}$) are shown for various radii $r$ as functions of the multipole number $l$. The cosmological parameters are the same ones used in the analysis: $\Omega_b h^2 = 0.024$, $\Omega_m h^2 = 0.14$, $h = 0.72$, $\tau = 0.17$. With these parameters, the present conformal time $\tau_0$ is 13.24 Gpc and the recombination time $\tau_R$ is 0.27 Gpc.

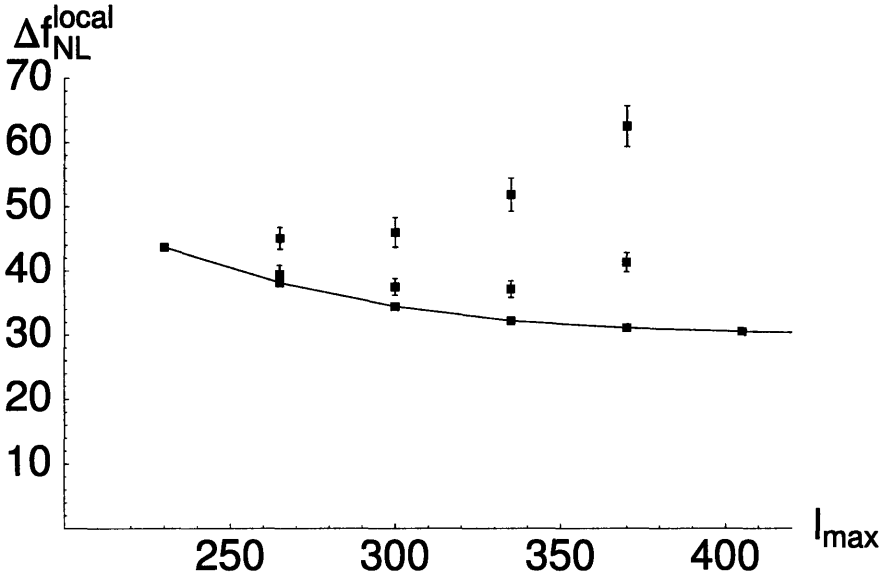


Figure 5-4: Standard deviation for estimators of $f_{\rm NL}^{\rm local}$ as a function of the maximum $l$ used in the analysis. Lower curve: lower bound deduced from the full sky variance. Lower data points: standard deviations for the trilinear + linear estimator. Upper data points: the same for the estimator without linear term, for which the divergence at high $l$'s caused by noise anisotropy had already been noticed in [11].

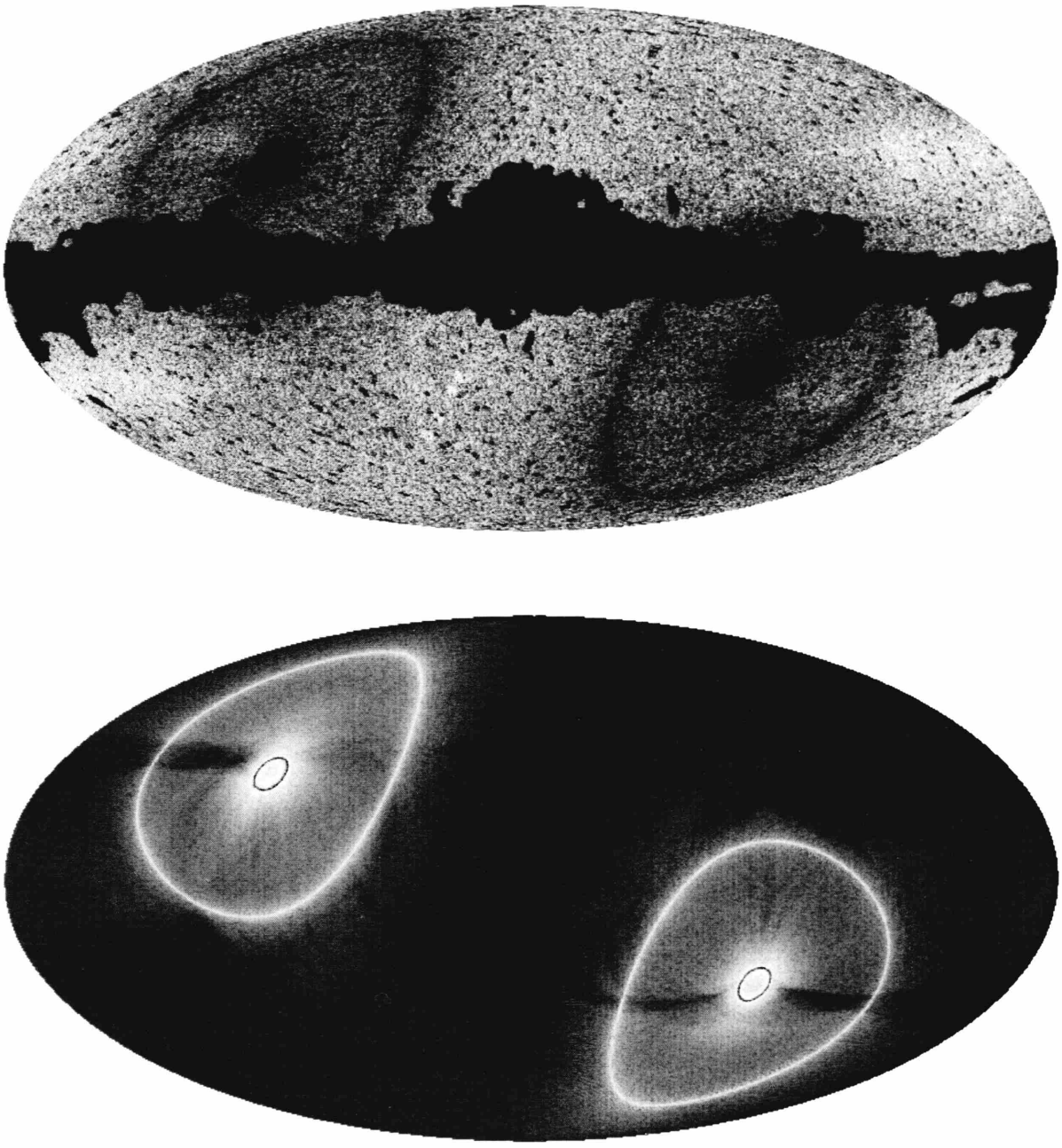

Figure 5-5: Top: $S_{AB}(\hat{n}, r)$ map for $r$ around recombination calculated with noise only. Bottom: number of observations as a function of the position in the sky for the Q1 band (the plot is quite similar for the other bands). A lighter color indicates points which are observed many times.

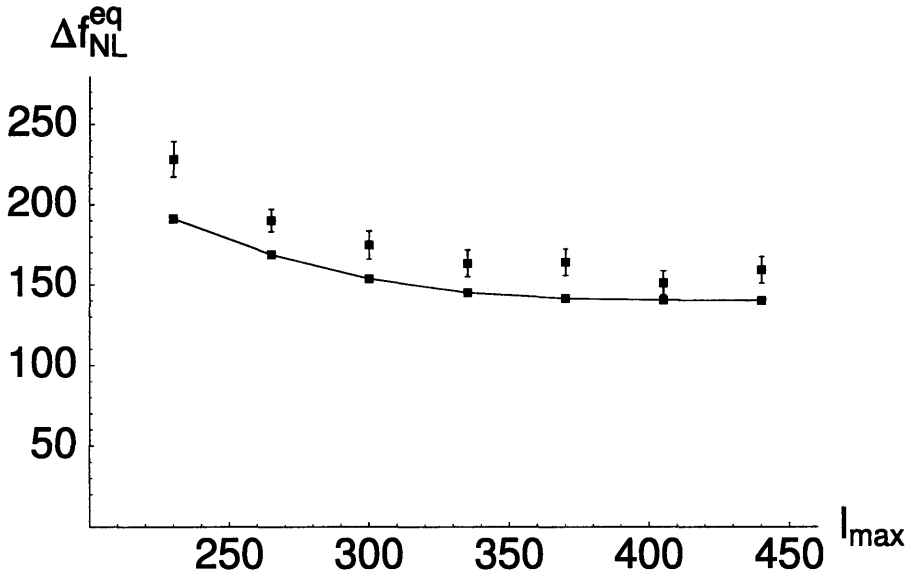


Figure 5-6: Standard deviations for estimators of $f_{\rm NL}^{\rm equil.}$ as a function of the maximum $l$ used in the analysis. Lower curve: lower bound deduced from the full sky variance. Data points: standard deviations for the estimator without linear term.

# Bibliography


[1] J. Maldacena, "Non-Gaussian features of primordial fluctuations in single field inflationary models," JHEP **0305**, 013 (2003) [astro-ph/0210603].

[2] V. Acquaviva, N. Bartolo, S. Matarrese and A. Riotto, "Second-order cosmological perturbations from inflation," Nucl. Phys. B **667**, 119 (2003) [astro-ph/0209156].

[3] P. Creminelli and M. Zaldarriaga, "CMB 3-point functions generated by non-linearities at recombination," Phys. Rev. D **70**, 083532 (2004) [astro-ph/0405428].

[4] D. Babich, P. Creminelli and M. Zaldarriaga, "The shape of non-Gaussianities," JCAP **0408**, 009 (2004) [astro-ph/0405356].

[5] D. H. Lyth, C. Ungarelli and D. Wands, "The primordial density perturbation in the curvaton scenario," Phys. Rev. D **67**, 023503 (2003) [astro-ph/0208055].

[6] M. Zaldarriaga, "Non-Gaussianities in models with a varying inflaton decay rate," Phys. Rev. D **69**, 043508 (2004) [astro-ph/0306006].

[7] P. Creminelli, "On non-Gaussianities in single-field inflation," JCAP **0310**, 003 (2003) [astro-ph/0306122].

[8] N. Arkani-Hamed, P. Creminelli, S. Mukohyama and M. Zaldarriaga, "Ghost inflation," JCAP **0404**, 001 (2004) [hep-th/0312100].

[9] M. Alishahiha, E. Silverstein and D. Tong, "DBI in the sky," Phys. Rev. D **70**, 123505 (2004) [hep-th/0404084].

[10] L. Senatore, "Tilted ghost inflation," Phys. Rev. D **71**, 043512 (2005) [astro-ph/0406187].

[11] E. Komatsu *et al.*, "First Year Wilkinson Microwave Anisotropy Probe (WMAP) Observations: Tests of Gaussianity," Astrophys. J. Suppl. **148**, 119 (2003) [astro-ph/0302223].

[12] A. F. Heavens, "Estimating non-Gaussianity in the microwave background," astro-ph/9804222.

[13] D. Babich, "Optimal Estimation of Non-Gaussianity," astro-ph/0503375.

[14] L. M. Wang and M. Kamionkowski, "The cosmic microwave background bispectrum and inflation," Phys. Rev. D **61**, 063504 (2000) [astro-ph/9907431].

[15] E. Komatsu, D. N. Spergel and B. D. Wandelt, "Measuring primordial non-Gaussianity in the cosmic microwave background," astro-ph/0305189.

[16] Heron of Alexandria, *Metrica*, Alexandria, *circa* 100 B.C. – 100 A.D.

[17] U. Seljak and M. Zaldarriaga, "A Line of Sight Approach to Cosmic Microwave Background Anisotropies," Astrophys. J. **469**, 437 (1996) [astro-ph/9603033].

[18] C. Bennett *et al.*, "First Year Wilkinson Microwave Anisotropy Probe (WMAP) Observations: Foreground Emission," Astrophys. J. Suppl. **148**, 97 (2003) [astro-ph/0302208].

[19] R. Juszkiewicz, D. H. Weinberg, P. Amsterdamski, M. Chodorowski and F. Bouchet, "Weakly nonlinear Gaussian fluctuations and the Edgeworth expansion," Astrophys. J. **442** (1995) 39.

[20] A. Taylor and P. Watts, "Parameter information from nonlinear cosmological fields," Mon. Not. Roy. Astron. Soc. **328**, 1027 (2001) [astro-ph/0010014].

[21] F. Bernardeau and L. Kofman, "Properties of the Cosmological Density Distribution Function," Astrophys. J. **443** (1995) 479 [astro-ph/9403028].

[22] G. Hinshaw *et al.*, "First Year Wilkinson Microwave Anisotropy Probe (WMAP) Observations: Angular Power Spectrum," Astrophys. J. Suppl. **148**, 135 (2003) [astro-ph/0302217].

[23] E. Komatsu, "The Pursuit of Non-Gaussian Fluctuations in the Cosmic Microwave Background," astro-ph/0206039.

[24] D. N. Spergel *et al.* [WMAP Collaboration], "First Year Wilkinson Microwave Anisotropy Probe (WMAP) Observations: Determination of Cosmological Parameters," Astrophys. J. Suppl. **148**, 175 (2003) [astro-ph/0302209].

[25] L. Page *et al.*, "First Year Wilkinson Microwave Anisotropy Probe (WMAP) Observations: Beam Profiles and Window Functions," Astrophys. J. Suppl. **148**, 39 (2003) [astro-ph/0302214].

[26] C. L. Bennett *et al.*, "First Year Wilkinson Microwave Anisotropy Probe (WMAP) Observations: Preliminary Maps and Basic Results," Astrophys. J. Suppl. **148**, 1 (2003) [astro-ph/0302207].

[27] M. Tegmark, A. de Oliveira-Costa & A.J.S. Hamilton, "A high resolution foreground cleaned CMB map from WMAP", Phys. Rev. D **68**, 123523 (2003) [astro-ph/0302496].

[28] L. Verde *et al.*, "First Year Wilkinson Microwave Anisotropy Probe (WMAP) Observations: Parameter Estimation Methodology," Astrophys. J. Suppl. **148**, 195 (2003) [arXiv:astro-ph/0302218].

[29] D. Babich and M. Zaldarriaga, "Primordial Bispectrum Information from CMB Polarization," Phys. Rev. D **70**, 083005 (2004) [astro-ph/0408455].

[30] K. M. Gorski, E. Hivon and B. D. Wandelt, "Analysis Issues for Large CMB Data Sets," astro-ph/9812350.

# Chapter 6

# The Minimal Model for Dark Matter and Unification

Gauge coupling unification and the success of TeV-scale weakly interacting dark matter are usually taken as evidence of low energy supersymmetry (SUSY). However, if we assume that the tuning of the higgs can be explained in some *unnatural* way, from environmental considerations for example, SUSY is no longer a necessary component of any Beyond the Standard Model theory. In this chapter we study the minimal model with a dark matter candidate and gauge coupling unification. This consists of the SM plus fermions with the quantum numbers of SUSY higgsinos, and a singlet. It predicts thermal dark matter with a mass that can range from 100 GeV to around 2 TeV and generically gives rise to an electric dipole moment (EDM) that is just beyond current experimental limits, with a large portion of its allowed parameter space accessible to next generation EDM and direct detection experiments. We study precision unification in this model by embedding it in a 5-D orbifold GUT where certain large threshold corrections are calculable, achieving gauge coupling and $b$-$\tau$ unification, and predicting a rate of proton decay just beyond current limits.

## 6.1 Introduction

Over the last few decades the search for physics beyond the Standard Model (SM) has largely been driven by the principle of naturalness, according to which the parameters of a low energy effective field theory like the SM should not be much smaller than the contributions that come from running them up to the cutoff. This principle can be used to constrain the couplings of the effective theory with positive mass dimension, which have a strong dependence on UV physics. Requiring no fine tuning between bare parameters and the corrections they receive from renormalization means that the theory must have a low cutoff. New physics can enter at this scale to literally cut off the high-energy contributions from renormalization.

In the specific case of the SM the effective lagrangian contains two relevant parameters: the higgs mass and the cosmological constant (c.c), both of which give rise to problems concerning the interpretation of the low energy theory. Any discussion of large discrepancies between expectation and observation must begin with what is known as the c.c. problem. This relates to our failure to find a well-motivated dynamical explanation for the factor of $10^{120}$ between the observed c.c and the naive contribution to it from renormalization which is proportional to $\Lambda^4$, where $\Lambda$ is the cutoff of the theory, usually taken to be equal to the Planck scale. Until very recently there was still hope in the high energy physics community that the c.c. might be set equal to zero by some mysterious symmetry of quantum gravity. This possibility has become increasingly unlikely with time since the observation that our universe is accelerating strongly suggests the presence of a non-zero cosmological constant [1, 2].

A less extreme example is the hierarchy between the higgs mass and the GUT scale which can be explained by SUSY breaking at around a TeV. Unfortunately the failure of indirect searches to find light SUSY partners has brought this possibility into question, since it implies the presence of some small fine-tuning in the SUSY sector. This 'little hierarchy' problem [3, 4] raises some doubts about the plausibility of low energy SUSY as an explanation for the smallness of the higgs mass.

Both these problems can be understood from a different perspective: the fact

that the c.c. and the higgs mass are relevant parameters means that they dominate low energy physics, allowing them to determine very gross properties of the effective theory. We might therefore be able to put limits on them by requiring that this theory satisfy the environmental conditions necessary for the universe not to be empty. This approach was first used by Weinberg [5] to deduce an upper bound on the cosmological constant from structure formation, and was later employed to solve the hierarchy problem in an analogous way by invoking the atomic principle [6].

Potential motivation for this class of argument can be found in the string theory landscape. At low energies some regions of the landscape can be thought of as a field theory with many vacua, each having different physical properties. It is possible to imagine that all these vacua might have been equally populated in the early universe, but observers can evolve only in the few where the low energy conditions are conducive to life. The number of vacua with this property can be such a small proportion of the total as to dwarf even the tuning involved in the c.c. problem; resolving the hierarchy problem similarly needs no further assumptions. This mechanism for dealing with both issues simultaneously by scanning all relevant parameters of the low energy theory within a landscape was recently proposed in [7, 8].

From this point of view there seems to be no fundamental inconsistency with having the SM be the complete theory of our world up to the Planck scale; nevertheless this scenario presents various problems. Firstly there is increasing evidence for dark matter (DM) in the universe, and current cosmological observations fit well with the presence of a stable weakly interacting particle at around the TeV scale. The SM contains no such particle. Secondly, from a more aesthetic viewpoint gauge couplings do not quite unify at high energies in the SM alone; adding weakly interacting particles changes the running so unification works better. A well-motivated example of a model that does this is Split Supersymmetry [7], which is however not the simplest possible theory of this type. In light of this we study the minimal model with a finely-tuned higgs and a good thermal dark matter candidate proposed in [8], which also allows for gauge coupling unification. Although a systematic analysis of the complete set of such models was carried out in [9], the simplest one we study here was missed because

the authors did not consider the possibility of having large UV threshold corrections that fix unification, as well as a GUT mechanism suppressing proton decay.

Adding just two 'higgsino' doublets[1] to the SM improves unification significantly. This model is highly constrained since it contains only one new parameter, a Dirac mass term for the doublets ('$\mu$'), the neutral components of which make ideal DM candidates for 990 GeV$\lesssim \mu \lesssim$ 1150 GeV (see [9] for details). However a model with pure higgsino dark matter is excluded by direct detection experiments since the degenerate neutralinos have unsuppressed vector-like couplings to the $Z$ boson, giving rise to a spin-independent direct detection cross-section that is 2-3 orders of magnitude above current limits[2] [10, 11]. To circumvent this problem, it suffices to include a singlet ('bino') at some relatively high energy ($\lesssim 10^9$ GeV), with yukawa couplings with the higgsinos and higgs, to lift the mass degeneracy between the 'LSP' and 'NLSP'[3] by order 100 keV [12], as explained in Appendix 6.8. The instability of such a large mass splitting between the higgsinos and bino to radiative corrections, which tend to make the higgsinos as heavy as the bino, leads us to consider these masses to be separated by at most two orders of magnitude, which is technically natural. We will see that the yukawa interactions allow the DM candidate to be as heavy as 2.2 TeV. There is also a single reparametrization invariant CP violating phase which gives rise to a two-loop contribution to the electron EDM that is well within the reach of next-generation experiments.

Our chapter is organized as follows: in Section 6.2 we briefly introduce the model, in Section 6.3 we study the DM relic density in different regions of our parameter space with a view to constraining these parameters; we look more closely at the experimental implications of this model in the context of dark matter direct detection and EDM experiments in Sections 6.4 and 6.5. Next we study gauge coupling unification at two loops. We find that this is consistent modulo unknown UV threshold corrections,

[1]Here 'higgsino' is just a mnemonic for their quantum numbers, as these particles have nothing to do with the SUSY partners of the higgs.

[2]A model obtained adding a single higgsino doublet, although more minimal, is anomalous and hence is not considered here.

[3]From here on we will refer to these particles and couplings by their SUSY equivalents **without** the quotation marks for simplicity.

however the unification scale is too low to embed this model in a simple 4D GUT. This is not necessarily a disadvantage since 4D GUTs have problems of their own, in splitting the higgs doublet and triplet for example. A particularly appealing way to solve all these problems is by embedding our model in a 5D orbifold GUT, in which we can calculate all large threshold corrections and achieve unification. We also find a particular model with $b$-$\tau$ unification and a proton lifetime just above current bounds. We conclude in Section 6.7.

## 6.2 The Model

As mentioned above, the model we study consists of the SM with the addition of two fermion doublets with the quantum numbers of SUSY higgsinos, plus a singlet bino, with the following renormalizable interaction terms:

$$\mu\Psi_u\Psi_d + \frac{1}{2}M_1\Psi_s\Psi_s + \lambda_u\Psi_u h\Psi_s + \lambda_d\Psi_d h^\dagger\Psi_s \tag{6.1}$$

where $\Psi_s$ is the bino, $\Psi_{u,d}$ are the higgsinos, $h$ is the finely-tuned higgs.

We forbid all other renormalizable couplings to SM fields by imposing a parity symmetry under which our additional particles are odd whereas all SM fields are even. As in SUSY conservation of this parity symmetry implies that our LSP is stable.

The size of the yukawa couplings between the new fermions and the higgs are limited by requiring perturbativity to the cutoff. For equal yukawas this constrains $\lambda_u(M_Z) = \lambda_d(M_Z) \leq 0.88$, while if we take one of the couplings to be small, say $\lambda_d(M_Z) = 0.1$ then $\lambda_u(M_Z)$ can be as large as 1.38.

The above couplings allow for the CP violating phase $\theta = \mathrm{Arg}(\mu M_1 \lambda_u^* \lambda_d^*)$, giving 5 free parameters in total. In spite of its similarity to the MSSM (and Split SUSY) weak-ino sector, there are a number of important differences which have a qualitative effect on the phenomenology of the model, especially from the perspective of the relic density. Firstly a bino-like LSP, which usually mixes with the wino, will generically annihilate less effectively in this model since the wino is absent. Secondly the new

yukawa couplings are free parameters so they can get much larger than in Split SUSY, where the usual relation to gauge couplings is imposed at the high SUSY breaking scale. This will play a crucial role in the relic density calculation since larger yukawas means greater mixing in the neutralino sector as well as more efficient annihilation, especially for the bino which is a gauge singlet.

Our 3×3 neutralino mass matrix is shown below:

$$M_N = \begin{pmatrix} M_1 & \lambda_u v & \lambda_d v \\ \lambda_u v & 0 & -\mu e^{i\theta} \\ \lambda_d v & -\mu e^{i\theta} & 0 \end{pmatrix}$$

for $v = 174$ GeV, where we have chosen to put the CP violating phase in the $\mu$ term. The chargino is the charged component of the higgsino with tree level mass $\mu$.

It is possible to get a feel for the behavior of this matrix by diagonalizing it perturbatively for small off-diagonal terms, this is done in Appendix 6.8.

## 6.3 Relic Abundance

In this section we study the regions of parameter space in which the DM abundance is in accordance the post-WMAP $2\sigma$ region $0.094 < \Omega_{\rm dm} h^2 < 0.129$ [2], where $\Omega_{\rm dm}$ is the fraction of today's critical density in DM, and $h = 0.72 \pm 0.05$ is the Hubble constant in units of 100 km/(s Mpc).

As in Split SUSY, the absence of sleptons in our model greatly decreases the number of decay channels available to the LSP [13, 14]. Also similar to Split SUSY is the fact that our higgs can be heavier than in the MSSM (in our case the higgs mass is actually a free parameter), hence new decay channels will be available to it, resulting in a large enhancement of its width especially near the $WW$ and $ZZ$ thresholds. This in turn makes accessible neutralino annihilation via a resonant higgs, decreasing the relic density in regions of the parameter space where this channel is accessible. For a very bino-like LSP this is easily the dominant annihilation channel, allowing the bino density to decrease to an acceptable level. We use a modified version of

the DarkSUSY [15] code for our relic abundance calculations, explicitly adding the resonant decay of the heavy higgs to $W$ and $Z$ pairs.

As mentioned in the previous section there are also some differences between our model and Split SUSY that are relevant to this discussion: the first is that the Minimal Model contains no wino equivalent (this feature also distinguishes this model from that in [16], which contains a similar dark matter analysis). The second difference concerns the size of the yukawa couplings which govern this mixing, as well as the annihilation cross-section to higgses. Rather than being tied to the gauge couplings at the SUSY breaking scale, these couplings are limited only by the constraint of perturbativity to the cutoff. This means that the yukawas can be much larger in our model, helping a bino-like LSP to both mix more and annihilate more efficiently. These effects are evident in our results and will be discussed in more detail below.

We will restrict our study of DM relic abundance and direct detection in this model to the case with no CP violating phase ($\theta = 0, \pi$); we briefly comment on the general case in Section 6.5. Our results for different values of the yukawa couplings are shown in Figure 6-1 below, in which we highlight the points in the $\mu$-$M_1$ plane that give rise to a relic density within the cosmological bound. The higgs is relatively heavy ($M_{\text{higgs}} = 160$ GeV) in this plot in order to access processes with resonant annihilation through an s-channel higgs. As we will explain below the only effect this has is to allow a low mass region for a bino-like LSP with $M_1 \sim M_{\text{higgs}}/2$.

Notice that the relic abundance seems to be consistent with a dark matter mass as large as 2.2 TeV. Although a detailed analysis of the LHC signature of this model is not within the scope of this study, it is clear that a large part of this parameter space will be inaccessible at LHC. The pure higgsino region for example, will clearly be hard to explore since the higgsinos are heavy and also very degenerate. There is more hope in the bino LSP region for a light enough spectrum.

While analyzing these results we must keep in mind that $\Omega_{\text{dm}} \sim 10^{-9}\text{GeV}^{-2}/\langle\sigma\rangle_{\text{eff}}$, where $\langle\sigma\rangle_{\text{eff}}$ is an effective annihilation cross section for the LSP at the freeze out temperature, which takes into consideration all coannihilation channels as well as the thermal average [17]. It will be useful to approximate this quantity as the cross-

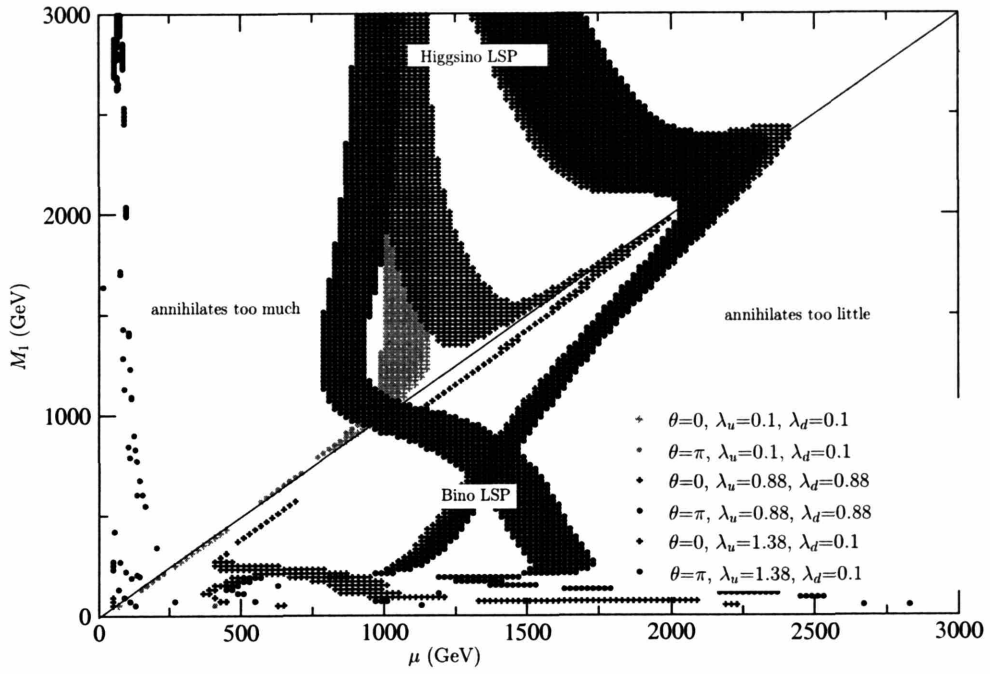


Figure 6-1: Graph showing regions of parameter space consistent with WMAP.

section for the dominant annihilation channel. Although rough, this approximation will help us build some intuition on the behavior of the relic density in different parts of the parameter space. We will not discuss the region close to the origin where the interpretation of the results become more involved due to large mixing and coannihilation.

### 6.3.1 Higgsino Dark Matter

In order to get a feeling for the structure of Figure 6-1, it is useful to begin by looking at the regions in which the physics is most simple. This can be achieved by diminishing the the number of annihilation channels that are available to the LSP by taking the limit of small yukawa couplings.

For $\theta = 0$, mixing occurs only on the diagonal $M_1 = \mu$ to a very good approximation (see Appendix 6.8 and Figure 6-2), hence the region above the diagonal corresponds to a pure higgsino LSP with mass $\mu$. For $\lambda_u = \lambda_d = 0.1$ the yukawa interactions are irrelevant and the LSP dominantly annihilates by t-channel neutral (charged) higgsino exchange to $ZZ$ ($WW$) pairs. Charginos, which have a tree-level

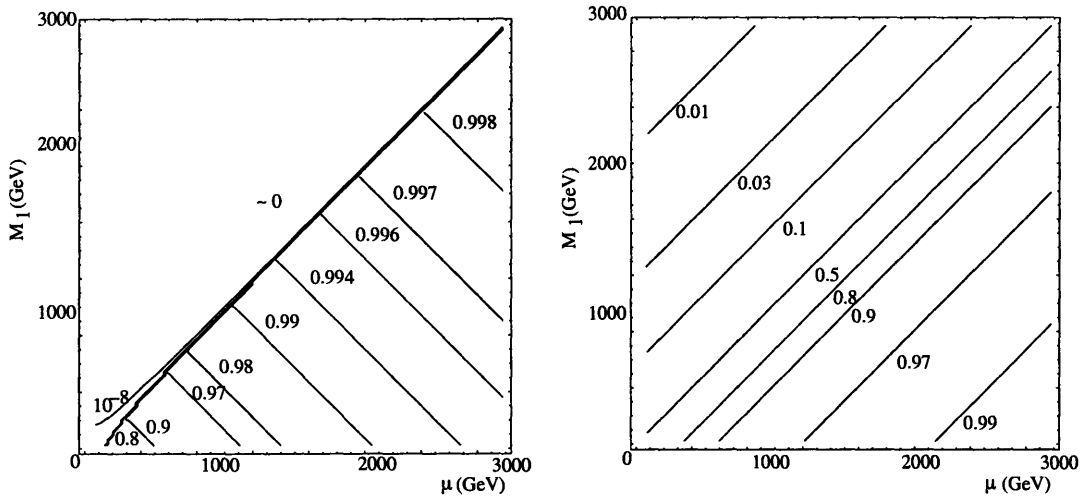


(a) $\theta$=0 (b) $\theta$=$\pi$

Figure 6-2: Gaugino fraction contours for $\lambda_u = \lambda_d = 0.88$ and $\theta$=0 (left),$\pi$ (right).

mass $\mu$ and are almost degenerate with the LSP, coannihilate with it, decreasing the relic density by a factor of 3. This fixes the LSP mass to be around $\mu = 1$ TeV, giving rise to the wide vertical band that can be seen in the figure; for smaller $\mu$ the LSP over-annihilates, for larger $\mu$ it does not annihilate enough.

Increasing the yukawa couplings increases the importance of t-channel bino exchange to higgs pairs. Notice that taking the limit $M_1 \gg \mu$ makes this new interaction irrelevant, therefore the allowed region converges to the one in which only gauge interactions are effective. Taking this as our starting point, as we approach the diagonal the mass of the bino decreases, causing the t-channel bino exchange process to become less suppressed and increasing the total annihilation cross-section. This explains the shift to higher masses, which is more pronounced for larger yukawas as expected and peaks along the diagonal where the higgsino and bino are degenerate and the bino mass suppression is minimal. The increased coannihilation between higgsinos and binos close to the diagonal does not play a large part here since both particles have access to a similar t-channel diagram.

Taking $\theta = \pi$ makes little qualitative difference when either of the yukawas is small compared to $M_1$ or $\mu$, since in this limit the angle is unphysical and can be rotated

away by a redefinition of the higgsino fields. However we can see in Figure 6-2 that for large yukawas the region above the diagonal $M_1 = \mu$ changes to a mixed state, rather than being pure higgsino as before. Starting again with the large $M_1$ limit and decreasing $M_1$ decreases the mass suppression of the t-channel bino exchange diagram like in the $\theta = 0$ case, but the LSP also starts to mix more with the bino, an effect that acts in the opposite direction and decreases $\langle\sigma\rangle_{\text{eff}}$. This effect happens to outweigh the former, forcing the LSP to shift to lower masses in order to annihilate enough.

With $\theta = \pi$ and yukawas large enough, there is an additional allowed region for $\mu < M_W$. In this region the higgsino LSP is too light to annihilate to on-shell gauge bosons, so the dominant annihilation channels are phase-space suppressed. Furthermore if the splitting between the chargino and the LSP is large enough, the effect of coannihilation with the chargino into photon and on-shell $W$ is Boltzmann suppressed, substantially decreasing the effective cross-section, and giving the right relic abundance even with such a light higgsino LSP. Although acceptable from a cosmological standpoint, this region is excluded by direct searches since it corresponds to a chargino that is too light.

### 6.3.2 Bino Dark Matter

The region below the diagonal $M_1 = \mu$ corresponds to a bino-like LSP. Recall that in the absence of yukawa couplings pure binos in this model do not couple to anything and hence cannot annihilate at all. Turning on the yukawas allows them to mix with higgsinos which have access to gauge annihilation channels. For $\lambda_u = \lambda_d = 0.1$ this effect is only large enough when $M_1$ and $\mu$ are comparable (in fact when they are equal, the neutralino states are maximally mixed for arbitrarily small off-diagonal terms), explaining the stripe near the diagonal in Figure 6-1. Once $\mu$ gets larger than $\sim 1$ TeV even pure higgsinos are too heavy to annihilate efficiently; this means that mixing is no longer sufficient to decrease the dark matter relic density to acceptable values and the stripe ends.

Increasing the yukawas beyond a certain value ($\lambda_u = \lambda_d = 0.88$, which is slightly

larger than their values in Split SUSY, is enough), makes t-channel annihilation to higgses become large enough that a bino LSP does not need to mix at all in order to have the correct annihilation cross-section. This gives rise to an allowed region which is in the shape of a stripe, where for fixed $M_1$ the correct annihilation cross-section is achieved only for the small range of $\mu$ that gives the right t-channel suppression. As $M_1$ increases the stripe converges towards the diagonal in order to compensate for the increase in LSP mass by increasing the cross-section. Once the diagonal is reached this channel cannot be enhanced any further, and there is no allowed region for heavier LSPs. In addition the cross-section for annihilation through an s-channel resonant higgs, even though CP suppressed (see Section 6.5 for details), becomes large enough to allow even LSPs that are very pure bino to annihilate in this way. The annihilation rate for this process is not very sensitive to the mixing, explaining the apparent horizontal line at $M_1 = \frac{1}{2}M_{\text{higgs}} \sim 80$ GeV. This line ends when $\mu$ grows to the point where the mixing is too small.

As in the higgsino case, taking $\theta = \pi$ changes the shape of the contours of constant gaugino fraction and spreads them out in the plane (see Figure 6-2), making mixing with higgsinos relevant throughout the region. For small $M_1$, the allowed region starts where the mixing term is small enough for the combination of gauge and higgs channels not to cause over-annihilation. Increasing $M_1$ again makes the region move towards the diagonal, where the increase in LSP mass is countered by increasing the cross-section for the gauge channel from mixing more.

For either yukawa very large ($\lambda_u = 1.38, \lambda_d = 0.1$), annihilation to higgses via t-channel higgsinos is so efficient that this process alone is sufficient to give bino-like LSPs the correct abundance. As $M_1$ increases the allowed region again moves towards the diagonal in such a way as to keep the effective cross-section constant by decreasing the higgsino mass suppression, thus compensating for the increase in LSP mass. As we remarked earlier since $\lambda_d$ is effectively zero in this case, the angle $\theta$ is unphysical and can be rotated away by a redefinition of the higgsino fields.

## 6.4 Direct Detection

Dark matter is also detectable through elastic scatterings off ordinary matter. The direct detection cross-section for this process can be divided up into a spin-dependent and a spin-independent part; we will concentrate on the former since it is usually dominant. As before we restrict to $\theta = 0$ and $\pi$, we expect the result not to change significantly for intermediate values.

The spin-independent interaction takes place through higgs exchange, via the yukawa couplings which mix higgsinos and binos. Since the only $\chi_1^0\chi_1^0 h$ term in our model involves the product of the gaugino and higgsino fractions, the more mixed our dark matter is the more visible it will be to direct detection experiments. This effect can be seen in Fig 6-3 below.

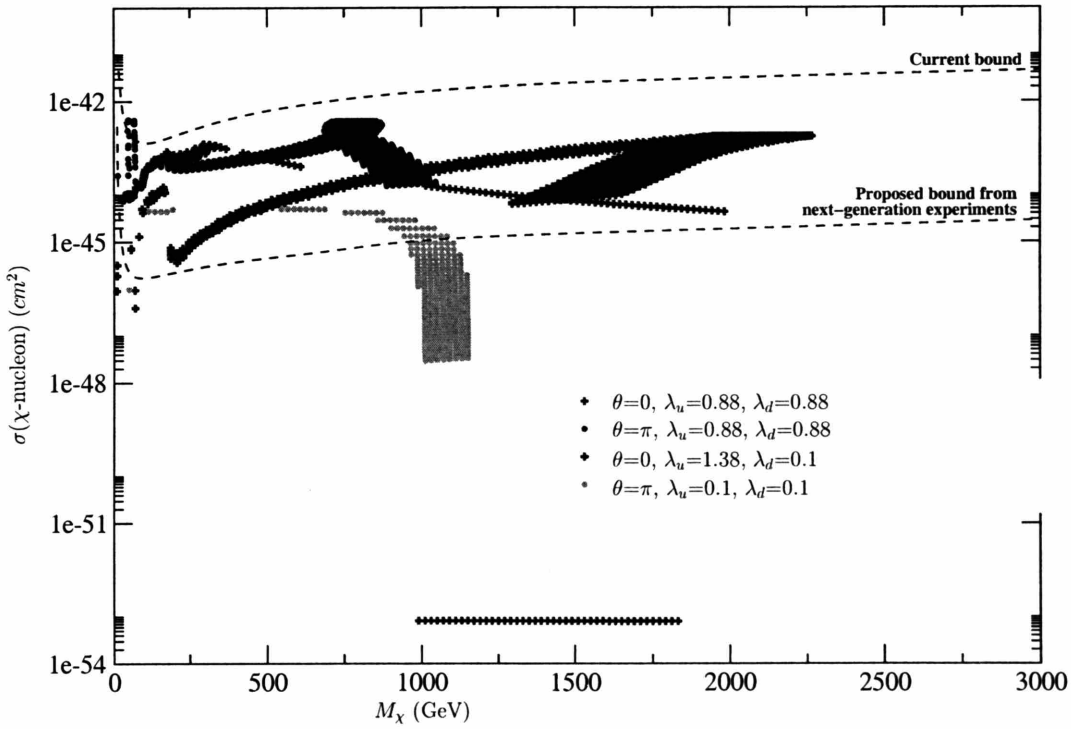


Figure 6-3: Spin-independent part of dark matter direct detection cross-section. The current bound represents the CDMS limit [11], and, as an indicative value for the proposed bound from next generation experiments, we take the projected sensitivity of SuperCDMS phase B [18].

Although it seems like we cannot currently use this measure as a constraint, the major proportion of our parameter space will be accessible at next-generation experiments. Since higgsino LSPs are generally more pure than bino-type ones, the former will

escape detection as long as there is an order 100 keV splitting between its two neutral components. This is is necessary in order to avoid the limit from spin-independent direct detection measurements [12].

Also visible in the graph are the interesting discontinuities mentioned in [13], corresponding to the opening up of new annihilation channels at $M_{LSP} = 1/2 M_{higgs}$ through an s-channel higgs. We also notice a similar discontinuity at the top threshold from annihilation to $t\bar{t}$; this effect becomes more pronounced as the new yukawa couplings increase.

## 6.5 Electric Dipole Moment

Since our model does not contain any sleptons it induces an electron EDM only at two loops, proportional to $\sin(\theta)$ for $\theta$ as defined above. This is a two-loop effect, we therefore expect it to be close to the experimental bound for $\mathcal{O}(1)$ $\theta$. The dominant diagram responsible for the EDM is generated by charginos and neutralinos in a loop and can be seen in Figure 6-4 below. This diagram is also present in Split SUSY where it gives a comparable contribution to the one with only charginos in the loop [19, 20].

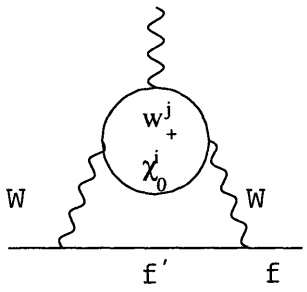


Figure 6-4: The 2-loop contribution to the EDM of a fermion f.

The induced EDM is (see [19]):

$$\frac{d_f^W}{e} = \pm \frac{\alpha^2 m_f}{8\pi^2 s_W^4 M_W^2} \sum_{i=1}^{3} \frac{m_{\chi_i} \mu}{M_W^2} \text{ Im } (O_i^L O_i^{R*}) \mathcal{G}\left(r_i^0, r^\pm\right) \tag{6.2}$$

where

$$\mathcal{G}\left(r_i^0, r^{\pm}\right) = \int_0^{\infty} dz \int_0^1 \frac{d\gamma}{\gamma} \int_0^1 dy \, \frac{y\, z\, (y + z/2)}{(z+y)^3 (z + K_i)}$$
$$= \int_0^1 \frac{d\gamma}{\gamma} \int_0^1 dy\, y \left[ \frac{(y - 3K_i)y + 2(K_i + y)y}{4y(K_i - y)^2} + \frac{K_i(K_i - 2y)}{2(K_i - y)^3} \ln \frac{K_i}{y} \right]$$

and

$$K_i = \frac{r_i^0}{1-\gamma} + \frac{r^{\pm}}{\gamma}, \quad r^{\pm} \equiv \frac{\mu^2}{M_W^2}, \quad r_i^0 \equiv \frac{m_{\chi_i}^2}{M_W^2},$$
$$O_i^R = \sqrt{2} N_{2i}^* \exp^{-i\theta}, \quad O_i^L = -N_{3i}$$

$N^T M_N N = \mathrm{diag}(\mathrm{m}_{\chi_1}, \mathrm{m}_{\chi_2}, \mathrm{m}_{\chi_3})$ with real and positive diagonal elements. The sign on the right-hand side of equation (6.2) corresponds to the fermion $f$ with weak isospin $\pm\frac{1}{2}$ and $f'$ is its electroweak partner.

In principle it should be possible to cross-correlate the region of our parameter space which is consistent with relic abundance measurements, with that consistent with electron EDM measurements in order to further constrain our parameters. However since the current release of DarkSUSY does not support CP violating phases and a version including CP violations seems almost ready for public release[4] we leave an accurate study of the consequences of non-zero CP phase in relic abundance and direct detection calculations for a future work. We can still draw some interesting conclusions by estimating the effect of non-zero CP phase. Because there is no reason for these new contributions to be suppressed with respect to the CP-conserving ones (for $\theta$ of $\mathcal{O}(1)$), we might naively expect their inclusion to enhance the annihilation cross-section by around a factor of 2, increasing the acceptable LSP masses by $\sim \sqrt{2}$ for constant relic abundance. This is discussed in greater detail in [21] (and [22] for direct detection) in which we see that this observation holds for most of the parameter space. We must note, however, that in particular small regions of the space the enhancement to the annihilation cross-section and the suppression to the elastic cross section can be much larger, justifying further investigation of this point in future

[4]Private communication with one of the authors of DarkSUSY.

work. With this assumption in mind we see in Figure 6-5 that although the majority of our allowed region is below the current experimental limit of $d_e < 1.7 \times 10^{-27} e$ cm at 95% C.L. [23], most of it will be accessible to next generation EDM experiments. These propose to improve the precision of the electron EDM measurement by 4 orders of magnitude in the next 5 years, and maybe even up to 8 orders of magnitude, funding permitting [24, 25, 26]. We also see in this figure that CP violation is enhanced on the diagonal where the mixing is largest. This is as expected since the yukawas that govern the mixing are necessary for there to be any CP violating phase at all. For the same reason, decoupling either particle sends the EDM to zero.

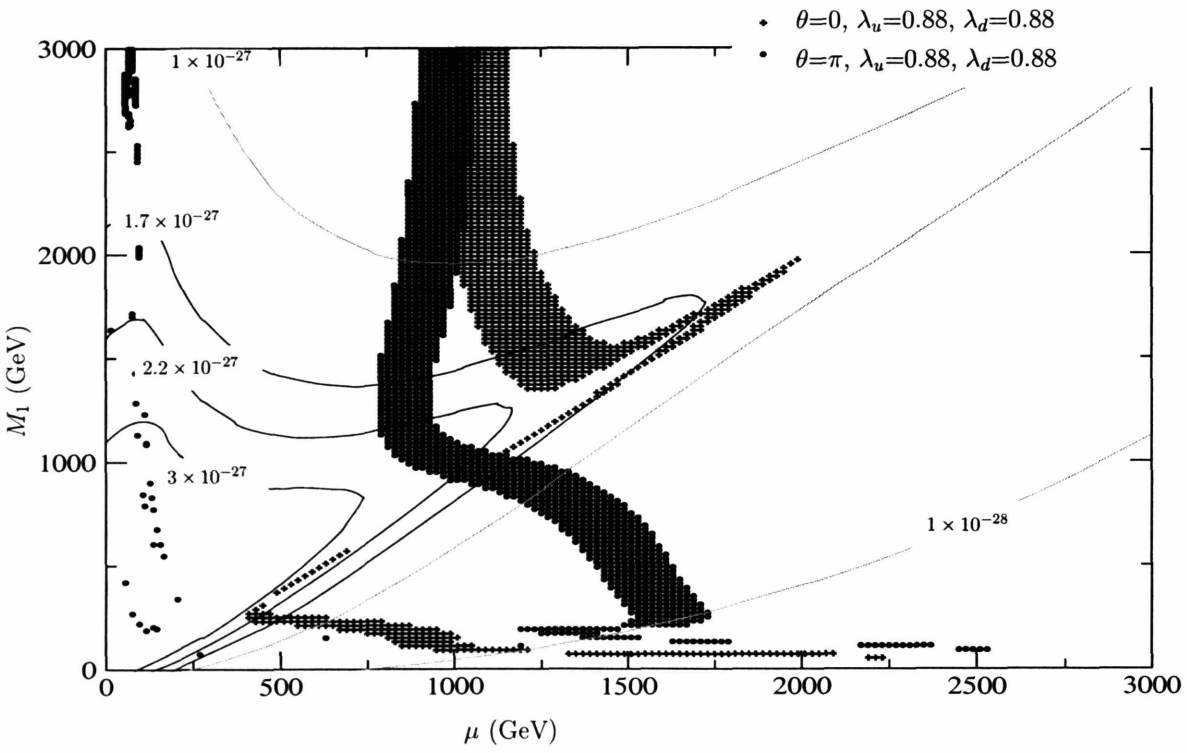


Figure 6-5: Electron edm contours for $\theta = \pi/2$. The excluded region is bounded by the black contours. Note that CP violation was not included in the relic density calculation, and the dark matter plot is simply intended to indicate the approximate region of interest for dark matter.

## 6.6 Gauge Coupling Unification

In this section we study the running of gauge couplings in our model at two loops. The addition of higgsinos largely improves unification as compared to the SM case,

but their effect is still not large enough and the model predicts a value for $\alpha_s(M_z)$ around $9\sigma$ lower than the experimental value of $\alpha_s(M_z) = 0.119 \pm 0.002$ [27]. Moreover the scale at which the couplings unify is very low, around $10^{14}$ GeV, making proton decay occur much too quickly to embed in a simple GUT theory[5]. These problems can be avoided by adding the Split SUSY particle content at higher energies, as in [29], at the cost of losing minimality; instead we choose to solve this problem by embedding our minimal model in an extra dimensional theory. This decision is well motivated: even though normal 4D GUTs have had some successes, explaining the quark-lepton mass relations for example, and charge quantization in the SM, there are many reasons why these simple theories are not ideal. In spite of the fact that the matter content of the SM falls naturally into representations of $SU(5)$, there are some components that seem particularly resistant to this. This is especially true of the higgs sector, the unification of which gives rise to the doublet-triplet splitting problem. Even in the matter sector, although $b$-$\tau$ unification works reasonably well the same cannot be said for unification of the first two generations. In other words, it seems like gauge couplings want to unify while the matter content of the SM does not, at least not to the same extent. This dilemma is easily addressed in an extra dimensional model with a GUT symmetry in the bulk, broken down to the SM gauge group on a brane by boundary conditions [30] since we can now choose where we put fields based on whether they unify consistently or not. Unified matter can be placed in the bulk whereas non-unified matter can be placed on the GUT-breaking brane. The low energy theory will then contain the zero modes of the 5D bulk fields as well as the brane matter. While solving many of the problems of standard 4D GUTs these extra dimensional theories have the drawback of having a large number of discrete choices for the location of the matter fields, as we shall see later.

We will consider a model with one flat extra dimension compactified on a circle of radius $R$, with orbifolds $S^1/(Z_2 \times Z_2')$, whose action is obtained from the identifications

[5]It is possible to evade the constraint from proton decay by setting some of the relevant mixing parameters to zero [28]. However we are not aware of any GUT model in which such an assertion is justified by symmetry arguments.

$$Z_2 : y \sim 2\pi\ R - y, \quad Z_2' : y \sim \pi R - y, \quad y \in [0, 2\pi] \tag{6.3}$$

where $y$ is the coordinate of the fifth dimension. There are two fixed points under this action, at $(0, \pi R)$ and $(\pi R/2, 3\pi R/2)$, at which are located two branes. We impose an $SU(5)$ symmetry in the bulk and on the $y = 0$ brane; this symmetry is broken down to the SM $SU(3) \times SU(2) \times U(1)$ on the other brane by a suitable choice of boundary conditions. All fields need to have definite transformation properties under the orbifold action - we choose the action on the fundamental to be $\phi \rightarrow \pm P\phi$ and on the adjoint, $\pm[P, A]$, for projection operators $P_Z = (+,+,+,+,+)$ and $P_{Z'} = (+,+,+,-,-)$. This gives SM gauge fields and their corresponding KK towers $A_\mu^a$ for $a = \{1, ..., 12\}$ $(+,+)$ parity; and the towers $A_\mu^{\hat{a}}$ for $\hat{a} = \{13, ..., 24\}$ $(+,-)$ parity, achieving the required symmetry-breaking pattern. By gauge invariance the unphysical fifth component of the gauge field, which is eaten in unitary gauge, gets opposite boundary conditions.[6] We still have the freedom to choose the location of the matter fields. In this model $SU(5)$-symmetric matter fields in the bulk will get split by the action of the $Z'$ orbifold: the SM $\overline{\mathbf{5}}$ for instance will either contain a massless $d^c$ or a massless $l$, with the other component only having massive modes. Matter fields in the bulk must therefore come in pairs with opposite eigenvalues under the orbifold projections, so for each SM generation in the bulk we will need two copies of $\mathbf{10} + \overline{\mathbf{5}}$. This provides us with a simple mechanism to forbid proton decay from $X$- and $Y$-exchange and also to split the color triplet higgs field from the doublet. To summarize, unification of SM matter fields in complete multiplets of $SU(5)$ cannot be achieved in the bulk but on the $SU(5)$ brane, while matter on the SM brane is not unified into complete GUT representations.

[6]From an effective field theory point of view an orbifold is not absolutely necessary, our theory can simply be thought of as a theory with a compact extra dimension on an interval, with two branes on the boundaries. Because of the presence of the boundaries we are free to impose either Dirichlet or Neumann boundary conditions for the bulk field on each of the branes breaking the $SU(5)$ to the SM gauge group purely by choice of boundary conditions and similarly splitting the multiplets accordingly. Our orbifold projection is therefore nothing more than a further restriction to the set of all possible choices we can make.

### 6.6.1 Running and matching

We run the gauge couplings from the weak scale to the cutoff $\Lambda$ by treating our model as a succession of effective field theories (EFTs) characterized by the differing particle content at different energies. The influence of the yukawa couplings between the higgsinos and the singlet on the two-loop running is negligible, hence it is fine to assume that the singlet is degenerate with the higgsinos so there is only one threshold from $M_{\text{top}}$ to the compactification scale $1/R$, at which we will need to match with the full 5D theory.

The $SU(5)$-symmetric bulk gauge coupling $g_5$ can be matched on to the low energy couplings at the renormalization scale $M$ via the equation

$$\frac{1}{g_i^2(M)} = \frac{2\pi R}{g_5^2} + \Delta_i(M) + \lambda_i(MR) \tag{6.4}$$

The first term on the right represents a tree level contribution from the 5d kinetic term, $\Delta_i$ are similar contributions from brane-localized kinetic terms and $\lambda_i$ encode radiative contributions from KK modes. The latter come from renormalization of the 4D brane kinetic terms which run logarithmically as usual.

To understand this in more detail let us consider radiative corrections to a $U(1)$ gauge coupling in an extra dimension compactified on a circle with no orbifolds, due to a 5D massless scalar field [32]. Since $1/g_5^2$ has mass dimension 1, by dimensional analysis we might expect corrections to it to go like $\Lambda + m \log \Lambda$ where $m$ is some mass parameter in the theory. The linearly divergent term is UV sensitive and can be reabsorbed into the definition of $g_5$, whereas the log term cannot exist since there is no mass parameter in the theory. Hence the 5D gauge coupling does not run, and neither does the 4D gauge coupling. This can also be interpreted from a 4D point of view, where the KK partners of the scalar cut off the divergences of the zero mode. Since there is no distinction between the wavefunctions for even (cosine) and odd (sine) KK modes in the absence of an orbifold, and we know that the sum of their contributions must cancel the log divergence of the 4D massless scalar, each of these must give a contribution equal to $-1/2$ times that of the 4D massless scalar.

When we impose a $Z_2$ orbifold projection and add two 3-branes at the orbifold fixed points, the scalar field must now transform as an eigenstate of this orbifold action and can either be even ($(+,+)$, with Neuman boudary conditions on the branes), or odd ($(-,-)$, with Dirichlet boundary conditions on the branes). This restricts us to a subset of the original modes and the cancellation of the log divergence no longer works. Since this running can only be due to 4D gauge kinetic terms localized on the branes, where the gauge coupling is dimensionless and can therefore receive logarithmic corrections, locality implies that the contribution from a tower of states on a particular brane can only be due to its boundary condition on that brane, with the total running equal to the sum of the contributions on each brane. In fact, it is only in the vicinity of the brane that imposing a particular boundary condition has any effect. As argued above, a $(+,+)$ tower (excluding the zero mode) and a $(-,-)$ tower must each give a total contribution equal to $-1/2$ times that of the zero mode, which corresponds to a coefficient of $-1/4$ to the running of each brane-localized kinetic term. Taking into account the contribution of the zero mode we can say that a tower of modes with $+$ boundary conditions on a brane contributes $+1/4$ times the corresponding 4D coefficient, while a $-$ boundary condition contributes $-1/4$ times the same quantity. This argument makes it explicit that the orbifold projection can be seen as a prescription on the boundary conditions of the fields in the extra dimension, which only affect the physics near each brane.

Adding another orbifold projection as we are doing in this case also allows for towers with $(+,-)$ and $(-,+)$ boundary conditions which, from the above argument, both give a contribution of $\pm 1/4 \mp 1/4 = 0$. The contribution of the $(+,+)$ and $(-,-)$ towers clearly remains unchanged.

Explicitly integrating out the KK modes at one loop at the compactification scale allows us to verify this fact, and also compute the constant parts of the threshold corrections, which are scheme-dependent. In $\overline{\text{DR}}$ [7] we obtain [32]:

[7] We use this renormalization scheme even though our theory is non-supersymmetric since 4D threshold corrections in this scheme contain no constant part [31].

$$\lambda_i(MR) = \frac{1}{96\pi^2}\left(\left(b_i^S - 21b_i^G + 8b_i^F\right)F_e(MR) + \left(\tilde{b}_i^S - 21\tilde{b}_i^G + 8\tilde{b}_i^F\right)F_0\right) \tag{6.5}$$

with

$$F_e(\mu R) = \mathcal{I} - 1 - \log(\pi) - \log(MR), \quad F_0 = -\log(2) \tag{6.6}$$
$$\mathcal{I} = \frac{1}{2}\int_1^{+\infty} dt\ \left(t^{-1} + t^{-1/2}\right)(\theta_3(it) - 1) \simeq 0.02, \quad \theta_3(it) = \sum_{n=-\infty}^{+\infty} e^{-\pi t n^2}$$

where $b_i^{S,G,F}$ ($\tilde{b}_i^{S,G,F}$) are the Casimirs of the KK modes of real scalars (not including goldstone bosons), massive vector bosons and Dirac fermions respectively with even (odd) masses $2n/R$ ($(2n+1)/R$). As explained above, the logarithmic part of the above expression is equal to exactly $-1/2$ times the contribution of the same fields in 4D [33, 34]. Since the compactification scale $1/R$ will always be relatively close to the unification scale $\Lambda$ (so our 5D theory remains perturbative), it will be sufficient for us to use one loop matching in our two loop analysis as long as the matching is done at a scale $M$ close to the compactification scale.

As an aside, from equation (6.4) we can get:

$$\frac{d}{dt}\Delta_i = \frac{b_i - b_i^{MM}}{8\pi^2} \tag{6.7}$$

where $b_i$ is shorthand for the combination $(b_i^S - 21b_i^G + 8b_i^F)/12$ and $b_i^{MM}$ are the coefficients of the renormalization group equations below the compactification scale (see Appendix 6.9 for details). It is clear from this equation that it is unnatural to require $\Delta_i(1/R) \ll 1/(8\pi^2)$. The most natural assumption $\Delta_i(\Lambda) \sim 1/(8\pi^2)$ gives a one-loop contribution comparable to the tree level term, implying the presence of some strong dynamics in the brane gauge sector at the scale $\Lambda$. We know that the 5D gauge theory becomes strong at the scale $24\pi^3/g_5^2$, so from naive dimensional analysis (NDA) (see for example [35]) we find that it is quite natural for $\Lambda$ to coincide with the strong coupling scale for the bulk gauge group.

Running equation (6.7) to the compactification scale we obtain

$$\Delta_i(1/R) = \Delta_i(\Lambda) + \frac{b_i - b_i^{MM}}{8\pi^2}\log(\Lambda R) \tag{6.8}$$

For $\Lambda R \gg 1$ the unknown bare parameter is negligible compared to the log-enhanced part, and can be ignored, leaving us with a calculable correction. Using $g_{GUT} = 2\pi R/g_5^2$ we expect $\Lambda R \sim 8\pi^2/g_{\rm GUT}^2 \sim 100$. Keeping this in mind, we shall check whether unification is possible in our model with $\Lambda R$ in the regime where the bare brane gauge coupling is negligible. To this purpose we will impose the matching equation (6.4) at the scale $\Lambda$ *assuming* $\Delta_i(\Lambda) = 0$; we will then check whether the value of $\Lambda R$ found justifies this approximation.

In order to develop some intuition for the direction that these thresholds go in, we can analyze the one-loop expression (with one-loop thresholds) for the gauge couplings at $M_z$:

$$\frac{1}{\alpha_i(M_z)} = \frac{4\pi}{g_{\rm GUT}^2} + 4\pi\lambda_i(\Lambda R) + \lambda_i^{\rm conv}(\Lambda R) + \frac{b_i^{\rm MM}}{2\pi}\log\left(\frac{\Lambda}{M_z}\right) + \frac{\left(b_i^{\rm SM} - b_i^{\rm MM}\right)}{2\pi}\log\left(\frac{\mu}{M_z}\right) \tag{6.9}$$

$b_i^{\rm SM}$ are the SM beta function coefficients (see Appendix 6.9), $\mu$ is the scale of the higgsinos and singlet, $\lambda^{\rm conv} = (-\frac{3}{12\pi}, -\frac{2}{12\pi}, 0)$ are conversion factors from $\overline{\rm MS}$, in which the low-energy experimental values for the gauge couplings are defined, to $\overline{\rm DR}$ [36]. Taking the linear combination $(9/14)\alpha_1^{-1} - (23/14)\alpha_2^{-1} + \alpha_3^{-1}$ allows us to eliminate the $\Lambda$ dependence as well as all $SU(5)$-symmetric terms, leaving

$$\frac{1}{\alpha_3(M_z)} = -\frac{9/14}{\alpha_1(M_z)} + \frac{23/14}{\alpha_2(M_z)} + 4\pi\lambda(\Lambda R) + \lambda^{\rm conv} + \frac{\left(b^{\rm SM} - b^{\rm MM}\right)}{2\pi}\log\left(\frac{\mu}{M_z}\right) \tag{6.10}$$

where $X = (9/14)X_1 - (23/14)X_2 + X_3$ for any quantity $X$. Recall that the leading threshold correction from the 5D GUT is proportional to $\log(\Lambda R)$. The low-energy value of $\alpha_3$ is therefore changed by

$$\delta\alpha_3(M_z) = \alpha_3(M_z)^2 \frac{b}{2\pi} \log(\Lambda R) \tag{6.11}$$

We still have the freedom to choose the positions of the various matter fields. In order to determine the best setup for gauge coupling unification we need to keep in mind two facts: the first is that adding $SU(5)$ multiplets in the bulk does not have any effect on $\alpha_3(M_Z)$; and the second is that $b$ contains only contributions from $(+,+)$ modes (in unitary gauge none of our bulk modes have $(-,-)$ boundary conditions; our $SU(5)$ bulk multiplets are split into $(+,+)$ and $(+,-)$ modes).

As stated at the beginning of this section our 4D prediction for $\alpha_3(M_z)$ is too low. Since fermions have a larger effect on running than scalars, this problem is most efficiently tackled by splitting up the fermion content of the SM into non-$SU(5)$ symmetric parts in order to make $b$ as positive as possible. Examining the particular linear combination that eliminated the dependence on $\Lambda$ at one loop we find that one or more $SU(5)$-incomplete colored multiplets are needed in the bulk, or equivalently the weakly-interacting part of the same multiplet has to be on one of the branes. Since matter in the bulk is naturally split by the orbifold projections, this just involves separating the pair of multiplets whose zero modes make up one SM family.

With this in mind we find that for fixed $\Lambda R$ and $\mu$, since separating different numbers of SM generations allows us to vary the low energy value of $\alpha_3$ anywhere from its experimental value to several $\sigma$s off, gauge coupling unification really does work in this model for some fraction of all available configurations. Although this may seem a little unsatisfactory from the point of view of predictivity, the situation can be somewhat ameliorated by further refining our requirements. For example, we can go some way towards explaining the hierarchy between the SM fermion masses by placing the first generation in the bulk, the second generation split between the bulk and a brane and the third generation entirely on a brane. This way, in addition to breaking the approximate flavor symmetry in the fermion sector we also obtain helpful factors of order $1/\sqrt{\Lambda R}$ between the masses of the different generations. The location of the higgs does not have a very large effect on unification, the simplest

choice would be to put it, as well as the higgsinos and singlet, on the $SU(5)$-breaking brane, where there is no need to introduce corresponding color triplet fields. This also helps to explain the hierarchy. In this model, which can be seen on the left-hand side

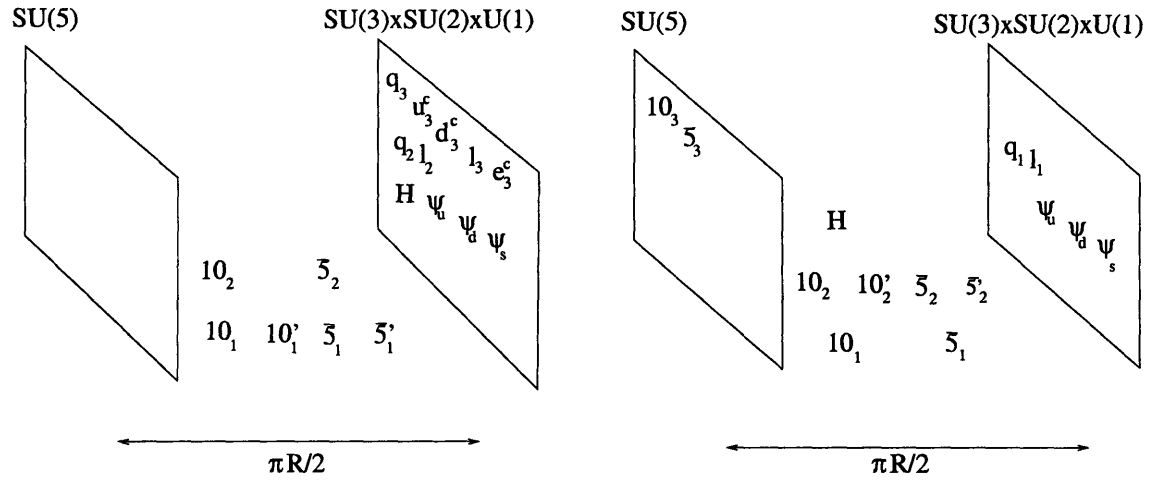


(a) Higgs on the broken brane

(b) Higgs in the bulk and third generation on the $SU(5)$ brane

Figure 6-6: Matter content of the two orbifold GUT models we propose.

of Figure 6-6, we also need to put our third generation and split second generation on the same brane in order for them to interact with the higgs.

On the right is another model which capitalizes on every shred of evidence we have about GUT physics: we put the higgs in the bulk in this case (recall that the orbifold naturally gives rise to doublet-triplet splitting) so that we can switch the third generation to the $SU(5)$-preserving brane and obtain $b$-$\tau$ unification (see Figure 6-7) without having analogous relationships for the other two generations[8]. We also need to flip the positions of the first and second generations if we want to keep the suppression of the mass of the first generation with respect to the second.

The low-energy values for $\alpha_3$ as a function of $\mu$ in these two models can be seen in Figure 6-8 for different $\Lambda R$. Note that unification can be acheived in the regime

[8]As explained in [37] the two yukawa couplings $\lambda_b$ and $\lambda_\tau$ run differently only below the compactification scale. Because of locality, the fields living on the $SU(5)$ brane do not feel the $SU(5)$ breaking until energies below the compactification scale; hence if they are unified at some high energy they keep being unified until this scale.

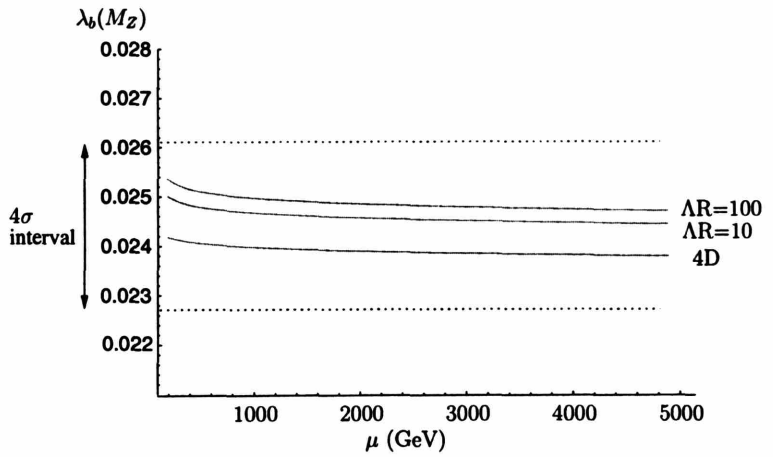


Figure 6-7: Low energy prediction for $\lambda_b(M_Z)$, as a function of the higgsino mass $\mu$, for the model with the higgs in the bulk, for $\Lambda R = 10, 100$ and for the 4D model. $4\sigma$ interval taken from [27].

where $\Lambda R \gg 1$, justifying our initial assumption that the brane kinetic terms could be neglected. We see that although the dependence on $\mu$ is very slight, small $\mu$ seems to be preferred. However we cannot use this observation to put a firm upper limit on $\mu$ because of the uncertainties associated with ignoring the bare kinetic terms on the branes.

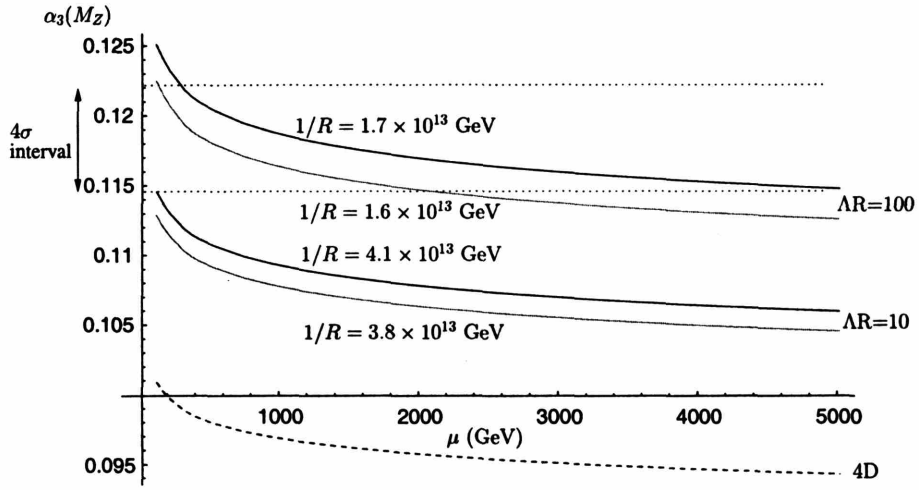


Figure 6-8: Low energy prediction for $\alpha_3(M_z)$, as a function of the higgsino mass $\mu$, for the model with the higgs on the brane (black line), and for the model with the higgs in the bulk (green line), for $\Lambda R = 10, 100$, and for the 4D case (dashed line). Some typical values of $1/R$ are shown.

The second configuration, Figure 6-6(b), also gives proton decay through the mixing of the third generation with the first two. From our knowledge of the CKM matrix we infer that all mixing matrices will be close to the unit matrix, proton

decay will therefore be suppressed by off-diagonal elements. To minimize this suppression it is best to have an anti-neutrino and a strange quark in the final state. The proton decay rate for this process was computed in [38] and is proportional to $\left(\frac{g_4^2}{(1/R)^2}\right)^2 \left(1 - \frac{m_{\text{kaon}}^2}{m_{\text{proton}}^2}\right) |(R_d^\dagger)_{23}(R_u^\dagger)_{13}(L_d)_{31}|^2$ where $R_{d,u}$ and $L_d$ are the rotation matrices of the right-handed down-type and up-type quarks, and the left-handed down-type quarks, which are unknown. We assume that the 2-3 and the 1-3 mixing elements are 0.05 and 0.01 respectively, similar to the corresponding CKM matrix elements, giving a proton lifetime of

$$\tau_p(p \to K^+ \bar{\nu}_\tau) \simeq 6.6 \times 10^{38} \text{ years } \times \left(\frac{1/R}{10^{14}\text{GeV}}\right)^4 \simeq 4 \times 10^{35} \text{ years} \qquad (6.12)$$

for $1/R = 1.6 \times 10^{13}$ GeV. This is above the current limit from Super-Kamiokande of $1.9 \times 10^{33}$ years at 90% C.L. [39, 40], although there are multi-megaton experiments in the planning stages that are expected to reach a sensitivity of up to $6 \times 10^{34}$ years [40] . Given our lack of information about the mixing matrices involved[9], we see that there might be some possibility that proton decay in this model will be seen in the not-too-distant future.

## 6.7 Conclusion

The identification of a TeV-scale weakly-interacting particle as a good dark matter candidate, and the unification of the gauge couplings are usually taken as indications of the presence of low-energy SUSY. However this might not necessarily be the case.

If we assume that the tuning of the higgs mass can be explained in some other unnatural way, through environmental reasoning for instance, then new possibilities open up for physics beyond the SM. In this chapter we studied the minimal model consistent with current experimental limits, that has both a good thermal dark matter candidate and gauge coupling unification. To this end we added to the SM two

[9]Experiments have only constrained the particular combination that appears in the SM as the CKM matrix.

higgsino-like particles and a singlet, with a singlet majorana mass of $\lesssim 100$ TeV in order to split the two neutralinos and so avoid direct detection constraints. Making the singlet light allowed for a new region of dark matter with mixed states as heavy as $\sim 2.2$ TeV, well beyond the reach of the LHC and the generic expectation for a weakly interacting particle. Nevertheless we do have some handles on this model: firstly via the 2-loop induced electron EDM contribution which is just beyond present limits for CP angle of order 1, and secondly by the spin-independent direct detection cross section, both of which should be accessible at next-generation experiments.

Turning to gauge coupling unification we saw that this was much improved at two loops by the presence of the higgsinos. A full 4D GUT model is nevertheless excluded by the smallness of the GUT scale $\sim 10^{14}$ GeV, which induces too fast proton decay. We embedded the model in a 5D orbifold GUT in which the threshold corrections were calculable and pushed $\alpha_3$ in the right direction for unification (for a suitable matter configuration). It is very gratifying that such a model can help explain the pattern in the fermion mass hierarchy, give $b$-$\tau$ unification, and predict a rate for proton decay that can be tested in the future.

## 6.8 Appendix A: The neutralino mass matrix

We have a 3×3 neutralino mass matrix in which the mixing terms (see equation (6.2)) are unrelated to gauge couplings and are limited only by the requirement of perturbativity to the cutoff. It is possible to get a feel for the behavior of this matrix by finding the approximate eigenvalues and eigenvectors in the limit of equal and small off-diagonal terms ($\lambda v \ll M_1 \pm \mu$). The approximate eigenvalues and eigenvectors are shown in the table below:

| $M^2$ | Gaugino fraction |
|---|---|
| $M_1^2 + 4\lambda^2 v^2 \frac{M_1}{M_1 \pm \mu}$ | $1 - 2\frac{\lambda^2 v^2}{(M_1 \pm \mu)^2}$ |
| $\mu^2$ | 0 |
| $\mu^2 \pm 4\lambda^2 v^2 \frac{\mu}{M_1 \pm \mu}$ | $2\frac{\lambda^2 v^2}{(M_1 \pm \mu)^2}$ |

for $\cos\theta = \pm 1$.

If $M_1 << \mu$ the first eigenstate will be the LSP. In the opposite limit the composition of the LSP is dependent upon the sign of $\cos(\theta)$. For $\cos(\theta)$ positive the second eigenstate, which is pure higgsino, is the LSP, while for $\cos(\theta)$ negative, the mixed third eigenstate becomes the LSP.

We also see from the table that in the pure higgsino case, a splitting of order 100 keV (sufficient to evade the direct detection constraint) can be achieved with a singlet mass lighter than $10^9$ GeV, where the upper limit corresponds to O(1) yukawa couplings.

## 6.9 Appendix B: Two-Loop Beta Functions for Gauge Couplings

The two-loop RGE for the gauge couplings in our minimal model is

$$(-2\pi)\frac{d}{dt}\alpha_i^{-1} = b_i^{MM} + \frac{1}{(4\pi)^2}\left[\sum_j^3 4\pi B_{ij}^{MM}\alpha_j - d_i\lambda_t^2 - d_i'(\lambda_u^2 + \lambda_d^2)\right]$$

with $\beta$-function coefficients

$$b^{MM} = \left(\frac{9}{2}, -\frac{15}{6}, -7\right); \qquad B^{MM} = \begin{pmatrix} \frac{104}{25} & \frac{18}{5} & \frac{44}{5} \\ \frac{6}{5} & 14 & 12 \\ \frac{11}{10} & \frac{9}{2} & -26 \end{pmatrix};$$

$$d = \left(\frac{17}{10}, \frac{3}{2}, 2\right); \qquad d' = \left(\frac{3}{20}, \frac{1}{4}, 0\right)$$

The running of the yukawa couplings is the same as in [9] but we will reproduce their RGEs here for convenience - we ignore all except the top yukawa coupling (we found that our two new yukawas do not have a significant effect).

$$(4\pi)^2\lambda_t = \lambda_t\left[-3\sum_{i=1}^3 4\pi c_i\alpha_i + \frac{9}{2}\lambda_t^2 + \frac{1}{2}(\lambda_u^2 + \lambda_d^2)\right]$$

with $c = \left(\frac{17}{60}, \frac{3}{4}, \frac{8}{3}\right)$.

The two-loop coupled RGEs can be solved analytically if we approximate the top yukawa coupling as a constant over the entire range of integration (see [36] for a study on the validity of this approximation). The solution is

$$\begin{aligned}\alpha_i^{-1}(M) &= \alpha_G^{-1} + \frac{1}{2\pi} b^{MM} \ln \frac{\Lambda}{M} + \\ &\quad \frac{1}{4\pi} \sum_{j=1}^{3} \frac{B_{ij}^{MM}}{b_j^{MM}} \ln \left(1 + \frac{1}{4\pi} b_j^{MM} \alpha_G(\Lambda) \ln \frac{\Lambda}{M}\right) - \frac{1}{32\pi^3} d_i \lambda_t^2 \ln \frac{\Lambda}{M}\end{aligned}$$

# Bibliography


[1] S. Perlmutter *et al.* [Supernova Cosmology Project Collaboration], "Measurements of Omega and Lambda from 42 High-Redshift Supernovae," Astrophys. J. **517** (1999) 565, astro-ph/9812133.

[2] D. N. Spergel *et al.* [WMAP Collaboration], "First Year Wilkinson Microwave Anisotropy Probe (WMAP) Observations: Determination of Cosmological Parameters," Astrophys. J. Suppl. **148** (2003) 175, astro-ph/0302209. C. L. Bennett *et al.*, "First Year Wilkinson Microwave Anisotropy Probe (WMAP) Observations: Preliminary Maps and Basic Results," Astrophys. J. Suppl. **148**, 1 (2003), astro-ph/0302207.

[3] R. Barbieri and A. Strumia, "What is the limit on the Higgs mass?," Phys. Lett. B **462**, 144 (1999), hep-ph/9905281.

[4] L. Giusti, A. Romanino and A. Strumia, "Natural ranges of supersymmetric signals," Nucl. Phys. B **550** (1999) 3, hep-ph/9811386.

[5] S. Weinberg, "Anthropic Bound On The Cosmological Constant," Phys. Rev. Lett. **59** (1987) 2607.

[6] V. Agrawal, S. M. Barr, J. F. Donoghue and D. Seckel, "The anthropic principle and the mass scale of the standard model," Phys. Rev. D **57**, 5480 (1998), hep-ph/9707380.

[7] N. Arkani-Hamed and S. Dimopoulos, "Supersymmetric unification without low energy supersymmetry and signatures for fine-tuning at the LHC," JHEP **0506**, 073 (2005) [arXiv:hep-th/0405159].

[8] N. Arkani-Hamed, S. Dimopoulos and S. Kachru, "Predictive landscapes and new physics at a TeV," arXiv:hep-th/0501082.

[9] G. F. Giudice and A. Romanino, "Split supersymmetry," Nucl. Phys. B **699**, 65 (2004) [Erratum-ibid. B **706**, 65 (2005)], hep-ph/0406088.

[10] M. W. Goodman and E. Witten, "Detectability Of Certain Dark-Matter Candidates," Phys. Rev. D **31**, 3059 (1985).

[11] D. S. Akerib *et al.* [CDMS Collaboration], "Limits on spin-independent WIMP nucleon interactions from the two-tower run of the Cryogenic Dark Matter Search," arXiv:astro-ph/0509259.

[12] D. R. Smith and N. Weiner, "Inelastic dark matter," Phys. Rev. D **64**, 043502 (2001), hep-ph/0101138.

[13] A. Pierce, "Dark matter in the finely tuned minimal supersymmetric standard model," Phys. Rev. D **70** (2004) 075006, hep-ph/0406144.

[14] A. Masiero, S. Profumo and P. Ullio, "Neutralino dark matter detection in split supersymmetry scenarios," Nucl. Phys. B **712**, 86 (2005) [arXiv:hep-ph/0412058]. L. Senatore, "How heavy can the fermions in split SUSY be? A study on gravitino and extradimensional LSP," Phys. Rev. D **71**, 103510 (2005) [arXiv:hep-ph/0412103].

[15] P. Gondolo, J. Edsjo, P. Ullio, L. Bergstrom, M. Schelke and E. A. Baltz, "DarkSUSY: A numerical package for supersymmetric dark matter calculations,",astro-ph/0211238; J. Edsjo, M. Schelke, P. Ullio and P. Gondolo, "Accurate relic densities with neutralino, chargino and sfermion coannihilations in mSUGRA," JCAP **0304**, 001 (2003), hep-ph/0301106]; P. Gondolo and G. Gelmini, "Cosmic Abundances Of Stable Particles: Improved Analysis," Nucl. Phys. B **360**, 145 (1991).

[16] A. Provenza, M. Quiros and P. Ullio, "Electroweak baryogenesis, large Yukawas and dark matter," JHEP **0510**, 048 (2005) [arXiv:hep-ph/0507325].

[17] J. Edsjo and P. Gondolo, "Neutralino relic density including coannihilations," Phys. Rev. D **56**, 1879 (1997), hep-ph/9704361];

[18] P. L. Brink *et al.* [CDMS-II Collaboration], "Beyond the CDMS-II dark matter search: SuperCDMS," eConf **C041213**, 2529 (2004) [arXiv:astro-ph/0503583]. Useful comparison can be done using the tools of http://dendera.berkeley.edu/plotter/entryform.html

[19] D. Chang, W. F. Chang and W. Y. Keung, "Electric dipole moment in the split supersymmetry models," Phys. Rev. D **71** (2005) 076006, hep-ph/0503055.

[20] N. Arkani-Hamed, S. Dimopoulos, G. F. Giudice and A. Romanino, "Aspects of split supersymmetry," Nucl. Phys. B **709**, 3 (2005) [arXiv:hep-ph/0409232].

[21] P. Gondolo and K. Freese, "CP-violating effects in neutralino scattering and annihilation," JHEP **0207**, 052 (2002), hep-ph/9908390.

[22] T. Falk, A. Ferstl and K. A. Olive, "Variations of the neutralino elastic cross-section with CP violating phases," Astropart. Phys. **13**, 301 (2000) [arXiv:hep-ph/9908311].

[23] B. C. Regan, E. D. Commins, C. J. Schmidt and D. DeMille, "New limit on the electron electric dipole moment," Phys. Rev. Lett. **88** (2002) 071805.

[24] D. Kawall, F. Bay, S. Bickman, Y. Jiang and D. DeMille, "Progress towards measuring the electric dipole moment of the electron in metastable PbO," AIP Conf. Proc. **698** (2004) 192.

[25] S. K. Lamoreaux, "Solid state systems for electron electric dipole moment and other fundamental measurements," nucl-ex/0109014.

[26] Y. K. Semertzidis, "Electric dipole moments of fundamental particles," arXiv:hep-ex/0401016.

[27] S. Eidelman *et al.* [Particle Data Group], "Review of particle physics," Phys. Lett. B **592** (2004) 1.

[28] I. Dorsner and P. F. Perez, "How long could we live?," Phys. Lett. B **625**, 88 (2005) [arXiv:hep-ph/0410198].

[29] I. Antoniadis, A. Delgado, K. Benakli, M. Quiros and M. Tuckmantel, "Splitting extended supersymmetry," arXiv:hep-ph/0507192.

[30] Y. Kawamura, "Gauge symmetry reduction from the extra space S(1)/Z(2)," Prog. Theor. Phys. **103**, 613 (2000), hep-ph/9902423. A. Hebecker and J. March-Russell, "A minimal S(1)/(Z(2) x Z'(2)) orbifold GUT," Nucl. Phys. B **613**, 3 (2001), hep-ph/0106166. L. J. Hall and Y. Nomura, "Gauge coupling unification from unified theories in higher dimensions," Phys. Rev. D **65**, 125012 (2002), hep-ph/0111068. G. Altarelli and F. Feruglio, "SU(5) grand unification in extra dimensions and proton decay," Phys. Lett. B **511**, 257 (2001), hep-ph/0102301. L. J. Hall and Y. Nomura, "Grand unification in higher dimensions," Annals Phys. **306**, 132 (2003), hep-ph/0212134. P. C. Schuster, "Grand unification in higher dimensions with split supersymmetry," hep-ph/0412263. A. B. Kobakhidze, "Proton stability in TeV-scale GUTs," Phys. Lett. B **514**, 131 (2001) [arXiv:hep-ph/0102323].

[31] I. Antoniadis, C. Kounnas and K. Tamvakis, "Simple Treatment Of Threshold Effects," Phys. Lett. B **119**, 377 (1982).

[32] R. Contino, L. Pilo, R. Rattazzi and E. Trincherini, "Running and matching from 5 to 4 dimensions," Nucl. Phys. B **622**, 227 (2002), hep-ph/0108102.

[33] S. Weinberg, "Effective Gauge Theories," Phys. Lett. B **91**, 51 (1980).

[34] L. J. Hall, "Grand Unification Of Effective Gauge Theories," Nucl. Phys. B **178**, 75 (1981).

[35] Z. Chacko, M. A. Luty and E. Ponton, "Massive higher-dimensional gauge fields as messengers of supersymmetry breaking," JHEP **0007**, 036 (2000), hep-ph/9909248.

[36] P. Langacker and N. Polonsky, "Uncertainties in coupling constant unification," Phys. Rev. D **47**, 4028 (1993), hep-ph/9210235.

[37] L. J. Hall and Y. Nomura, "A complete theory of grand unification in five dimensions," Phys. Rev. D **66**, 075004 (2002), hep-ph/0205067.

[38] A. Hebecker and J. March-Russell, "Proton decay signatures of orbifold GUTs," Phys. Lett. B **539**, 119 (2002), hep-ph/0204037.

[39] Y. Hayato *et al.* [Super-Kamiokande Collaboration], "Search for proton decay through p $\rightarrow$ anti-nu K+ in a large water Cherenkov detector," Phys. Rev. Lett. **83** (1999) 1529, hep-ex/9904020.

[40] Y. Suzuki *et al.* [TITAND Working Group], "Multi-Megaton water Cherenkov detector for a proton decay search: TITAND (former name: TITANIC)," hep-ex/0110005.

# Chapter 7

# Conclusions

I have reported on some of the research work I have done during my years as a graduate student.

My research interest has focused mainly on the connections between Particle Physics and Cosmology, of which I think I have been able to explore many of the different aspects.

Thanks to the very recent improvement in the experimental techniques in Observational Cosmology, the field of Cosmology has become a field where new observations can motivate new ideas from Theoretical Physics, as for example with the observation of Dark Matter, of the tyne anisotropy of the CMB, and recently of the acceleration of the universe. Viceversa it has become also a field where new ideas from Theoretical Physics can be applied to the early universe with the purpose either of testing them against some phases that we consider well understood, or of gaining through them some insight on phases less understood, as for example is the case of the inflationary phase.

During my research work, I think I have been able to deepen most of these aspects.

Concerning that part which deals with using new high energy theories to develop new possible models for the early universe, in chapter 2 I have shown a model for the early universe where a new kind of inflation is developed. This new inflationary model is based on the condensate of a ghost field, which is a new mechanism for obtaining a stable Lorentz violating state in quantum field theory which has been

understood only very recently. When applied to the inflationary phase, the ghost condensate predicts some new features, such as a large amount of non-Gaussianities, which, because of the large information this kind of signal carries on, if detected, it would both tell us with great confidence that inflation did occur in the past, and also that it occurred in a way very similar to the one of ghost condensation. This inflationary model is also the first one in which it is shown that the Hubble rate $H$ can actually grow with time.

The work on non-Gaussianities has found a natural development in the direct analysis of the data from the most advanced experiment on the CMB: the WMAP experiment, as I have shown in chapter 5. Experimental data are at the origin of Physics, and it is really emotional to be able to deal with them. The work on the analysis of the non-Gaussian signal in the WMAP data originates from a long theoretical work during which the generation of a non-Gaussian inflationary signal in the CMB and its importance as a possible smoking gun for inflation was progressively understood. In the very last few years, several inflationary models have emerged which are distinguishable from the standard slow roll scenario exactly for the predicted amount and characteristics of the non-Gaussian signal. After this theoretical work, my collaborators and I realized that in the WMAP data there was more information on the non-Gaussian signal than what had already been extracted. We therefore decided to develop a method to better exploit the experimental data, and we directly did the analysis. No evidence of a non-Gaussian signal was found, but we improved and completed the available limits, so that the limits we give are at present the best currently available.

This last work represents to me that part of the field of Cosmology in which new theoretical ideas begin to be tested by new cosmological observations. In this thesis I have shown some other works in this direction, in which some other aspects of the history of the universe that we consider well understood are used to constraint models of Physics beyond the Standard Model.

In chapters 3,4 and 6, I have shown how some observational constraints coming from Dark Matter relic abundance, Baryogenesis, or Big Bang Nucleosynthesis, can

be applied to test ideas motivated by the Landscape.

The Landscape itself, istead, represent the most recent important idea in Theoretical Physics which is, at least partially, motivated by Cosmological Observations. In fact, the Landscape is a scenario which has recently emerged from String Theory in which the UV theory which describes our universe has a huge number of different low energy configurations, in which the parameters that we are able to observe scan from vacuum to vacuum. Together with the cosmological observation that the cosmological constant in our universe is not-null, and that it is roughly comparable to the upper limit it has in order for structures to be present in our universe, these theoretical considerations have led to the proposal that the reason why the cosmological constant (as well as the higgs mass) are small is not dynamical, as usually thought, but rather environmental, where by environmental we mean that their value should be such that the environment in our universe is such that physical observers can form in it. This has led to the proposal of several specific models, some of which I have then applied to the early universe and studied their constraint.

In chapter 3, I have considered the case of Split Susy, the first of these theories, where it is proposed that the supersymmetric partners of the Standard Model are split into scalar, which are very heavy at an intermediate scale between the weak scale and the GUT scale, and the fermions, which are instead at the weak scale protected by chiral symmetry. The lightness of the higgs is then not explained dynamically, but it is tuned to be light for environmental reasons. In this model it is the fact that the lightest supersymmetric partner (LSP) should be a thermal relic and made up the dark matter of the universe that fixes the fermions at around the weak scale, with deep consequences for a possible detection at LHC. This would in fact not be true if the gravitino or another dark sector particle were the LSP, and I have studied in detail the dark matter relic abundance in this case, and its consequences on the spectrum of the weakly interacting fermionic partners.

In the same direction, in chapter 4, I have studied a model which explains the tuning of the higgs through a mechanism in which baryons, which are necessary for in our universe there to be life, are present in our universe only if the higgs is

parametrically light. Baryons are produced at the electroweak phase transition in the so called electroweak baryogenesis scenario, and I have studied in detail the predicted baryon abundance. Taking this into account, the Physics associated with the CP violation then becomes very interesting when it is realized that the natural predicted electron electric dipole moment is parametrically just beyond current experimental limits, at a level reachable by next generation experiments.

Eventually, in chapter 6, I have illustrated a study of the minimal model beyond the standard model which accounts for the dark matter in the universe and gauge coupling unification, where again the higgs is assumed to be light for environmental reasons. We have realized that the right amount of dark matter abundance can be achieved with particles of unusual large mass, while gauge coupling unification works extremely well, as we have explicitly shown embedding the model in a five dimensional theory.

I think that thanks to these works I have been able to gain some good understanding of the field of Cosmology and Particle Physics. It is then very exciting to realize that in the very next few years, with the turning on of new experiments in Cosmology, such as the Planck satellite, and in Particle Physics as LHC, many of the ideas I have worked on during my studies for a PhD will be possibly tested, and our understanding of both the fields potentially revolutionized. A detection in the CMB of a tilt in the power spectrum of the scalar perturbations, or of a polarization induced by a background of gravitational waves, or of a non-Gaussian signal would shed light into the inflationary phase of the universe, and therefore also on the physics at very high energies. Combined with a definite improvement in the data on the Supernovae, expected in the very near future, these new experiments might shed light also on the great mystery of the present value of the Dark Energy, ruling out or giving further support to the idea of the Landscape. Similar in this will be the turning on of LHC which will probably help us understand if the solution to the hierarchy problem is to be solved in some natural way, as for example with TeV scale Supersymmetry, or if there is evidence of a tuning which points towards the presence of a Landscape.